TDP-43 Aberrant Phosphorylation in Amyotrophic Lateral Sclerosis (ALS) and in Niemann-Pick type C (NPC) Disease

Thesis

TDP-43 Aberrant Phosphorylation in Amyotrophic Lateral Sclerosis (ALS) and in Niemann-Pick type C (NPC) Disease

A thesis submitted in fulfilment for the requirements of the Open University (UK) for the degree of Doctor of Philosophy

Life Sciences

International Centre for Genetic Engineering and Biotechnology (ICGEB)
Trieste, Italy

Candidate: Francesca Paron
Supervisor: Prof. Emanuele Buratti
External Supervisor: Prof. Sebastian Oltean

To my husband and my parents

Publications

"**Dysregulation of TDP-43 intracellular localization and early onset ALS are associated with a TARDBP S375G variant**". Kathy Newell*, **Francesca Paron***, Miguel Mompean, Jill Murrell, Elisa Salis, Cristiana Stuani, Gary Pattee, Maurizio Romano, Douglas Laurents, Bernardino Ghetti, Emanuele Buratti. **Brain Pathol**. **2019 May**;29(3):397-413. doi:10.1111/bpa.12680.

*these authors contributed equally to the work

"**Pre-mRNA splicing defects and RNA binding protein involvement in Niemann Pick type C disease**". **Francesca Paron**, Andrea Dardis, Emanuele Buratti. **J Biotechnol**. **2020 Jul 20**;318:20-30. doi:10.1016/j.jbiotec.2020.03.012.

"**Somatic TARDBP variants as a cause of semantic dementia**". Jeroen van Rooij, Merel O Mol, Shamiram Melhem, Pelle van der Wal, Pascal Arp, **Francesca Paron**, Laura Donker Kaat, Harro Seelaar, Netherlands Brain Bank; Suzanne S M Miedema, Takuya Oshima, Bart J L Eggen, André Uitterlinden, Joyce van Meurs, Ronald E van Kesteren, August B Smit, Emanuele Buratti, John C van Swieten. **Brain**. **2020 Dec 1**;143(12):3827-3841. doi:10.1093/brain/awaa317.

"**Antibody against TDP-43 phosphorylated at serine 369 suggests conformational differences of TDP-43 aggregates among FTLD-TDP subtypes**". Manuela Neumann, Petra Frick, **Francesca Paron**, Jonas Kosten, Emanuele Buratti, Ian R Mackenzie. **Acta Neuropathol**. **2021 Jan**;141(1):137. doi:10.1007/s00401-020-02242-7.

Table of content

List of Tables 11
List of abbreviations 13
Abstract 21
1 INTRODUCTION 23
1.1 Trans-Active Regulator DNA Binding Protein (TDP-43) – general characteristics 24
1.1.1 The TDP-43 gene 24
1.1.2 TDP-43 protein structure 26
1.1.3 The TDP-43 cellular function 28
1.2 TDP-43 proteinopathies 33
1.2.1 Neurodegenerative disorders 33
1.2.1.1 Amyotrophic Lateral Sclerosis – ALS 33
1.2.1.2 Frontotemporal Lobar Degeneration – FTLD 34
1.2.1.3 Motoneuron Disease – MND 36
1.2.2 TDP-43, RNA-binding proteins, and metabolic disorders 36
1.2.2.1 Niemann-Pick type C Disease (NPC) 37
1.2.2.2 NPC neurodegeneration and TDP-43 40
1.3 TDP-43 pathogenic mechanisms in neurodegenerative disorders 42
1.3.1 Loss-Of-Function mechanism (LOF) 43
1.3.2 Gain-Of-Function mechanism (GOF) 44
1.4 TDP-43 mutations 45
1.5 Post-Translational Modifications (PTMs): TDP-43 phosphorylation 48
2 AIM OF THE PROJECT 51
3 MATERIAL AND METHODS 53
3.1 DNA plasmid preparation, purification, and mutagenesis 54
3.1.1 *Escherichia coli* DH5α competent cells preparation 54
3.1.2 DH5α plasmid transformation 54
3.1.3 Miniprep: small scale purification of DNA plasmid 55
3.1.4 Midiprep: middle scale purification of DNA plasmid 55
3.1.5 Site-directed mutagenesis technique (QuickChange) and DNA sequencing 56
3.2 Cell culture techniques 59
3.2.1 Gene knockdown 59
3.2.1.1 Knockdonw in HeLa cell line 59
3.2.1.2 Knockdown in SH-Sy5Y ECACC (European Collection of Authenticated Cell Cultures, England) cell line 60
3.2.2 Cellular transfection 60

3.2.2.1 Transfection in HeLa cell line and Hek293 Flp-In T-Rex (Life Technology, Carlsbad, California, USA) cell line 64
3.2.2.2 Transfection in SHSy5Y ECACC cell line 65
3.2.3 Generation of Constitutive Expression Cell Lines 65
3.2.4 Sodium arsenate treatment 66
3.2.5 Toxicity study: Lactate Dehydrogenase (LDH) release toxicity assay 67
3.2.6 Mitochondria marker: MitoTracker Red CMXRos kit (ThermoFisher Scientific, Waltham, Massachusetts, USA) 67
3.2.7 Multipotent stem cells derived from skin biopsies differentiated in neuronal cells 68
3.3 Propidium iodide cell cycle assay and flowcytometry analysis 69
3.4 Immunohistochemical and immunocytochemical analysis 70
3.4.1 Immunohistochemical analysis on brain region derived from S375G patient.. 70
3.4.2 Immunocytochemical analysis 70
3.4.2.1 Standard immunofluorescence assay 71
3.4.2.2 Immunocytochemical assay: mitochondria and Apoptosis Inducing Factor 1 (AIF1) protein tracking 72
3.4.2.3 Region of Interest (ROI) calculation 73
3.5 Protein and Peptide analysis 74
3.5.1 Nuclear-cytoplasmic fractionation 74
3.5.2 Solubility assay: soluble-insoluble fractionation 75
3.5.3 Sodium Dodecyl Sulphate (SDS) - Polyacrylamide Gel Electrophoresis (SDS-PAGE) and Western Blot assay 76
3.5.3.1 Sample preparation: brain tissue 76
3.5.3.2 Sample preparation: cell lysate 77
3.5.3.3 Sample preparation: concentration detection using Bradford colorimetric assay 77
3.5.3.4 Sample preparation: denaturation 77
3.5.3.5 Sodium Dodecyl Sulphate - Polyacrylamide Gel Electrophoresis (SDS-PAGE) 77
3.5.3.6 Western Blot assay 78
3.5.4 Molecular Dynamic Simulation on peptides 80
3.6 Nucleic acids analysis 81
3.6.1 DNA extraction and genetic analysis of the S375G patient's brain tissue 81
3.6.2 RNA extraction 81
3.6.2.1 Sample preparation: brain tissue 81
3.6.2.2 Sample preparation: cell lysate 81
3.6.2.3 miRNeasy Mini Kit (Qiagen, Hilden, Germany) 81
3.6.3 Reverse transcription reaction: complementary DNA (cDNA) preparation 82

3.6.4 Pre-mRNA splicing analysis 83
3.6.5 Gene expression analysis: real time quantitative PCR (qPCR) 85
3.6.6 RNA sequencing analysis of differentially expressed genes 89
3.6.7 RNA immunoprecipitation (RNA-IP) assay 92
3.7 Statistical analysis 97
3.8 Standard solutions 98
4 RESULTS 99
4.1 Characterization of a TDP-43 mutation in an ALS case that might affect phosphorylation sites in the C-terminal region of this protein. 100
4.1.1 Clinical case: TDP-43 S375G unpublished variant associated with ALS 100
4.1.2 Characterization of S375G variant and of the adjacent G376D, N378D, and Y374X TDP-43 disease-associated mutants. 103
4.1.2.1 Splicing capability 103
4.1.2.2 Immunolocalization analysis 106
4.1.2.3 TDP-43 mutants' cellular toxicity: LDH release assay 107
4.1.2.4 Functional effects of mimicking post-translational phosphorylation at the S375 position 108
4.1.2.5 Analysis of the effects of other sites in TDP-43 CTD that have been shown to undergo phosphorylation 110
4.1.2.6 Molecular dynamic (MD) simulation: propensity of β-sheet formation in TDP-43 371-376 CTD segment upon S375G and phosphomimic S375E substitutions 113
4.1.3 Creation of a stable cell line expressing S375G and S375E 115
4.2 Involvement of TDP-43 in neurological defects of Niemann-Pick type C: new therapeutic target for the disease 125
4.2.1 RNA sequencing analysis on human NPC disease model 125
4.2.2 RNA sequencing gene expression validation 131
4.2.3 RNA sequencing functional validation 133
4.2.3.1 RNA immunoprecipitation assay 134
4.2.3.2 Down-regulated genes functional analysis 135
4.2.3.2.1 Down-regulated genes functional analysis: LDH release assay 136
4.2.3.2.2 Down-regulated genes functional analysis: TDP-43 and pTDP-43 immunolocalization analysis upon *ITPR1* knockdown 138
5 DISCUSSION 139
5.1 Characterization of TDP-43 mutation in an ALS case affecting a potential phosphorylation site 141
5.2 Involvement of TDP-43 in neurological defects of Niemann-Pick type C 146
6 CONCLUSIONS 149
7 FUTURE PERSPECTIVES 151
Bibliography 154

List of Figures

Figure 1 - TAR-DNA binding protein locus and position on chr1.....24

Figure 2 - TARDBP coding exons structure.....24

Figure 3 - Amino acid sequence alignment of the eukaryotic TDP-43 proteins in different organisms.....25

Figure 4 - TDP-43 protein structure.....26

Figure 5 - TDP-43 nuclear and cytoplasmic physiological roles.....28

Figure 6 - Examples of TDP-43 target genes.....29

Figure 7 - TDP-43 and hnRNPs complex on CFTR exon 9.....30

Figure 8 -TDP-43 autoregulation mechanism.....31

Figure 9 – MVBs cellular pathway.....37

Figure 10 – NPC1 and NPC2 lysosomal interaction and cholesterol binding.....39

Figure 11 – TDP-43 cytoplasmic mislocalization in NPC human cellular model.....40

Figure 12 – TDP-43 mislocalization and hyper-phosphorylation in NPC human cellular model.....41

Figure 13 - TDP-43 misregulated genes by qPCR in human NPC model.....41

Figure 14 - TDP-43 LOF model leading cell death.....43

Figure 15 - TDP-43 GOF model leading cell death.....44

Figure 16 -TDP-43 mutations.....46

Figure 17 - Possible alterations promoted by TDP-43 mutation.....47

Figure 18 - TDP-43 most prevalent PTMs.....49

Figure 19 - TDP-43 aberrant phosphorylation.....50

Figure 20 – pFLAG-CMV4 TDP-43 siRNA resistent map.....61

Figure 21 – pFLAG-CMV4 TDP-43 siRNA resistent map.....62

Figure 22 – p5cDNA FRT/TO flag TDP-43 map.....63

Figure 23 – p5cDNA FRT/TO flag TDP-43 map. 64

Figure 24 – NEB library proposed by Novogene. 90

Figure 25 – Illumina sequencing scheme. 91

Figure 26 – phosphoTDP-43 density and distribution of immunoreactive neurons and glia of the motor cortex. 100

Figure 27 – phosphoTDP-43 density and distribution of different brain areas. 101

Figure 28 – pTDP4-43 amount in glial and neuronal cells versus total TDP-43 expressed. 102

Figure 29 – TDP-43 S375G variant. 103

Figure 30 – Addback splicing assay. 104

Figure 31 – TDP-43 Y374X nonsense mutation addback analysis. 105

Figure 32 – pFlagSiRTDP-43 intracellular localization. 107

Figure 33 – Y374X TDP-43 mutant immunolocalization. 107

Figure 34 - LDH release. 108

Figure 35 - S375E phosphomimic analysis. 109

Figure 36 - S375G and S375E immunolocalization under sodium arsenate stress conditions. 110

Figure 37 - TDP-43 phosphomimic analyzed residues. 112

Figure 38 – TDP-43 CTD phosphomimic analysis. 113

Figure 39 – Molecular dynamic simulation analysis. 114

Figure 40 - Western blot analysis of all the stable clones prepared. 116

Figure 41 - Western blot analysis testing stable clones' expression at three different time points: 24, 48 and 72 hours. 117

Figure 42 - POLDIP3 gene splicing analysis. 118

Figure 43 - S375G and S375E stable alleles autoregulation on the endogenous TDP-43. 119

Figure 44 - Western Blot analysis of the solubility assay performed on the stable clones. 119

Figure 45 - Western Blot solubility assay of the stable clones upon arsenate treatment.. 120

Figure 46 – Stable clones immunolocalization analysis. 121

Figure 47 - Immunolocalization analysis upon sodium arsenate treatment..... 121

Figure 48 - Western Blot against CdK6. 122

Figure 49 - Cell cycle analysis performed with flow cytometry and propidium iodide staining. 123

Figure 50 – AIF expression and immunolocalization analysis on stable cell line expressing WT, S375G, and S375E TDP-43. 124

Figure 51 – Multipotent stem cells isolated from skin biopsies reprogrammed in neurons. 126

Figure 52 – RNA quality check. 127

Figure 53 – Gene expression analysis of differentially expressed genes. 127

Figure 54 – Volcano plot representing the 799 differentially expressed genes.. 128

Figure 55 – GO enrichment analysis..... 129

Figure 56 – KEGG enrichment analysis. 129

Figure 57 – Volcano plot representing the RNA sequencing data on SHSy5Y silenced for TDP-43 130

Figure 58 – Volcano plot of merged data between NPC RNA sequencing, and SH-SY-5Y cells silenced for TDP-43. 131

Figure 59 – Quantitative real-time PCR preliminary result on RNA sequencing validation. 133

Figure 60 – RNA immunoprecipitation assay on down regulated genes. 134

Figure 61 – RNA immunoprecipitation assay on up regulated genes. 135

Figure 62 – LDH release assay.. 137

Figure 63 – TDP-43 and pS409/S410 TDP-43 immunostaining upon ITPR1 silencing. ... 138

List of Tables

Table 1 – QuickChange negative control reagents. 56

Table 2 – QuickChange sample reagents. 57

Table 3 – Oligonucleotide sequences used for site directed mutagenesis. 58

Table 4 – Oligonucleotide sequence upstream (CMV 30 forward) and downstream (CM 24 reverse) the insert of interest, used for sequencing. 58

Table 5 – siRNA sequences. 59

Table 6 – Effectene transfection reagents reported according to the plate volume. 65

Table 7 – Immunocytochemical analysis: pramary and secondary antibodies. 70

Table 8 - NE-PER Nuclear and Cytoplasmic Extraction reagents volumes according to packed cell volume 74

Table 9 – Primary antibodies, dilution and blocking media, and their final concentrations are reported. 79

Table 10 - Secondary antibodies, dilution and blocking media, and their final concentrations are reported. 80

Table 11 – cDNA preparation: mix 1 containing random primers and RNA. 83

Table 12 - cDNA preparation: mix 2 containing reverse transcription reaction reagents. 83

Table 13 – PCR reaction mix. 84

Table 14 – Pre-mRNA splicing primer sequences. 84

Tabella 15 – Pre-mRNA splicing protocols. 85

Table 16 – Quantitative Real Time PCR primer sequences. 87

Table 17 – Quantitative Real Time PCR protocols and related master mix reagents. 88

Table 18 – Quantitative Real Time PCR reagents mix. 88

Table 19 – RNA-IP lysis reagents volume, according to cell range. 93

Table 20 – IP-buffer preparation mix. 94

Table 21 - TDP-43 potential phosphorylation sites and disease-associated mutations already described in literature. 111

Table 22 – Controls (CTR) and patients (PT) details in terms of allele mutations and sample concentration..... 126

Table 23 – Selected genes for the RNA-sequencing validations. 132

List of abbreviations

18s	Ribosomal RNA subunit 18
28s	Ribosomal RNA subunit 28
A315E	Alanine in position 315 changing in a Glutamic acid
A382T	Alanine in position 382 changing in a Threonine
ACRV1/SP10	Acrosomal Vesicle Protein 1/Sperm protein 10
AD	Alzheimer disease
AIF1	Apoptosis-inducing factor 1
AKT	Protein kinase B
ALS	Amyotrophic lateral sclerosis
ANG	Angiogenin
B27	Human leukocyte antigen (HLA) B27
bFGF	Basic fibroblast growth factor
BSA	Bovine Serum Albumin
bvFTD	Behavioral variant FTD
C9orf72	C9orf72-SMCR8 Complex Subunit
cAMP	Cyclic adenosine monophosphate
CDH18	Cadherin 18
CDK6	Cyclin dependent kinase 6
cDNA	Complementary DNA
CDON	Cell Adhesion Associated, Oncogene Regulated
CFTR	Cystic Fibrosis Transmembrane Regulator
CNTFR	Ciliary Neurotrophic Factor Receptor
CTD	C-terminal domain

CTNND1	Catenin Delta 1
CTR	Control
Cα–Cα	Carbonium alpha distance intra-β-sheet
DCLK1	Doublecortin Like Kinase 1
DDX17	DEAD-Box Helicase 17
DEPTOR	DEP Domain Containing MTOR Interacting Protein
D-MEM	Dulbecco's Modified Eagle's Medium
D-MEM/HG	D-MEM with High glucose
D-MEM:F12	Dulbecco's Modified Eagle's Medium/Nutrient Mixture F-12 Ham
dNTP	Deoxynucleotide
DTT	Dithiothreitol
E. coli	*Escherichia coli*
ECL	Enhanced chemiluminescence
EGF	Epidermal growth factor
EMSA	Electromobility shift assay
EPDR1	Ependymin Related 1
F4L	TDP-43 RRM1 domain mutant in which four Phenylalanine were mutated in Leucine
FACS	Fluorescence activated cell sorting, flow cytometry
fALS	Familiar ALS
FBS	Fetal bovine serum
FC	Fold change
FIG4	Phosphatidylinositol 3,5-Bisphosphate 5-Phosphatase
Flp	Flippase recombinase

FPKM	Million mapped reads
FRT	Flippase recognition target
FTLD/FTD	Frontotemporal lobar degeneration
FTLD-FUS	FTLD with FUS positive inclusions
FTLD-TAU	FTLD with TAU positive inclusions
FTLD-TDP	FTLD with TDP positive inclusions
FTLD-U	FTLD negative for TDP/TAU/FUS
FUS	Fuses-in-sarcoma
G295S	Glycine in position 295 changing in a Serine
G376D	Glycine in position 376 changing in an Aspartic acid
GAPDH	Glyceraldehyde-3-phosphate Dehydrogenase
Gln/Asn	Glutammine/Asparagine
GO	Gene ontology
GOF	Gain-of-function
h	Hour
HB9	Motor neuron and pancreas homeobox 1
HDAC6	Histone deacetylase 6
HIV-1	Human immunodeficiency virus 1
*h*NFL	Human low molecular weight neurofilament
hnRNP	Heterogeneous nuclear ribonucleoprotein
Hoechst	Bisbenzimide H33342 trihydrochloride
HPRT1	Hypoxanthine Posphoribosyltransferase 1
hSKIN-MASCs	Human multipotent adult stem cells isolated from the skin
IBMX	3-isobutyl-1-methylxanthine

ITPR1	Inositol 1,4,5-Trisphosphate Receptor Type 1
KEGG	Kyoto encyclopedia of genes and genomes
KIF1B	Kinesin Family Member 1B
KIF2	Kinesin Family Member 2
LB	Luria-Bertani medium
LCP1	Lymphocyte Cytosolic Protein 1
LDH	Lactate dehydrogenase
LDL	Low-density lipoproteins
LDL-receptor	Low-density lipoproteins receptor
LGR4	Leucine Rich Repeat Containing G Protein-Coupled Receptor 4
LMN	Lower motoneuron
LOF	Loss-of-function
LSD	Lysosomal storage disorder
MADD	MAP Kinase Activating Death Domain
MASP2	Mammalian-binding lectin Serine-Protease 2
MCDB-201	With trace elements, L-glutamine and 30 mM HEPES
MEF2D	Myocyte Enhancer Factor 2D
miRNA	micro-RNA
M-MLV RT	Moloney murine leukemia virus reverse transcriptase
MMP	Mappable prefix
MN	Superoxide Dismutase 2
MND	Motoneuron disease
mRNA	messenger RNA

MVB	Multi-vesicular bodies
N352S	Asparagine in position 352 changing in a Serine
N_{371}-NSYGG$_{376}$	S375E segment
N_{371}-NSYGG$_{376}$	S375G segment
N_{371}-NSYSG$_{376}$	Wild type segment
N378D	Asparagine in position 378 changing in an Aspartic acid
N390S	Asparagine in position 390 changing in a Serine
NE-PER	Nuclear and cytoplasmic extraction reagent
NES	Nuclear Exporting Signal
NeuN	Hexaribonucleotide Binding Protein-3
NLS	Nuclear Localization Signal
NMR	Nuclear magnetic resonance
NP40	Nonidet P40
NPC	Niemann-Pick type C disease
NPC1	NPC Intracellular Cholesterol Transporter 1
NPC2/HE1	NPC Intracellular Cholesterol Transporter 2/ Human Epididymis-Specific Protein 1
NTD	N-terminal domain
Opti-MEM	Opti-MEM® Reduced-Serum Medium
pAdj	p-value adjusted
PBS	Phosphate Buffer Saline
PBST	PBS with Tween
PCR	Polymerase chain reaction
PD	Parkinson disease

PDGF-BB	Platelet-derived growth factor
PFA	Para-formaldehyde
PI3K	Phosphoinositide 3-kinases
PNFA	Non-fluent aphasia
POLDIP3	DNA polymerase Delta interacting protein 3
PolyPhen-2	Polymorphism Phenotyping v2
Pre-mRNA	pre-messenger RNA
PT	Patient
pTDP-43	Phospho-TDP-43 (in S409/S410 residues)
PTMs	Post-translational modifications
qPCR	Real time quantitative PCR
R361S	Arginine in position 361 changing in a Serine
RBP	RNA binding protein
RIPA buffer	Radioimmunoprecipitation assay buffer
RIS	RNA integrity score
RNA-IP/RIP	RNA immunoprecipitation
RNase H	M-MuLV reverse transcriptase
ROI	Region of interest
Rq	Relative quantification
RRM	RNA-recognition motive
S242E	Serine in position 242 changing in a Glutamic acid
S305E	Serine in position 305 changing in a Glutamic acid
S375E	Serine in position 375 changing in a Glutamic acid
S375G	Serine in position 375 changing in a Glycine

S387-95E	Serine in position 387-389-393-395 changing in a Glutamic acid
S387T	Serine in position 387 changing in a Threonine
S396L	Serine in position 396 changing in a Leucine
S397E	Serine in position 397 changing in a Glutamic acid
S403/404E	Serine in position 403 and 404 changing in a Glutamic acid
S404/410E	Serine in position 409 and 410 changing in a Glutamic acid
S404E	Serine in position 404 changing in a Glutamic acid
sALS	Sporadic ALS
SD	Semantic dementia
SDS-PAGE	Sodium dodecyl sulphate – polyacrylamide gel electrophoresis
Ser	Serine
SHANK1	SH3 And Multiple Ankyrin Repeat Domains 1
SIFT	Sorting intolerant form tolerant
siLUC	siRNA against *Fire-fly luciferase*
siRNA	Short interfering RNA
SNAP	Predict effect of non-synonymous polymorphisms on function
SOD1	Superoxide Dismutase 1
STCS	Decision Tree Classifier Software
TAU	Microtubule Associated Protein Tau
TB	Terrific Broth
TDP-43/TAR DNA binding protein	Trans-Active Regulator DNA Binding Protein

TFAP2A	Transcription Factor AP-2 Alpha
TLE1	Transducing-Like Enhancer Protein 1
TNG	Trans-Golgi Network
TNIK	TRAF2 And NCK-Interacting Protein Kinase
TSS	Transformation & Storage Solution
UMN	Upper motoneuron
UPS	Ubiquitin-proteasome system
UTR	Untranslated region
Wnt	Catenin Beta 1
WT	Wild type
Y374X	Tyrosine in position 374 changing in stop codon

Abstract

In 2006, human Trans-Active Regulator DNA Binding Protein (TDP-43) was identified as the major ubiquitinated component of inclusion bodies in Amyotrophic Lateral Sclerosis (ALS) and Frontotemporal Lobar Degeneration (FTLD), two important neurodegenerative diseases in the human population. In ALS/FTLD, TDP-43 that is normally present in the nucleus, is found aggregated in the cytoplasm where it is also abnormally phosphorylated, poly-ubiquitinated, and cleaved to release toxic C-terminal fragments. Recently, evidences of TDP-43 involvement were also reported by our laboratory in Niemann-Pick type C (NPC) disease, a Lysosomal Storage Disorder (LDS) with visceral and neurological symptoms. In particular, in this disease, the protein TDP-43 does not aggregate in the cytoplasm like in the motor neurons of ALS patients. However, it is found mislocalized and abnormally phosphorylated in the cytoplasm of three different models: mouse *NPC1*$^{-/-}$ brain; human NPC cellular model (multipotent stem cells derived from skin biopsies, reprogrammed to neuronal cells); and in patients' brain Purkinje cells.

Keeping these two observations in mind, the general aim of my work for this thesis has been to specifically study one of the major TDP-43 post-translational modifications (PTMs), phosphorylation, in two different diseases models: disease-associated TDP-43 mutations in ALS patients and aberrant phosphorylation of TDP-43 in NPC disease.

Regarding ALS, together with a group in Indiana/Kansas University I described a novel mutation in TDP-43 affecting a Serine residue changing to a Glycine in position 375 (S375G). The reason why this mutation was interesting is because it was discovered in an early-onset ALS case. The results of my study showed that the TDP-43 carrying this S375G variant localized more in the nucleus with respect to the wild-type (WT) form. This nuclear localization leads to a stronger cytotoxicity probably due to the lack of the phosphorylation site, that was suggested to strongly destabilize an amyloid-like structure in its C-terminal tail that promoted TDP-43 multimerization. In order to study in depth, the physiological/pathological behavior of this Serine residue, I created a cell line expressing constitutively the WT, S375G, and S375E (phosphomimic) TDP-43 forms. No significant changes were reported in splicing activity, autoregulation, or aggregation, but a cell-cycle analysis of the stable clones showed that the number of cells in the G2 phase decreased in the two phospho-mutants compared to WT. The exact reason for this alteration is still not known. However, preliminary experiments on the mitochondria apoptotic signal that I

performed showed that Apoptosis-Inducing Factor 1 (AIF1) seemed to be released from the mitochondria.

Regarding Niemann Pick C, in order to better understand the molecular mechanisms that lead to TDP-43 phosphorylation in NPC, I performed an RNA sequencing analysis using a human NPC cellular model and compared the detected list of gene expression changes with a list of changes that we previously described for neuronal SHSy5Y cells depleted of TDP-43. As described in depth in the thesis, approximately 800 genes were found differentially regulated between NPC patients and healthy controls, involving neuronal, inflammatory, and lipid metabolism pathway. Among these 800 genes, 64 were found to be commonly misregulated in the RNA sequencing performed on SHSy5Y cells upon TDP-43 silencing. Based on these preliminary results, I identified two particular targets of TDP-43 that were previously unknown: Inositol 1,4,5-Trisphosphate Receptor Type 1 (ITPR1), and the Ependymin Related 1 (EPDR1). Interestingly, the depletion (down regulation) of *ITPR1* gene induced changes in TDP-43 protein cellular localization, thus suggesting a direct link between alterations in this gene and aberrant TDP-43 regulation.

Taken together, the data contained in my thesis strongly support growing evidence that alterations of TDP-43 post-translational modifications, either due to disease-associated mutations or genes that control its cellular localization, can play a potentially important role in disease pathogenesis.

1 INTRODUCTION

1.1 Trans-Active Regulator DNA Binding Protein (TDP-43) – general characteristics

1.1.1 The TDP-43 gene

Human TDP-43 was isolated and described for the first time in 1995 as a novel transcriptional inactivator involved in the TAR (Tat Activation Response) DNA motive of the Human Immunodeficiency Virus (HIV-1) binding (Ou et al., 1995).

The human gene is located on chromosome 1 in *MASP2* (Mammalian-binding lectin Serine-Protease 2) locus, a highly conserved gene-rich region [chr1:11,013,728-11,022,651; 8,924bp] (**Fig.1**).

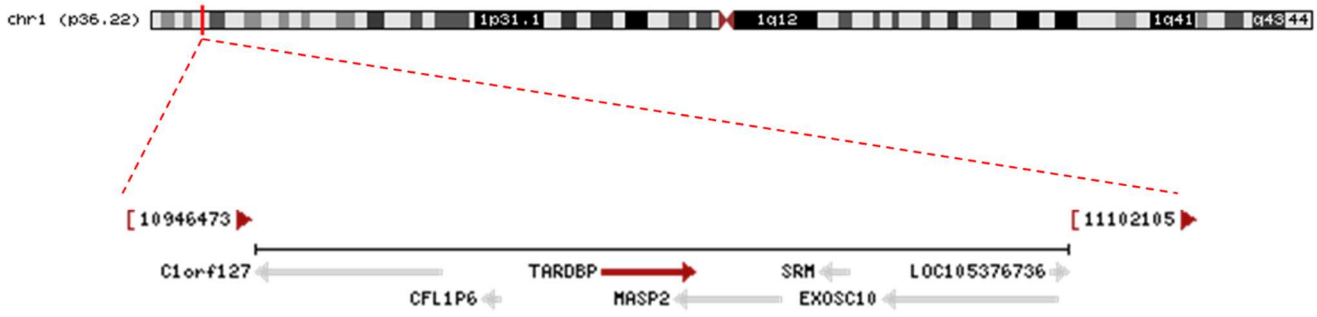

Figure 1 - TAR-DNA binding protein locus and position on chr1 - PubMed and UCSC Genome Browser (hg38)

In **Figure 2** is shown the *TAR-DNA binding protein* (*TDP-43*) gene structure composed of 6 exons: the coding region starts from exon 2 to exon 6, whilst the first one is a non-coding exon (Banks et al., 2008; Wang et al., 2004).

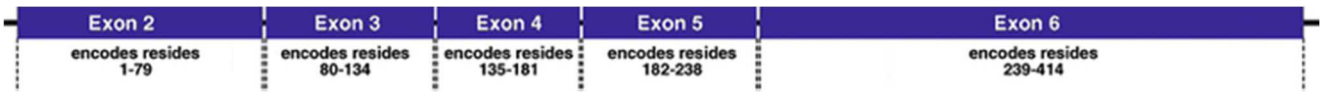

Figure 2 - TARDBP coding exons structure (Banks et al., 2008).

During evolution, *TDP-43* has been highly conserved among many species, like *Drosophila melanogaster*, *Xenopus laevis* and *Caenorhabditis elegans* (**Fig.3**) (Ayala et al., 2005; Stover et al., 2004; Wang et al., 2004). The high sequence conservation in such distant organism indicates that this protein has played a fundamental role during evolution (Buratti and Baralle, 2008).

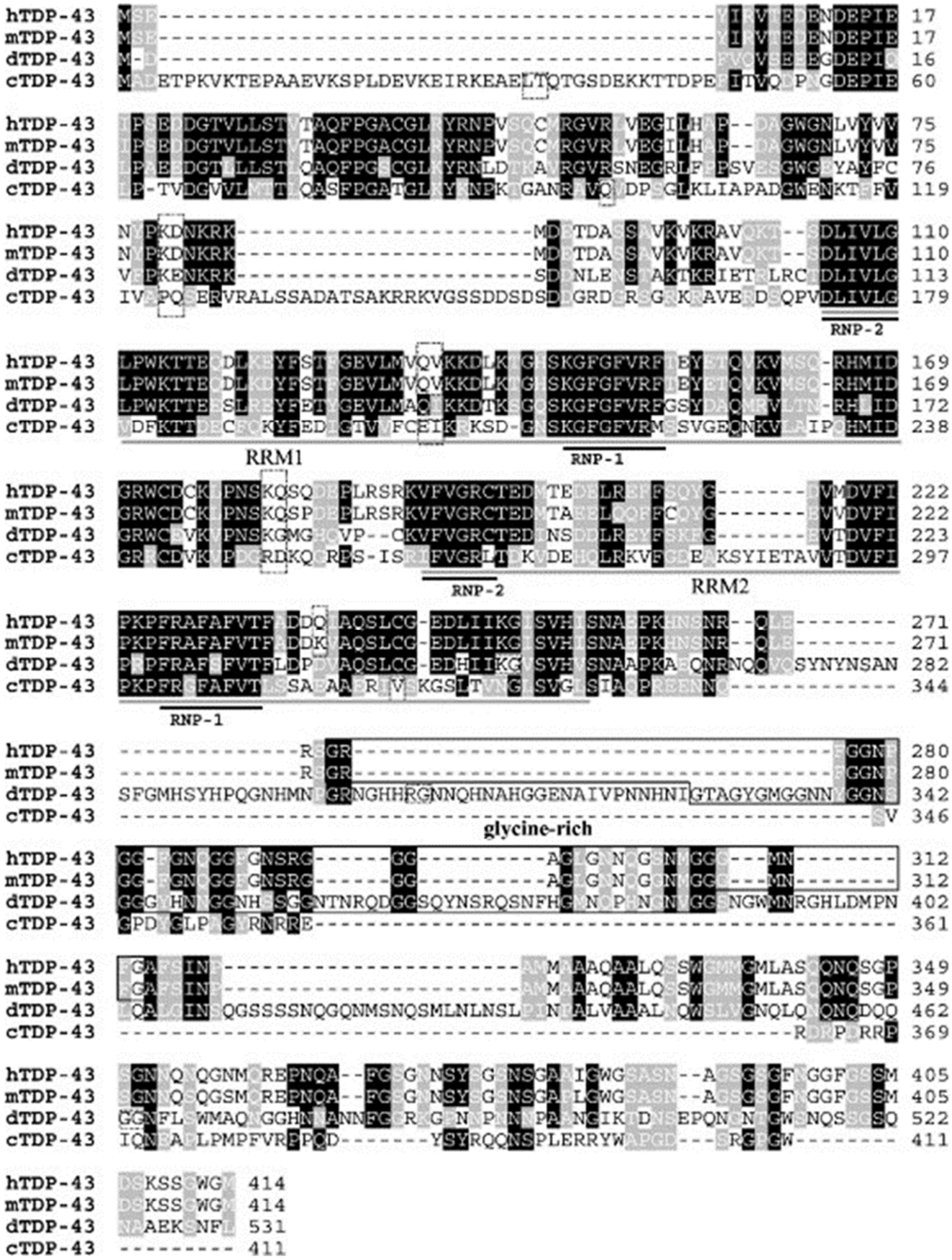

Figure 3 - Aminoacid sequence alignment of the eukaryotic TDP-43 proteins in different organisms: human (hTDP-43), mouse (mTDP-43), D. melanogaster (dTDP-43), and C. elegans (cTDP-43) (Wang et al., 2004).

1.1.2 TDP-43 protein structure

From a structural and functional point of view, TDP-43 belongs to the heterogeneous nuclear ribonucleoprotein (hnRNP) family, known to associate with heterogeneous RNA in a sequence-specific manner, thanks to the presence of specific domains able to mediate protein-RNA interactions and protein-protein interactions. The hnRNP proteins play an important role in multiple steps of gene expression regulation including transcription, splicing, mRNA stability, DNA replication/repair, protein translation, and export or retention of nascent RNA. They are able to interfere with different processes depending on their subcellular localization, by binding to RNA, other proteins, or cellular components (Buratti and Baralle, 2012; Y. M. Ayala et al., 2008; Krecic and Swanson, 1999).

The TDP-43 primary structure can be split in three basic domain composition, as shown in **Figure 4** (Buratti and Baralle, 2012; Krecic and Swanson, 1999).

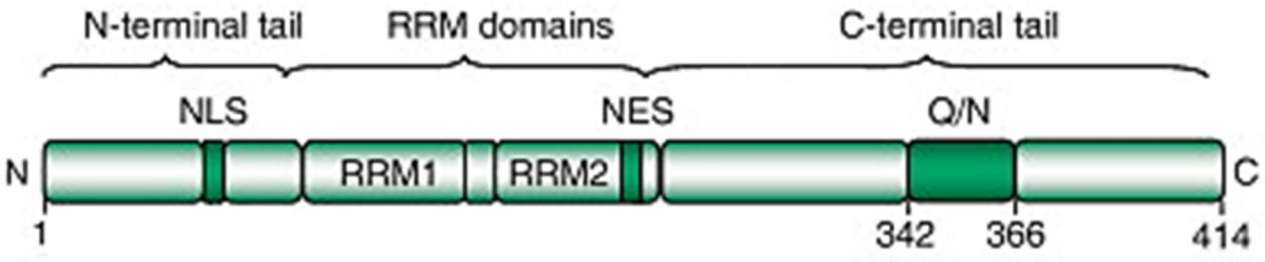

Figure 4 - TDP-43 protein structure (Buratti and Baralle, 2012).

- The N-terminal domain (NTD): very little is known about this region. It is very well conserved during evolution especially the residues encoding for the Nuclear Localization Signal regions, (NLS) composed by NLS1 (K82RK84) and NLS2 (K95VKR98), mediating the protein nuclear localization. Mutations in those sites reduce the presence of TDP-43 in the nucleus (Buratti and Baralle, 2001, 2008; Winton et al., 2008; Y. M. Ayala et al., 2008). Recently, the NMR structure of this region has been solved and it has been shown to be important in mediating protein oligomerization (Mompeán et al., 2016).
- The RNA-Recognition Motives (RRM): RRMs are two highly-conserved domains involved in the binding to specific RNA or DNA sequences and act by mediating the nucleic acid direct recognition (Y. M. Ayala et al., 2008; Buratti and Baralle, 2001). In particular, the RRM-1 region is necessary and sufficient to mediate binding to UG or

TG repeated motifs (Ayala et al., 2005; Buratti and Baralle, 2001). Using Electromobility Shift Assay (EMSA), it has been shown that a mutant lacking of this region was sufficient to abolish completely the ability of TDP-43 to bind RNA molecules (Buratti and Baralle, 2001). Also, RRM-2 region was studied together with RRM-1 domain. Using a mutant lacking of RRM-2, it has been discovered that the deletion of RRM-2 domain did not compromise completely RNA binding capability of the protein, concluding that the two domains have different binding characteristics and RRM-2 can help RRM-1 in RNA recognition (Buratti and Baralle, 2001). Recently, RRM-2 was described to play a role in chromatin organization by the co-crystallization with single-stranded DNA forming thermal-stable dimeric complex (Y. M. Ayala et al., 2008). Moreover, RRM2 is predicted to contain a nuclear export signal (NES) (**Fig. 4**) (Strong et al., 2007; Buratti and Baralle, 2001) that acts together with the NLS signal in the N-terminus to determine the nuclear-cytoplasmic balance of TDP-43.

- The C-terminal Domain (CTD): this sequence mediates protein-protein interaction especially with other hnRNPs, promoting the recruitment of TDP-43 to the macromolecular complexes that are necessary to carry out its functions. For example, by immunoprecipitation and proteomic studies it has been discovered that TDP-43 can interact with another abundant hnRNP protein, hnRNP A2/B1, through residues 342 to 366 in the C-terminal tail (**Fig.4**) (Budini et al., 2012; D'Ambrogio et al., 2009). In addition to protein-protein interactions, the C-terminal domain is essential for affecting protein solubility and sub-cellular localization. The fact that it is poor in charged residues means that pH switches can lead to aggregative phase changes and microdroplet formation to bring RNA molecules in the right sub-cellular localization. As a consequence, deletions in the CTD lead to large nuclear and cytoplasmic aggregates formation (Buratti and Baralle, 2012; Y. M. Ayala et al., 2008). In fact, even in normal conditions, this region tends to induce TDP-43 aggregation due to the presence of glycine-rich motif and a Gln/Asn-rich region identified as a potential prion-like domain (Udan and Baloh, 2011). Most importantly, the C-terminal tail is strongly linked to the pathogenesis of neurodegenerative disorders because this is the region where most of the disease-associated mutations associated with Amyotrophic Lateral Sclerosis (ALS), and Frontotemporal Dementia (FTLD) are localized, except for a few mutations that are located in the RRM domain regions (Budini et al., 2012).

1.1.3 The TDP-43 cellular function

Due to its structure, TDP-43 is involved in many cellular functions, both in the nucleus and in the cytoplasm (**Fig.5**).

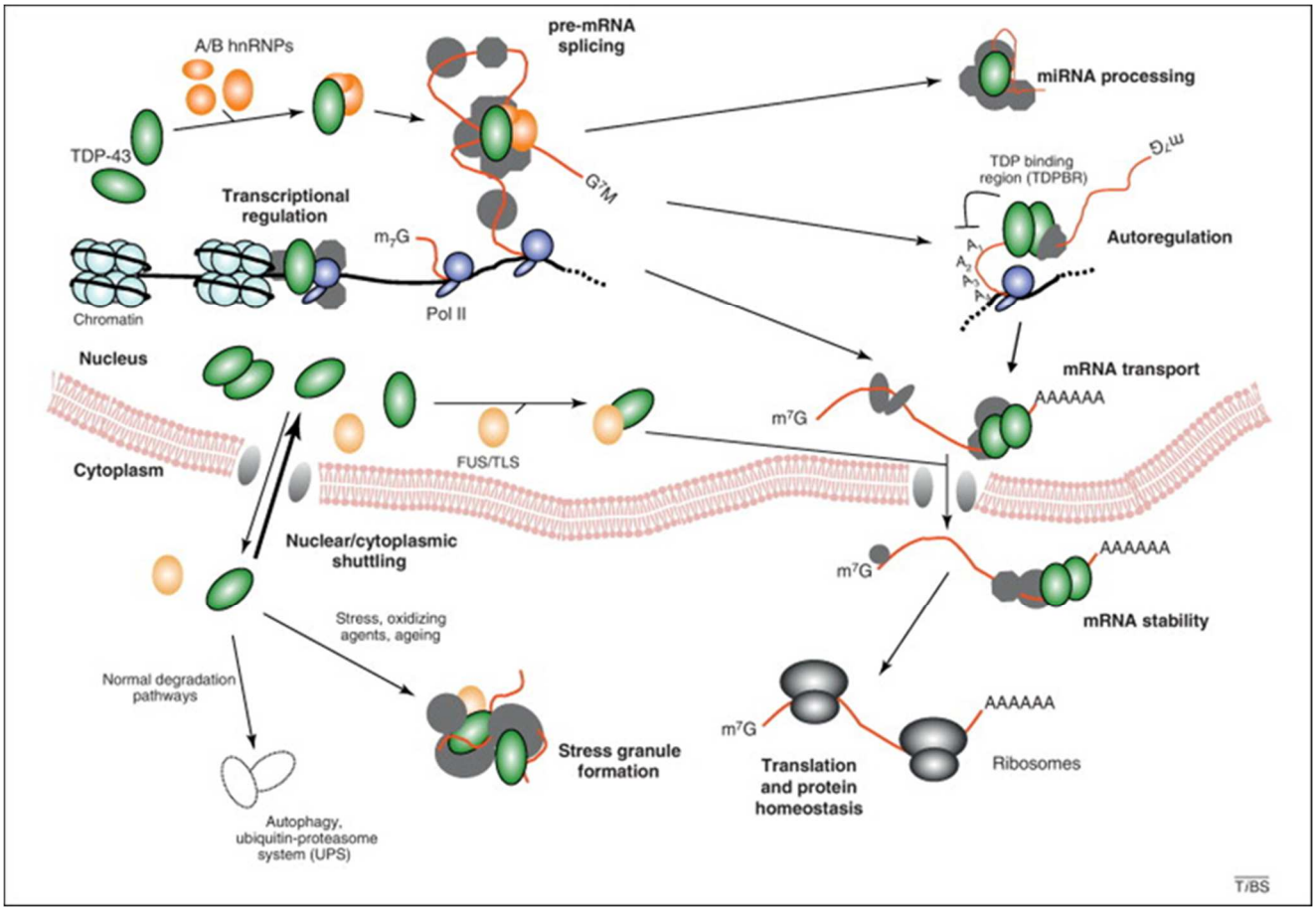

Figure 5 - TDP-43 nuclear and cytoplasmic physiological roles (Buratti and Baralle, 2012).

First of all, as a typical member of the hnRNP protein family, TDP-43 has been shown to be involved in multiple levels of RNA processing, like splicing, transcription, transport and translation (Lagier-Tourenne et al., 2010). In particular, TDP-43 is mostly known for its involvement in splicing regulation. In **Figure 6**, several TDP-43 target genes are shown characterized by the presence of an UG-rich region bound specifically by the RRMs (Buratti and Baralle, 2001).

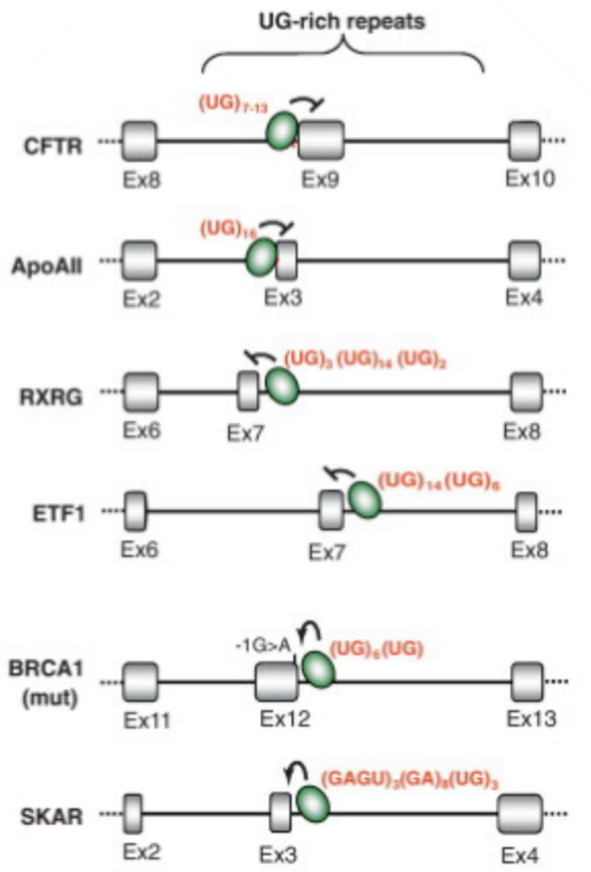

Figure 6 - Examples of TDP-43 target genes (Buratti and Baralle, 2012).

An example of TDP-43 mechanism of action in regulating the splicing process is reported in **Figure 7**, where TDP-43 is shown binding to one of its best characterized targets, the *Cystic Fibrosis Transmembrane Regulator* (*CFTR*) gene. In this case, TDP-43 recognizes specifically the splicing regulatory (UG)m elements located near the 3'splice-site of *CFTR* exon 9 through the RRMs (Buratti and Baralle, 2001, 2008). The RRMs alone are not enough to promote splicing regulation; indeed TDP-43 inhibits the recognition of basic splicing factors through the Glycine-rich C-terminal domain that recalls other hnRNP proteins and together create an inhibitory complex that abolish the assembling of the spliceosome in the early stage (Lagier-Tourenne et al., 2010).

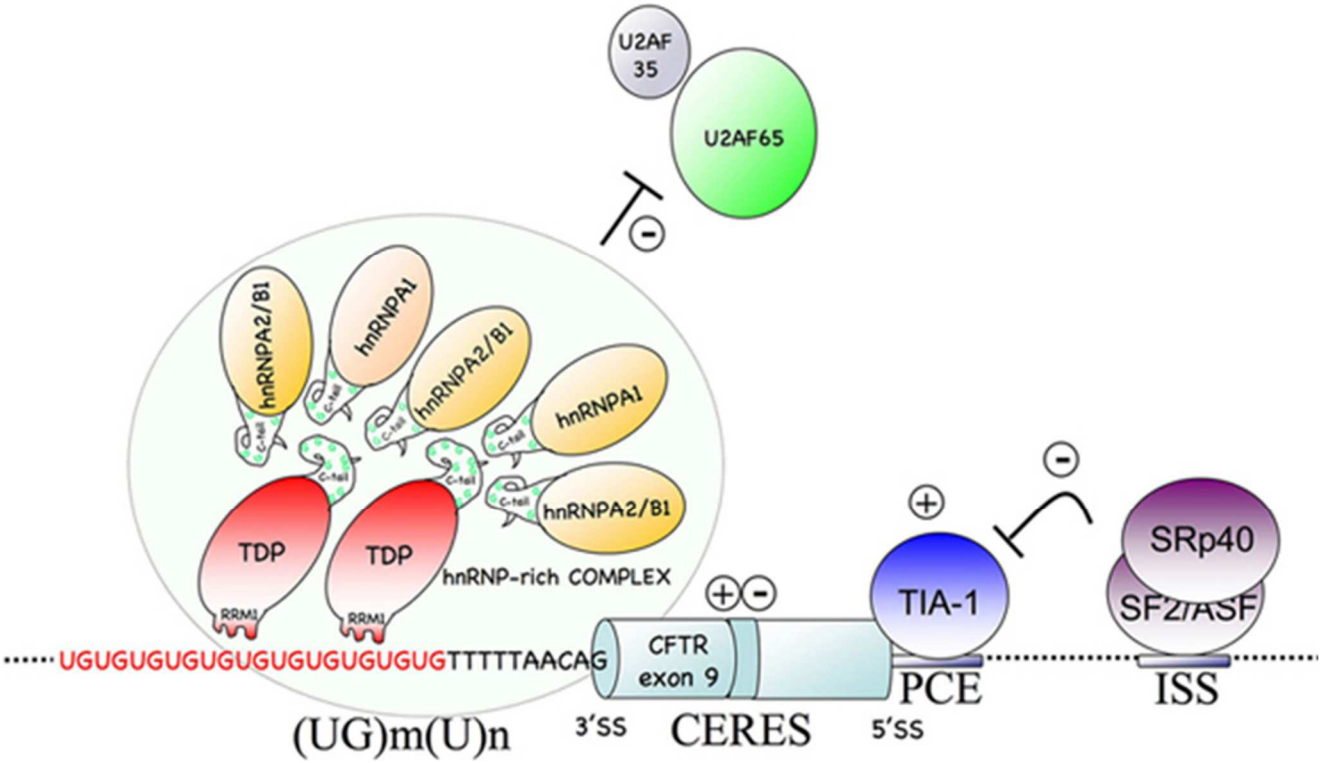

Figure 7 - TDP-43 and hnRNPs complex on CFTR exon 9 (Buratti and Baralle, 2008).

In physiological conditions, TDP-43 is able to modulate its own protein levels through a negative feedback loop by binding its own mRNA in the 3'UTR region, leading to mRNA instability and degradation (Buratti and Baralle, 2012; Budini and Buratti, 2011). **Figure 8** schematically shows the TDP-43 autoregulation mechanism: low concentrations of nuclear TDP-43 allow the use of the most efficient poly-A1 site instead the others two, pA2 and pA4. On the other hand, abundant TDP-43 protein levels result in the binding with sub-optimal sites that lead to the rapid degradation of the mRNA. Using this negative feedback mechanism, the TDP-43 concentration within cells can remain constant and alterations in this process could be a major driver of aberrant TDP-43 production and aggregation in neurons (Budini and Buratti, 2011).

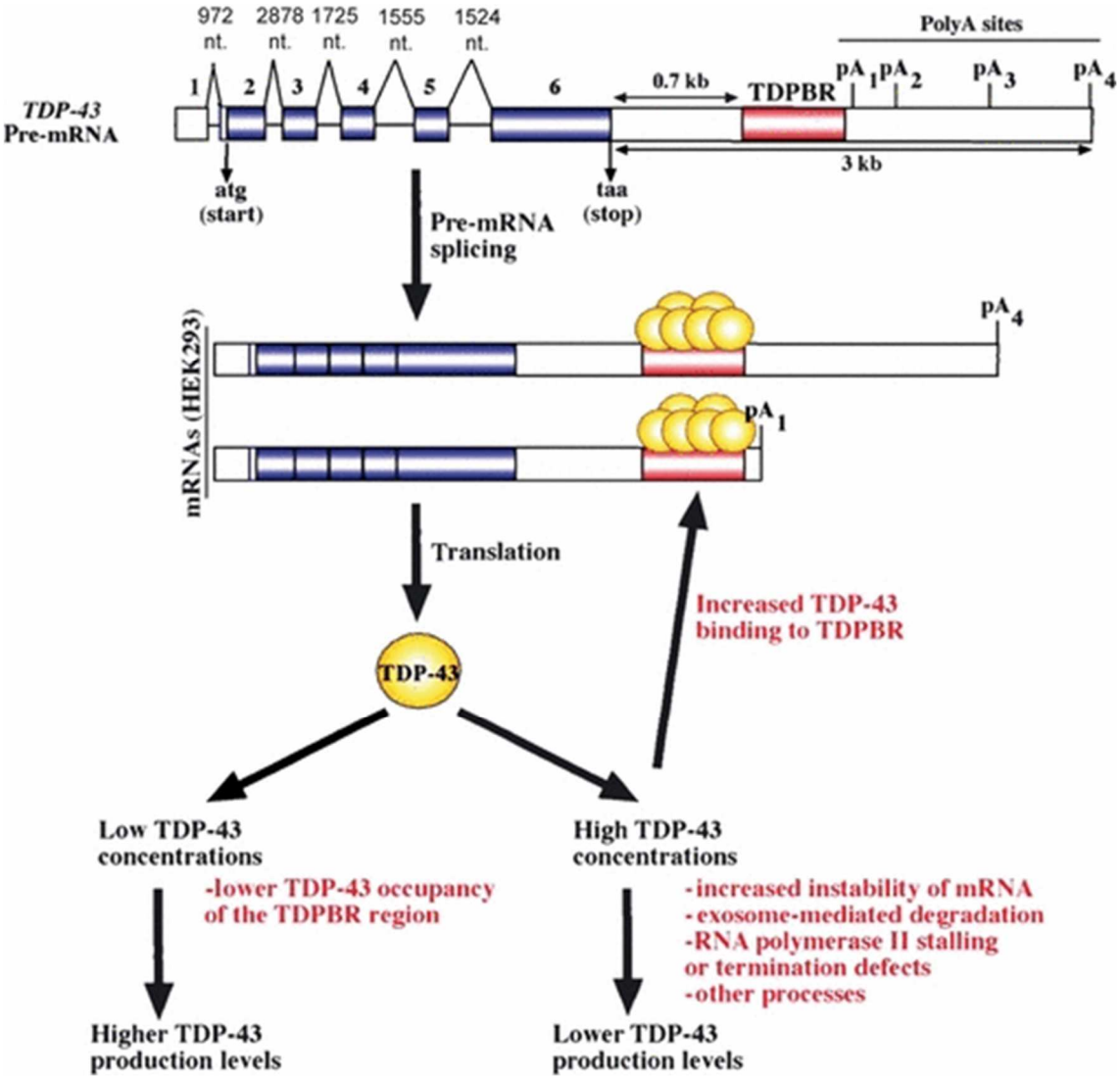

Figure 8 -TDP-43 autoregulation mechanism (Budini and Buratti, 2011).

In addition to pre-mRNA splicing, TDP-43 plays also an important role in micro-RNA (miRNA) biogenesis (Lee et al., 2012). Although the mechanism through which this occurs is still not clearly known, TDP-43 is thought to be involved in the cytoplasmic cleavage step of miRNA by interacting with Argonaute-2 and DDX17, two proteins implied in this process (Lagier-Tourenne et al., 2010).

TDP-43 is implicated in mRNA turnover by regulating mRNA levels of different genes (Lee et al., 2012). An example is TDP-43 inhibition of Cyclin Dependent Kinase 6 (CdK6) expression through its recruitment to the GU-rich transcript. The depletion of TDP-43 in human cells leads to a significantly increase of CdK6 protein and transcript level resulting with a major phosphorylation of CdK6 targets (Youhna M Ayala et al., 2008). In addition, TDP-43 influences also the expression of the histone deacetylase 6 (HDAC6), a protein involved in other proteins aggregation and degradation (Fiesel et al., 2010). TDP-43

knockdown/loss leads to HDAC6 downregulation and accumulation of its substrates (Fiesel et al., 2010). Another example is the human low molecular weight neurofilament (*h*NFL), where TDP-43 has been shown to stabilize *h*NFL with a direct interaction of the 3'UTR of this mRNA (Strong et al., 2007). TDP-43 binding to *h*NFL is important for this mRNA cytoplasmic translocation and its translation in the correct subcellular compartment (Strong et al., 2007). TDP-43 loss or altered function could affect also the regulation of downstream genes, that taken together can potentially lead to a disease status (Lee et al., 2011).

According to its functions, TDP-43 in physiological conditions is present also in the cytoplasm working on mRNA destination in the cell's compartment, subcellular localization, translation, and degradation acting as a nucleus-cytoplasmic shuttle (Lagier-Tourenne et al., 2010). In particular, TDP-43 was found in RNA transporting granules and, by altering mRNA transport and localization, it is involved in neuroplasticity modulation (King et al., 2012; Lagier-Tourenne et al., 2010).

Finally, in a rather limited set of examples, TDP-43 is known to interact with DNA, in particular with single stranded DNA, acting as transcriptional regulator. Indeed, this protein was first discovered as a regulator of studied as a potential regulator of the HIV-1 TAR DNA sequence motif (Lee et al., 2012; Ou et al., 1995). More recently, it has been shown to be involved in the regulation of the spermatid-specific SP-10 gene (*ACRV1*), preventing the enhancer-promoter interaction (Lee et al., 2012). In this particular event, TDP-43 interacts with SP-10 insulator, abolishing SP-10 translation. TDP-43 knockdown or mutations suppressed this capability. This role is tissue specific, as far as TDP-43 is present also in testis, but this function is not detectable in male germline (Abhyankar et al., 2007).

1.2 TDP-43 proteinopathies

As previously described, TDP-43 plays an important role in cell metabolism, and in particular in the regulation of RNA homeostasis. TDP-43 disfunctions can disrupt RNA metabolism with devastating consequences for the cells, especially for neurons in which RNA processing events are particularly important to increase their potential ability to modulate transcriptome and gene expression (Conlon and Manley, 2017; Sephton and Yu, 2015). In recent times, considering the increasing number of diseases that are characterized by misregulation of TDP-43, a new term has been coined and they are now classified under the term of TDP-43 proteinopathies (Barmada and Finkbeiner, 2010).

1.2.1 Neurodegenerative disorders

As already mentioned, in 2006 TDP-43 was identified for the first time as the major ubiquitinated component of inclusion bodies in Amyotrophic Lateral Sclerosis (ALS) and Frontotemporal Lobar Degeneration (FTLD) patients' brain. Under pathological conditions, the protein is depleted from the nucleus and sequestered as hyperphosphorylated/ubiquitinated insoluble aggregates, disturbing the physiological nuclear functions of TDP-43 and its trafficking to the cytosol (Arai et al., 2006; Neumann et al., 2006). A brief overview will therefore follow with regards to some of these pathologies.

1.2.1.1 Amyotrophic Lateral Sclerosis – ALS

Amyotrophic Lateral Sclerosis (ALS) is a fatal motoneuron disease characterized by progressive loss of function of the upper and lower motoneurons at the spinal or bulbar level, resulting in muscle weakness, atrophy and spasticity (Zarei et al., 2015; Gendron et al., 2013).

It was first described in 1869 by the French neurologist, Jean-Martin Charcot, but the disease became well known when it was diagnosed in 1939 to Lou Gehrig, a baseball player (Zarei et al., 2015).

ALS is the third most common adult neurodegenerative disease after Alzheimer Disease (AD) and Parkinson Disease (PD) (Banks et al., 2008). The incidence of ALS is

similar throughout the world, affecting 1.5-2.5 patients per 100000 individuals (Barmada and Finkbeiner, 2010).

The pathology is categorized in two forms:

- Sporadic (sALS), the most common form which affects 90-95% of the patients with no genetic inheritance.
- Familiar (fALS) type, that includes the remaining 5-10%, associated to genetic inheritance factors (Zarei et al., 2015).

Approximately 20% of all fALS is caused by mutations in the ubiquitously expressed enzyme Super-Oxide Dismutase1 (SOD1) and about 1% of sALS are caused by mutations in the same gene (Banks et al., 2008). Some recent studies have described another prominent genome region where mutations are present in fALS cases, *C9orf72* (Cooper-Knock et al., 2015).

ALS is a clinically and genetically heterogeneous disorder arising between the fourth and the seventh decade, and the median time from symptom onset to death is 30-36 months, often due to respiratory muscle involvement. Patients may present a predominantly upper motoneuron (UMN) loss, a lower motoneuron (LMN) degeneration, or a combination of the two. Some patients can also present an early bulbar involvement but in other cases the muscles of the head and neck may be not involved during the disease progress (Barmada and Finkbeiner, 2010).

Most importantly, as disease progresses ALS seems to affect different brain areas, from the frontal and temporal cortices, brainstem and cerebellum, adding different symptoms to the traditionally recognized motor system degeneration (Barmada and Finkbeiner, 2010).

1.2.1.2 Frontotemporal Lobar Degeneration – FTLD

Frontotemporal Lobar Degeneration (FTLD) is the most common cause of presenile dementia after Alzheimer disease below 65 years (Banks et al., 2008). It is a clinically and pathologically heterogeneous syndrome, characterized by a progressive decline in behavior or language, associated with degeneration of the frontal and anterior temporal lobes (Rabinovici and Miller, 2010). Patients may also display movement abnormalities with clinical features overlapping with Motoneuron Disease (MND) that recall ALS characteristics (Gendron et al., 2013).

First evidence of the disease was described in 1892 by Arnold Pick who studied a patient with progressive aphasia and lobar atrophy. In 1911, the presence of neuronal inclusions at neuropathological examination, later called Pick bodies, was reported by Alois Alzheimer (Seelaar et al., 2011).

FTLD patients are clinically classified into three different groups depending on the early and predominant symptoms, such as a behavioral variant (bvFTD), and two language variants, called semantic dementia (SD), and progressive non-fluent aphasia (PNFA). Each variant is associated with a different brain atrophy pattern and has peculiar histopathologic characteristics. Sometimes the symptoms can overlap, in particular during the later course of the disease when it spreads and involves the entire frontal and temporal lobes (Rabinovici and Miller, 2010).

From a histopathological point of view, FTLD patients are characterized by atrophy of the frontal and temporal lobes and by the presence of glial and neuronal inclusion bodies composed by: TAU, TDP-43, or fused-in-sarcoma (FUS) (Rabinovici and Miller, 2010). FTLD patients can be classified in sub-molecular groups depending on the inclusion type:

- FTLD with TAU inclusion (FTLD-TAU). FTLD tauopathy is characterized by the presence of Pick bodies, which are solitary, round or oval, argyrophilic inclusions found in the cytoplasm of neurons (Rabinovici and Miller, 2010).
- FTLD with ubiquitin TDP-43 positive inclusions (FTLD-TDP) is characterized by the presence of TDP-43 as the major ubiquitinated component. Like in ALS, under pathologic conditions TDP-43 is displaced from the cell nucleus to the cytoplasm, hyperphosphorylated, ubiquitinated and cleaved to produce C-terminal fragments (CTF) which aggregate and form the inclusion bodies. Neuronal and glial TDP-43 inclusions are found in the majority of cases previously classified as FTLD-TAU negative (FTLD-U) with and without motor neuron disease symptoms (Rabinovici and Miller, 2010).
- FTLD-FUS positive cases cover about the 5–20% of all FTLD-U cases that remain negative for TDP-43. FUS is a ubiquitously expressed DNA/RNA binding protein that regulates gene expression and, like TDP-43, is also involved in ALS. The clinical phenotype is characterized by early onset and important behavior clinical signs (Rabinovici and Miller, 2010).

FTLD patients can also be recognized by the presence or the absence of motoneuron disease features:

- FTLD with Motor-Neuron Disease (MND) can be also divided in two subtypes: presenile dementia with MND or ALS with dementia (Arai et al., 2006);
- FTLD with MND-type inclusions, but without MND phenotype (Arai et al., 2006);
- FTLD phenotype lacking of distinct histology, without TAU or ubiquitin-positive inclusions (Arai et al., 2006).

1.2.1.3 Motoneuron Disease – MND

Based on the predominant symptoms, FTLD and ALS could seem two different disorders: FTLD is characterized by progressive changes in social behavior or/and language dysfunctions whilst ALS shows weakness and wasting of the muscles. However, in some cases the two phenotypes can eventually match. For example, some FTLD patients develop a MND phenotype and around 1/3 of ALS patients eventually show some form of dementia (Neumann et al., 2006). Moreover, families in which the two diseases segregated together were identified, speculating a clinical and pathological overlap between the two disorders. This hypothesis was confirmed by biochemical and immunohistochemical analyses suggesting that they could represent two manifestations of the same basic neurodegenerative disorder (Achi and Rudnicki, 2012; Neumann et al., 2006).

1.2.2 TDP-43, RNA-binding proteins, and metabolic disorders

Interestingly, neurological impairment is also associated with many metabolic disorders, such as monogenic diseases characterized by single gene mutations leading to metabolic disfunctions, in particular those involving lysosomal pathways (Fiorenza et al., 2018). Alterations in the lysosomal system can contribute to protein accumulation, a classical feature of neurodegenerative disorders. Therefore, Lysosomal Storage Disorder (LSD) patients often show early neurodegenerative symptoms recalling ALS and FTLD disease (Bahr and Bendiske, 2002).

In this context, RNA-binding proteins (RBP), like TDP-43, can play an important role in the appearance of the neurological disfunction. In particular, they can disrupt axonal transport, and cell metabolism through Golgi apparatus fragmentation of by impairing the exosome/lysosome pathway (Janas et al., 2016; Jellinger, 2009; Potashkin and Meredith, 2006). In neuronal cells, the axonal transport through multi-vesicular bodies (MVBs – like lysosome and exosome) is directly implicated in synaptic function playing an important role

in the intra/inter cellular communication that is fundamental for neuronal homeostasis (Janas et al., 2016). In this regard, it is important to note that spatial and temporal mRNA translation is a fundamental requirement in neurons because RNA is often associated with RBPs and the resulting RNA-RBP complex can be loaded into exosomes to facilitate the axonal transport and the correct subcellular translation or localization. Alternatively, the complex can be load in the lysosome promoting its degradation (**Fig.9**) (Paron et al., 2020; Janas et al., 2016).

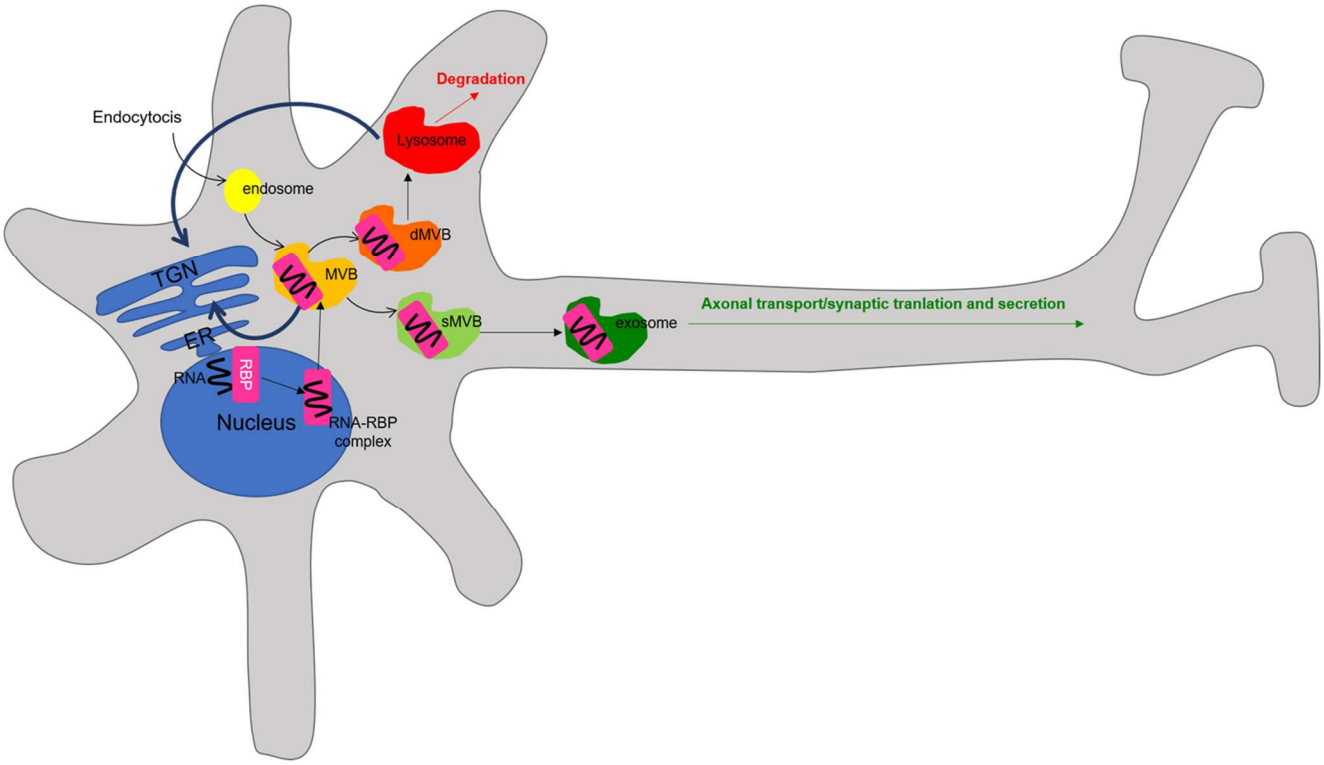

Figure 9 – MVBs cellular pathway. The RNA-RBP complex loaded in the MVBs can follow exosomal secreting pathway (sMVB); or the lysosomal degradation pathway (dMVB) (Paron et al., 2020).

In this context, therefore, lysosomal pathway disfunctions can impair RNA metabolism, explaining the neurological features in many LSDs (Conlon and Manley, 2017).

1.2.2.1 Niemann-Pick type C Disease (NPC)

In this work, I focused my attention on a specific LSD that is known as Niemann-Pick type C disease (NPC). NPC was described for the first time in the late 1920's by Albert Niemann and Ludwig Pick as a heterogeneous group of LSD, characterized by cholesterol storage disfunction with milder visceral symptoms, and a progressive fatal neurodegeneration (Vanier, 2010; Ong et al., 2001).

Genetically, NPC is an autosomal recessive disorder due to the presence of mutations in two genes *NPC1* and *NPC2* (Vanier et al., 1996). Around 95% of the patients display mutations on *NPC1,* gene whilst the other 5% stroke on *NPC2* (Vanier, 2010; Vanier and Millat, 2004).

NPC1 is located on chromosome 18, and its protein was described as a 1278 amino acid transmembrane glycoprotein able to associate with the membranes of different cytoplasmic vesicles (Storch and Xu, 2009; Higgins et al., 1999). On the other hand, *NPC2* maps on chromosome 14 and it was first studied as Human-Epididymis (HE1) Specific protein1, a secretory protein of the human epididymis. Later studies demonstrated that its absence or its mutation was correlated with NPC disease (Storch and Xu, 2009; Vanier and Millat, 2004). The mature human NPC2 protein is a small soluble 132 amino acid glycoprotein able to bind cholesterol with high affinity (Storch and Xu, 2009).

In physiological conditions, the cholesterol acquired with the diet is transported in the blood vessels through the low-density lipoproteins (LDL) that are then internalized by the cells exposing the LDL receptor (Brown and Goldstein, 1986). In cells, the endosome maturates in the lysosome and in this compartment the mature NPC1 and NPC2 proteins cooperate together to carry out correct cholesterol transport. The proposed model suggests that NPC2 is binding the cholesterol molecules inside the lysosomes, and through this complex, the cholesterol molecule can physically interact with the N-terminal domain of NPC1 protein. At this point, NPC1 transports the cholesterol to the trans-Golgi network (TGN) thanks to the cooperation of the sterol sensing domain and the C-terminal tail (**Fig.10**) (Estiu et al., 2013; Storch and Xu, 2009; Vanier and Millat, 2004). In this manner, mutations in these two proteins lead to cholesterol accumulation and the onset of visceral symptoms (Vanier, 2010).

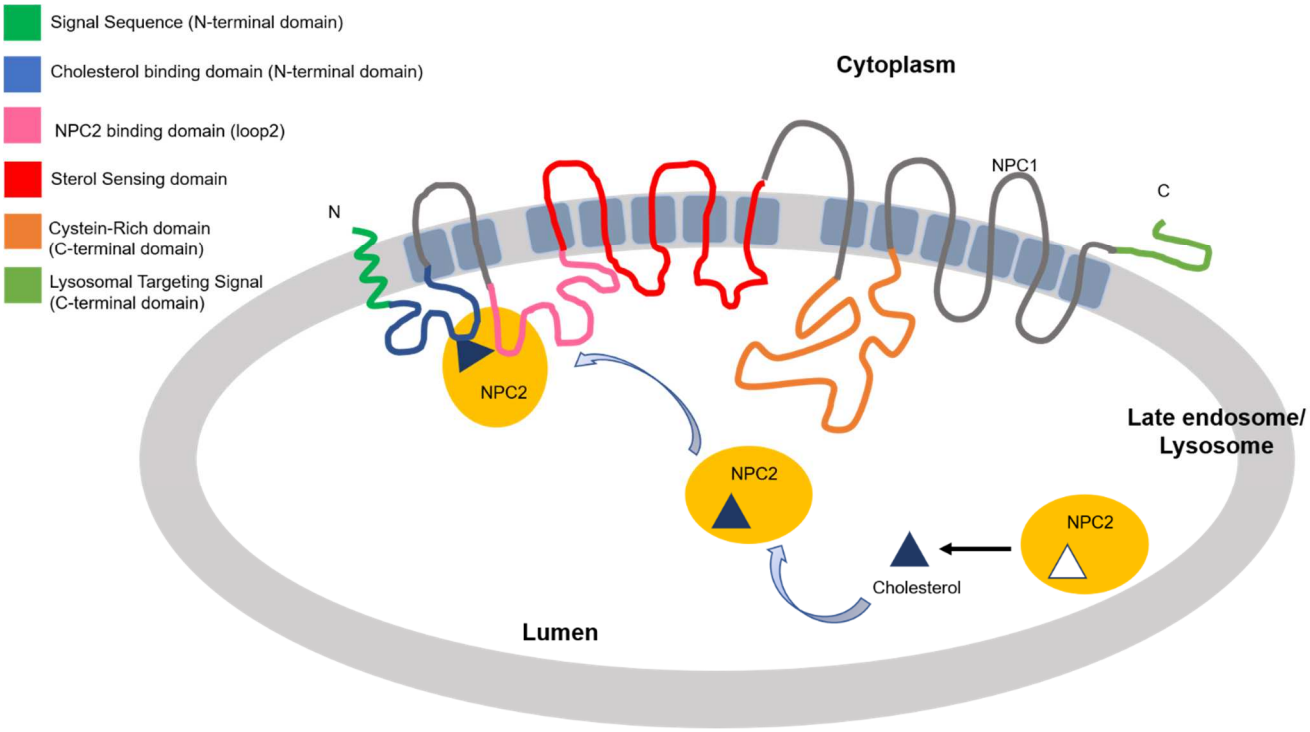

Figure 10 – NPC1 and NPC2 lysosomal interaction and cholesterol binding (Paron et al., 2020).

This model holds true for the visceral organs but not for the brain where the cholesterol is synthetized by the astrocyte and oligodendrocytes without any LDL-uptake (Björkhem et al., 2004). This clarification is very important because probably the molecular mechanism that undergoes to neurodegeneration in NPC disease is more subtle and not simply linked to the cholesterol pathway, but more similar to the one occurring in classical neurodegenerative disorders (Paron et al., 2020).

For this reason, NPC disease is not simply limited to visceral symptoms but it can be classified as a neurologic and neurodegenerative disorder. It is important to underline that the systemic diseases occurs prior to the neurological impairment. In fact, except for the perinatal period, NPC systemic disease is not very severe and quite well tolerated in most of the patients (Vanier, 2010).

At present, NPC neuro-pathogenetic mechanisms are still not clear but if we consider that RNA metabolism is very well known to be stricter controlled and regulated in the nervous system it is likely that the disruption of these pathways can represent a promising candidate to explain the pathogenesis of neurodegenerative diseases (Conlon and Manley, 2017).

1.2.2.2 NPC neurodegeneration and TDP-43

As previously described, TDP-43 has a fundamental role inside the cells, especially regarding RNA metabolism. Relying on this, in 2016 a correlation between NPC and TDP-43 was established by our lab (Dardis et al., 2016). In this work, Andrea Dardis and colleagues found TDP-43 mislocalized in the cytoplasm of Purkinje cells of *NPC1*$^{-/-}$ mouse model and in neuronal cells derived from multipotent stem cells isolated from skin biopsies of NPC patients, comparing to healthy controls (**Fig.11**) (Dardis et al., 2016).

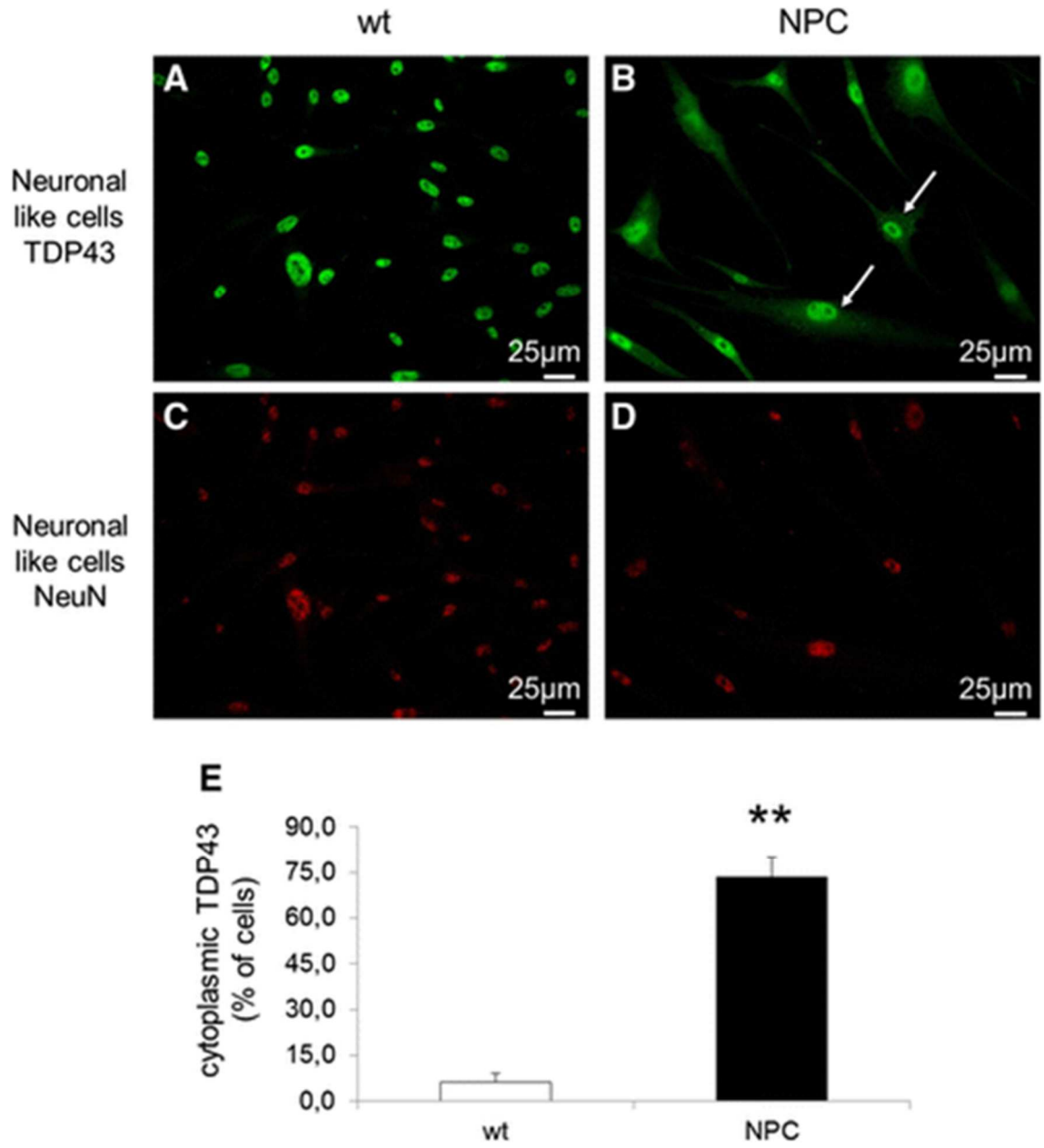

Figure 11 – TDP-43 cytoplasmic mislocalization in NPC human cellular mode. A) TDP-43 staining in wild type neuronal-like cells. B) NPC neuronal-like cells stained for TDP-43. C) and D) panels are reporting neuronal-like cells stained for a neuronal marker (NeuN) respectively wild type and NPC samples (Dardis et al., 2016).

They also discovered that TDP-43 was not just mislocalized but also hyperphosphorylated, like in ALS patients (**Fig.12**) (Newell et al., 2018; Dardis et al., 2016; Neumann et al., 2009).

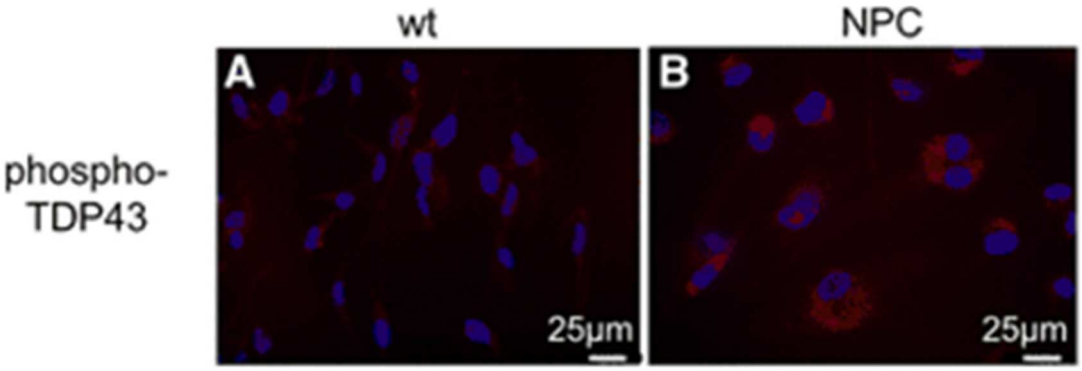

Figure 12 – TDP-43 mislocalization and hyper-phosphorylation in NPC human cellular model. Neuronal-like cells were stained with phospho-TDP-43 antibody (against the 409 and 410 Serine) in wild type (A) and NPC (B) samples (Dardis et al., 2016).

In addition, the expression of genes involved in neuronal survival and neuronal differentiation, like TFAP2A, CNTFR, MADD, MEF2D, CTNND1, KIF2, KIF1B, TLE1, TNIK, already described in literature as TDP-43 targets, was tested. The observation that 6 out of 9 genes tested were misregulated, supported the idea that TDP-43 mislocalization could play a role in neurodegeneration feature of NPC disease (**Fig.13**) (Dardis et al., 2016).

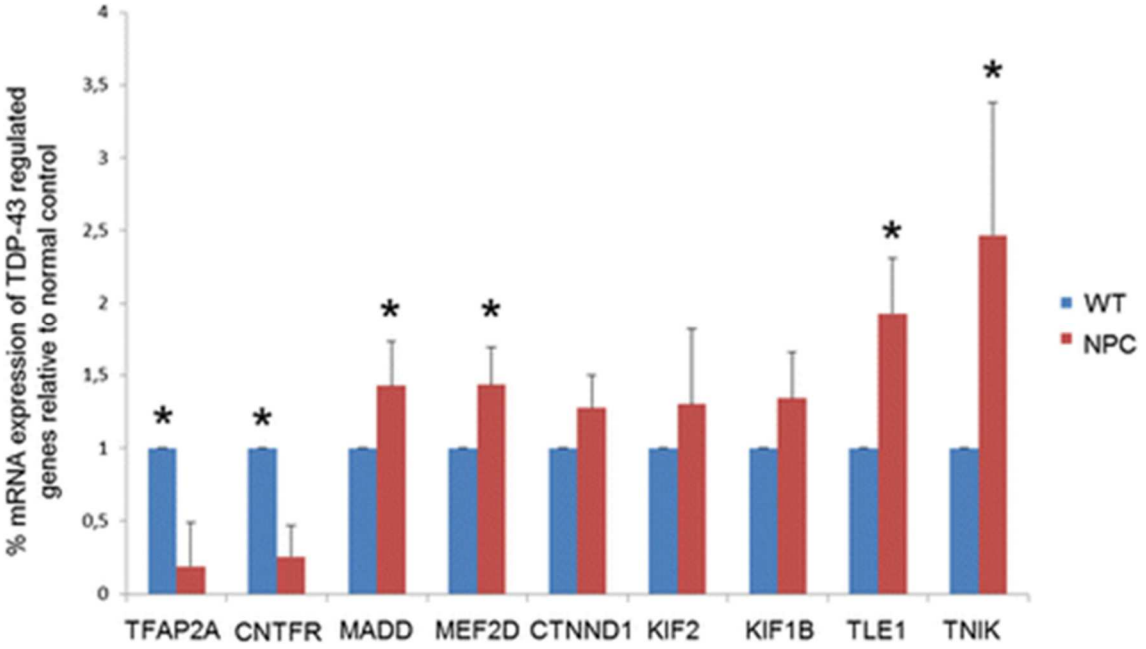

Figure 13 - TDP-43 misregulated genes by qPCR in human NPC model (Dardis et al., 2016).

1.3 TDP-43 pathogenic mechanisms in neurodegenerative disorders

After TDP-43 discovery as the major component of the inclusion bodies, many efforts have been performed aiming to describe its pathogenic mechanisms.

In TDP-43 disorders, the protein is found ubiquitinated and hyperphosphorylated, it is present in insoluble inclusions or in a C-terminal truncated form (20-25kDa fragments), it is mislocalized in the cytoplasm, and a loss of nuclear TDP-43 is detectable. However, the border between physiological and pathological aggregation is very subtle: the association with RNA, post-translational modification, and the formation of RNA granules is necessary to regulate mRNA transport and its final translation, but upon cellular stress this mechanism can become pathological with the irreversible aggregation of RNA-protein granules (Conlon and Manley, 2017; Vanderweyde et al., 2013). The balance between two cellular compartment is very delicate: a small perturbation can lead to the formation of TDP-43 aggregates that recapitulate TDP-43 pathologies features (Winton et al., 2008). Owing to this complexity, it is still unknown which of these processes should be considered primary characteristics of the disease and directly linked to neurodegeneration, as opposed to represent secondary features or epiphenomena (Lee et al., 2012).

In general, two models have been proposed to explain TDP-43 pathogenesis: Loss-Of-Function (LOF) and Gain-Of-Function (GOF) mechanisms.

1.3.1 Loss-Of-Function mechanism (LOF)

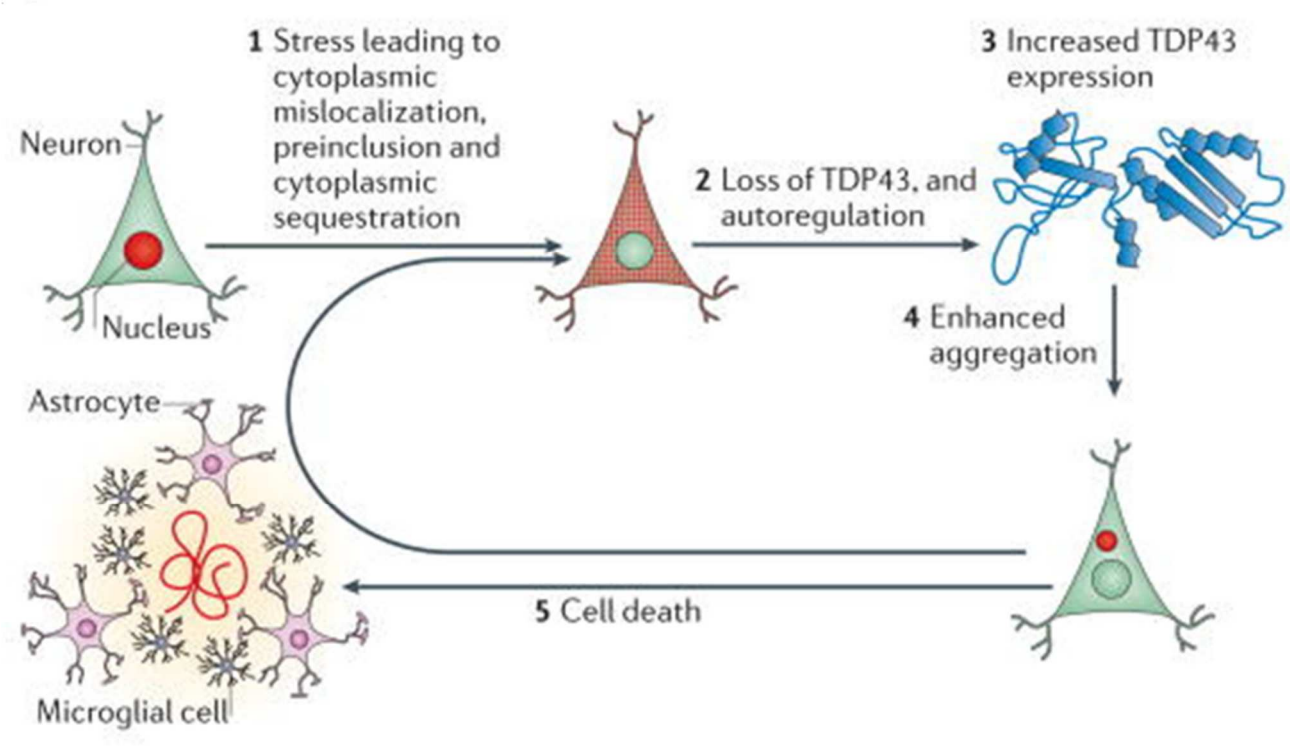

Figure 14 - TDP-43 LOF model leading cell death (Lee et al., 2012).

The LOF mechanism is thought to occur when cellular stress causes a redistribution of TDP-43 in pre-inclusion of the phosphorylated and/or ubiquitinated protein (stress granules). The presence of prolonged stress conditions and abnormal post-translational modifications eventually makes the aggregates difficult to be degraded. In this model, the increase in aggregates numbers/size induce nuclear clearance of the functional protein, the formation of truncated C-terminal fragments, and loss of autoregulation. The LOF toxicity is therefore induced by the sequestration of functional TDP-43 into the aggregates and consequent loss of all its normal cellular functions (**Fig.14**) (Lee et al., 2012; Barmada and Finkbeiner, 2010).

1.3.2 Gain-Of-Function mechanism (GOF)

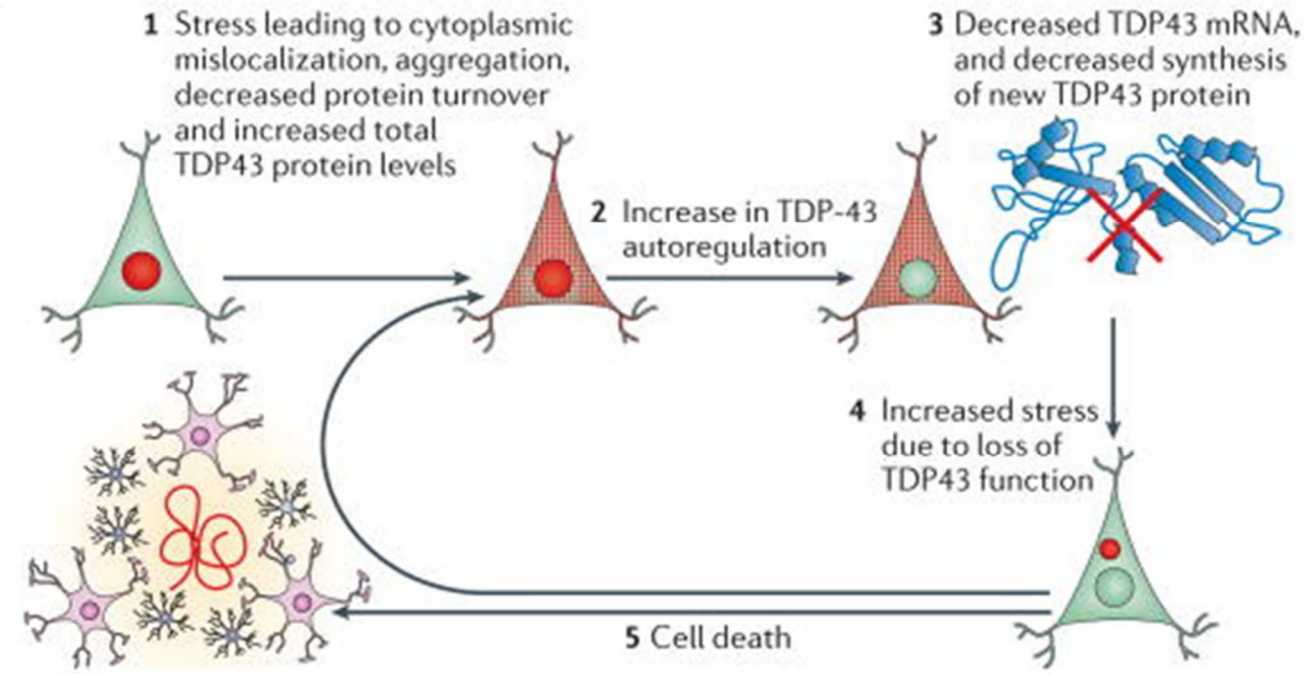

Figure 15 - TDP-43 GOF model leading cell death (Lee et al., 2012).

In addition to aggregation, a prolonged stress condition can also lead to abnormal cytoplasmic distribution, aggregation, changes in the autoregulation process, that occurs in the nucleus, leading to increas total protein levels (which are known to be toxic), and escape from degradation of partially folded protein oligomers by the ubiquitin-proteasome system (UPS) (**Fig.15**) (Lee et al., 2012). All these changes can be considered pathological when they have deleterious downstream effects and when the cell is not able anymore to limit their toxicity (Barmada and Finkbeiner, 2010).

Finally, it is important to note that these two models are not mutually exclusive and together they can cooperate in TDP-43 mediated neurodegeneration (Lee et al., 2012).

1.4 TDP-43 mutations

Since 2008, many papers have been published describing disease-associated mutations in the *TDP-43* gene, supporting the idea of TDP-43 direct involvement in neurodegenerative disorders, like ALS and FTLD. Even if mutations are sporadic events (3% in fALS and 1.5% in sALS), their characterization is important to better understand their functional significance and therefore TDP-43 pathogenic mechanisms (Buratti, 2015; Banks et al., 2008). Interestingly, mutations can display both LOF and GOF characteristics.

The presence of pathological TDP-43 mutations may result in a loss of function mechanism affecting the protein functions through two hypothetic scenarios:

- Haploinsufficiency or dominant-negative effect of the mutant protein, in which the mutant TDP-43 is not able to carry out the normal functions of the wild type. TDP-43 pathogenic mutations disrupt the physiological function of the protein and the mutant form cannot rescue the normal phenotype.
- The mutations affect the subcellular localization of the protein. In this situation, the mutant TDP-43 is able to reduce the nuclear protein levels by dimerizing with the wild type and sequestering it in the cytoplasm (Barmada and Finkbeiner, 2010).

Also, gain of function mechanisms can be promoted by disease-associated mutations resulting in new deleterious functions with TDP-43 aggregation in the neurons. These inclusions can acquire toxic functions with lethal downstream effects compromising neuronal survival. The molecular pathways involved in this process are unknown, but two mechanisms have been proposed:

- TDP-43 may induce toxicity by abnormal interaction with other cellular components: for example, aggregating TDP-43 can sequester cellular factors (other proteins; mRNA; etc.) disrupting other important pathways for the maintenance of nuclear survival.
- alternatively, pathogenic TDP-43 mutations may affect the binding of the protein with other factors, such as ubiquitin-1, thus interfering with the Ubiquitin-Proteasome System (UPS), escaping from the degradation (Barmada and Finkbeiner, 2010).

In keeping with this view, most TDP-43 pathogenetic mutations lie in the C-terminal domain (**Fig.16**) suggesting that they may affect the protein-protein interaction network, leading to the development of TDP-43 proteinopathies (Banks et al., 2008).

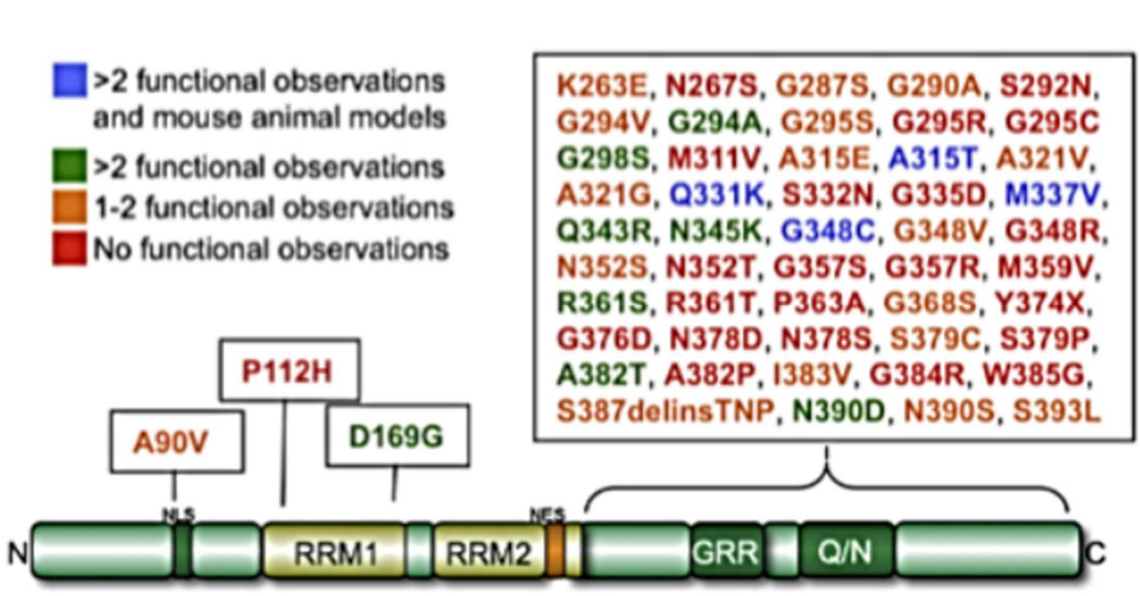

Figure 16 -TDP-43 mutations (Buratti, 2015).

In **Figure 16**, are reported all TDP-43 mutations already described to this date. Each mutation can lead to different alterations from the wild-type protein: for example, some mutations have been described to be able to increase aggregation, to change TDP-43 protein-protein interactions profile, to increase the half-life of the protein or its localization (**Fig.17**). It is important to underline that these functional alterations are not common to all mutations and different mutations may acquire specific properties (Buratti, 2015).

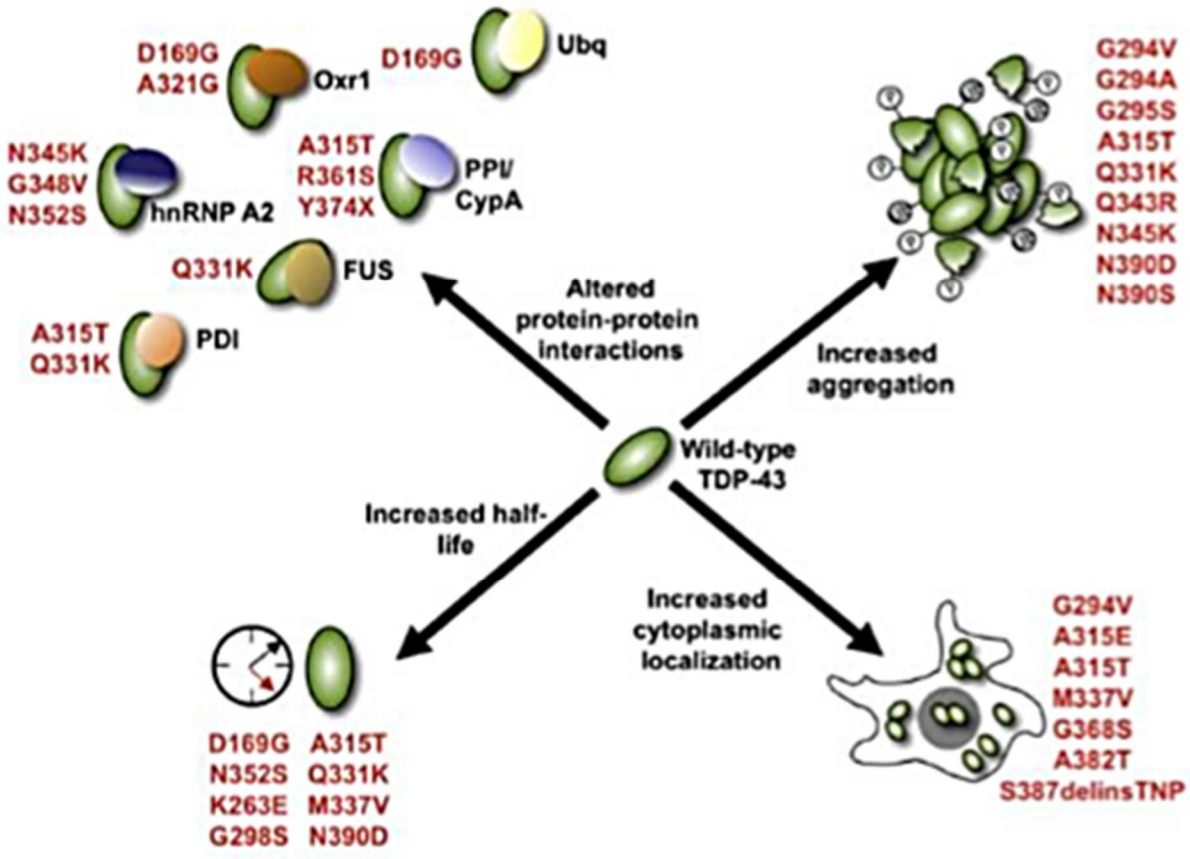

Figure 17 - Possible alterations promoted by TDP-43 mutation (Buratti, 2015).

Nonetheless, the study of single TDP-43 mutations is important because it can reveal novel potential pathological pathways that should be examined beyond the mutation itself. For this reason, a systematic approach to their study will be important in the future in order to analyze and characterize each mutation as soon as they are discovered (Buratti, 2015).

1.5 Post-Translational Modifications (PTMs): TDP-43 phosphorylation

Like other proteins involved in neurodegenerative disorders, TDP-43 undergoes to post-translational modification (PTMs) that can affect its function and cellular status both in physiological and pathological conditions (Buratti, 2018; Lee et al., 2012).

In general, PTMs allow proteins to quickly change their structural and functional properties in response to internal and external stimuli. For this reason, analyzing PTMs is important for better characterize protein profiles during health and disease conditions, potentially improving diagnostic and prognostic capabilities. Moreover, PTM analysis may provide potentially new specific therapeutic targets in neurodegenerative diseases (Buratti, 2018).

The presence of PTM-modified TDP-43 in ALS and FTLD is an issue that has been studied for a long time in TDP-43 proteinopathies. However, for many of these PTMs it is still unclear whether these modifications lead to aggregate formation/functional alterations or whether they are simply a physiological reaction to a cell stress condition. Whatever the case, the most prevalent modifications affecting TDP-43 in the ALS/FTD spectrum are as follows: phosphorylation; generation of C-terminal domain (CTD) fragments; ubiquitination; acetylation; cysteine oxidation; SUMOylating (Buratti, 2018; Lee et al., 2012). In **Figure 18** are summarized all the PTMs involved in TDP-43 pathology: the disease spectrum is wider than ALS/FTLD and include other diseases, like NPC and myopathies. At the moment, altered phosphorylation seems to be the most common PTM between the different disorders (Buratti, 2018).

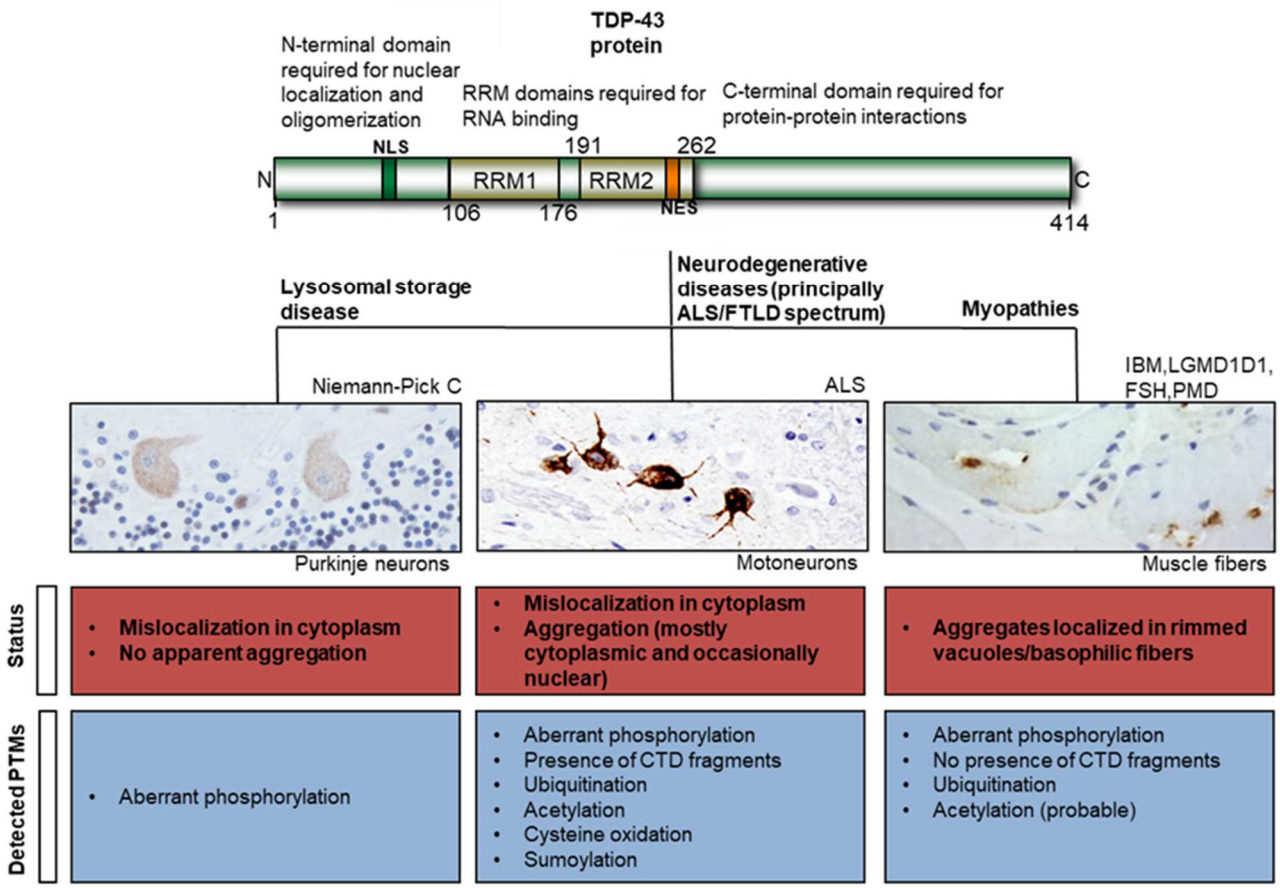

Figure 18 - TDP-43 most prevalent PTMs (Buratti, 2018).

Following many studies, the molecular events that activate aberrant TDP-43 phosphorylation were discovered to be related to endogenous or exogenous cell stress conditions (Buratti, 2015; Colombrita et al., 2009).

In **Figure 19**, are reported the known events in which TDP-43 phosphorylation is involved: in pathological cases, the main residues triggered by phosphorylation are two Serine residues in the C-terminal region, Ser409/Ser410. Also, phosphorylation at Ser379, Ser403, and Ser404 were described to correlate with disease pathology. Recently, a mass-spectrometry analysis and *in vitro* studies has been performed to detect the other possible phosphorylation on patient's brain samples and, as more samples are analyzed, it is probable that this picture will be considerably widened in the near future (Newell et al., 2018; Kametani et al., 2016; Neumann et al., 2009). The potentially important role of phosphorylation in disease is also highlighted in **Figure 19** where a clear correlation may be observed between phosphorylation and disease-associated mutations in the TDP-43 C-terminal region. Many mutated residues, in fact, seem to be involved either the

creation/disruption of Serine/Threonine residues or in the formation of a potential 'phosphomimic' by the introduction of an Aspartic or Glutamic acid (Buratti, 2018).

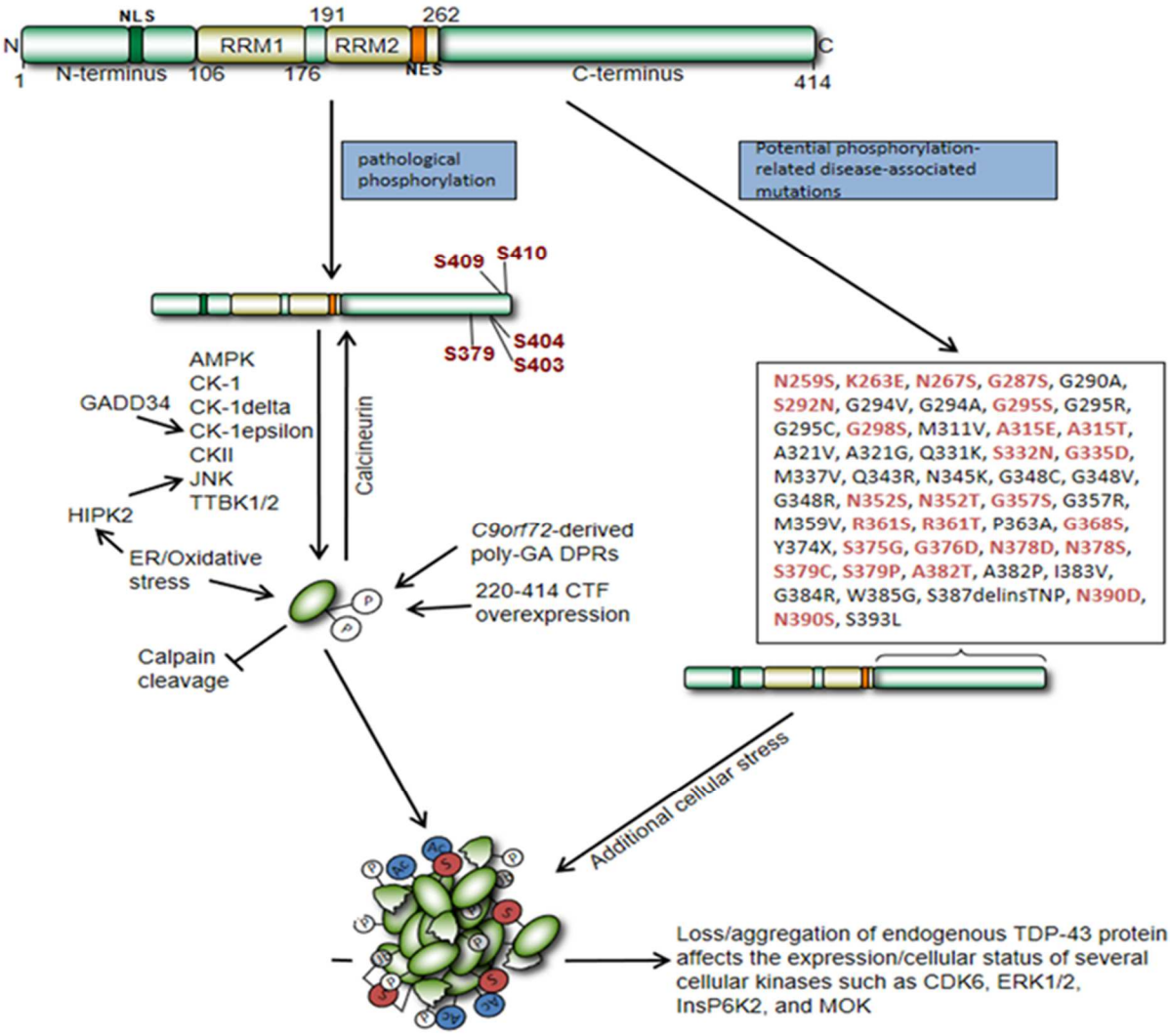

Figure 19 - TDP-43 aberrant phosphorylation(Buratti, 2018).

In the future, considering the importance of phosphorylation in TDP-43 pathology, many targeting kinases compounds should be tested in various experimental TDP-43 systems to check for their ability to modify TDP-43-mediated pathology. Moreover, the use of TDP-43 phosphorylation-specific antibodies as biomarkers of disease should improve the clinic diagnosis and prognosis of patients (Buratti, 2018).

2 AIM OF THE PROJECT

The aim of this work has been to study in detail a specific TDP-43 PTMs, namely phosphorylation, in two different diseases models. In particular, in the first part of the project I have focused on the characterization of a novel disease-associated TDP-43 mutation, S375G that was described in very early-onset ALS cases, that might affect the phosphorylation sites in the C-terminal region of this protein. In the second part of my study, I have focused on the involvement of TDP-43 phosphorylation in neurological defects linked to Niemann-Pick type C, which could become a new therapeutic target for the disease. Taken together, the hope is that my two aims will allow to better understand the impaired cellular processes that are induced by aberrant phosphorylation of TDP-43.

3 MATERIAL AND METHODS

3.1 DNA plasmid preparation, purification, and mutagenesis

3.1.1 *Escherichia coli* DH5α competent cells preparation

E. coli DH5α strain competent cells were generated starting from frozen glycerol stock (1:1), stored at -80°C. DH5α glycerol was defrosted on ice, and plated on LB[1]-agar Petri dish, without antibiotics, overnight at 37°C. The day after, one colony of DH5α, was picked up and it was grown overnight in 10ml LB media, without antibiotics, at 37°C (pre-inoculum). The third day, 3ml of this growth was inoculated in 100ml of LB[2] media and it was grown at 37°C by shaking. The bacterial growing was followed by measuring the optical density (OD) at 590nm by using the D30 Eppendorf BioSpectometre (Eppendorf, Hamburg, Germany), until it reached 0.35-0.37. The suspension was centrifuged at 1000xg for 10 minutes at 4°C. The supernatant was removed and the pellet was resuspended in 1/10 of the initial volume of 1% TSS[3] solution. The resuspended cells were aliquoted in 1.5ml tubes, immediately frozen with liquid nitrogen, and then the competent cells were stored at -80°C.

The competence of the generated DH5α cells was evaluated by transforming 100µL of DH5α with 0.1 ng/µl of pUC18 plasmid. The cells were plated in LB-agar Petri dish without antibiotics, overnight at 37°C. The day after were counted the grown colonies. The competence was calculated using the following formula:

$$Competence\ (10^6) = \frac{Colony\ Forming\ Units}{pUC18\ Concentration}$$

3.1.2 DH5α plasmid transformation

Competent *E. coli* DH5α were transformed in order to amplify the amount of the DNA plasmid of interest, that carries the resistance for a specific antibiotic. From this transformation, only the colonies that have inserted the plasmid grow in the media containing the specific antibiotic.

60µl of competent cells DH5α were defrosted in ice and transformed with 1µg of plasmid using a heat shock protocol. The cells were incubated with the plasmid in ice for 30 minutes. At the end of this incubation, the mix was shocked at 42°C for 2 minutes. In order

[1] Reference to 2.8 paragraph – standard solutions
[2] Reference to 2.8 paragraph – standard solutions
[3] Reference to 2.8 paragraph – standard solutions

to stop the reaction, the cells incubated with the plasmid were placed on ice for 1 minute, and then 60 µl of LB media was added; cells were left in a shaking incubator for 1 hour at 37°C. At the end, the reactions were plated in LB-agar petri dish with the specific antibiotic, and they were incubated at 37°C overnight.

The day after, one colony was inoculated overnight at 37°C, in 6ml (for Miniprep) or 50ml (for Midiprep) of TB[4] with the specific antibiotic. The suspension was centrifuged for 30 minutes at 1937xg and the resulting pellets were stored at -20 °C.

3.1.3 Miniprep: small scale purification of DNA plasmid

The Miniprep technique allows to extract a small amount of plasmid from bacterial cultures. In this work the Wizard Plus SV Minipreps DNA purification system (Promega, Fitchburg, WI, USA) was used following the manufacturer's instructions. The pellet was resuspended by vortexing in 250µL of resuspending solution and placed into a 1.5ml tube. 250µL of lysis solution and 10µL of alkaline protease were added and mixed by pipetting. The solution was left 5 minutes at room temperature. 350µL of neutralizing solution were added and gently turned. The samples were centrifuged 10 minutes at 16000xg (full speed). The supernatant was picked up and added on the top of the Promega kit column; it was then centrifuged for 1 minute at 16000xg. The column was then placed in another collecting tube, and on the top of it 750µL of washing solution were added. The column was centrifuged for 1 minutes at 16000xg. This step was repeated by adding 250µL of washing solution and it was centrifuged for 2 minutes at 16000xg. For the elution step the column was transferred in a 1.5 mL sterile tube and on the top of it 100µL of Nuclease-free water were added. It was centrifuged for 1 minute at 16000xg. Before storing it at -20°C, the amount of extracted and purified DNA plasmid was measured with the D30 Eppendorf BioSpectometre (Eppendorf, Hamburg, Germany).

3.1.4 Midiprep: middle scale purification of DNA plasmid

Middle scale preparation of DNA plasmid allows to extract medium amount of plasmid from total bacterial DNA. In this work, it was performed by using QIAGEN Plasmid Mini, Midi and Maxi kits (Qiagen, Hilden, Germany) following manufacturer's instructions.

[4] Reference to 2.8 paragraph – standard solutions

The bacterial pellet was resuspended in 4ml of P1 buffer, and 4ml of P2 buffer were added. It was then mixed by inverting and the resuspended pellet was left for 5 minutes at room temperature. After this resting time, 4ml of prechilled P3 solution were added and the tubes were vigorously inverted. The solution was left for 15 minutes on ice, and then it was centrifuged ≥20000xg for 30 minutes at 4°C. In the meantime, the QIAGEN-tip column was equilibrated with 4ml of QBT buffer. It was left at room temperature until the column becomes empty by gravity flow. After the centrifugation, the supernatant was applied to the QIAGEN-tip. The column was washed two times with 2ml of QC buffer. The DNA was then eluted in a clean vessel by adding 15ml of QF buffer, and DNA was precipitated by adding 3.5ml of isopropanol (Honeywell, Charlotte, North Carolina, USA). The precipitated DNA was centrifuged at ≥15000xg for 30 minutes at 4°C. The supernatant was gently removed, and the pellet was washed with 2ml 70% Ethanol (Honeywell, Charlotte, North Carolina, USA). It was centrifuged at ≥15000xg for 30 minutes at 4°C, and the supernatant was discarded. The pellet was left at room temperature to air-dry it, and it was resuspended in 200µl of sterile water. Before storing it at -20°C, the amount of extracted and purified DNA plasmid was measured with the D30 Eppendorf BioSpectometre (Eppendorf, Hamburg, Germany).

3.1.5 Site-directed mutagenesis technique (QuickChange) and DNA sequencing

The site directed mutagenesis technique (QuickChange, Promega) was employed; this is usually used to perform insertions, deletions or mutations smaller than 10bp.

Two different 0.2ml tube were prepared: one for the negative control and one for the sample. In table 1 are reported the reagents for the negative control:

Control Reaction	
Reagent	**Final Concentration (for 50µl of reaction)**
10X Pfu buffer	1X
Template	0,1-1ng/µl
Deoxynucleotide (dNTP) Solution Mix 2,5mM (Rovalab, Teltow, Germany)	0,05mM
Pfu enzyme	2,5U/µl

Table 1 – QuickChange negative control reagents.

In table 2 are shown the sample composition:

Sample Reaction	
Reagent	**Final Concentration (for 50µl of reaction)**
10X Pfu buffer	1X
Template	0,1-1ng/µl
Oligonucleotides Sense (100ng/µl)	2,5ng/µl
Oligonucleotides Antisense (100ng/µl)	2,5ng/µl
Deoxynucleotide (dNTP) Solution Mix 2,5mM (Rovalab, Teltow, Germany)	0,05mM
Pfu enzyme	2,5U/µl

Table 2 – QuickChange sample reagents.

Sterile water was used to reach the final volume and a drop of mineral oil (Sigma-Aldrich, St. Louis, Missouri, USA) was put on the top of each sample to avoid the evaporation.

As shown in table 1, in the negative control are not present the oligonucleotides in order to avoid the PCR reaction.

In table 3 are reported the oligonucleotides used to insert the nucleotides mismatches.

Name	**Sequence 5' → 3'**
S375G forward	ATAACTCTTATGGTGGCTCTAATTC
S375G reverse	GAATTAGAGCCACCATAAGAGTTAT
G376D forward	ACTCTTATAGTGACTCTAATTCTGG
G376D reverse	CCAGAATTAGAGTCACTATAAGAGT
N378D forward	TATAGTGGCTCTGATTCTGGTGCAG
N378D reverse	CTGCACCAGAATCAGAGCCACTATA
Y374X forward	CTGGAAATAACTCTTAGAGTGGCTCTAATTCTGG
Y374X reverse	CCAGAATTAGAGCCCACTCTAAGAGTTATTTCCAG
S375E forward	ATAACTCTTATGAGGGCTCAATTC
S375E reverse	GAATTAGAGCCCTCATAAGAGTTAT
S242E forward	GATGATCAGATTGCGCAGGAGCTTTGTGGAGAGGACTTG
S242E reverse	CAAGTCCTCTCCACAAAGCTCCTGCGCAATCTGATCCTC
S305E forward	AACAATCAAGGTGAGAATATGGGTGGTGGG
S305E reverse	CCCACCACCCATATTCTCACCTTGATTGTT
S387-395E forward	GCAGGTTGGGGAGAGGCAGAGAATGCAGGGGAGGGCGAGGGTTTTAATGGA

S387-395E reverse	TCCATTAAAACCCTCGCCCTCCCCTGCATTCTCTGCCTCTCCCCA ACCTGC
S404E forward	GGAGGCTTTGGCTCAGAGATGGATTCTAAG
S404E reverse	CTTAGAATCCATCTCTGAGCCAAAGCCTCC

Table 3 – Oligonucleotide sequences used for site directed mutagenesis.

The PCR protocol was carried out using 2720 Thermal Cycler (Applied Biosystem, Foster City, California, USA), following the manufacture's instruction:

1. 95°C for 30 seconds (first denaturation);
2. 95°C for 30 seconds;
3. 55°C for 60 seconds;
4. 68°C for 1minute/kb of plasmid length;
5. 4°C.

From step 2 to step 4 the number of cycles were set from 12 to 18, depending on the number of mutations that need to be inserted. When the PCR finished, 20U/µl of the DpnI enzyme (New England Biolabs, Ipswich, Massachusetts, USA) was added. The reaction was incubated for 3 hours at 37°C. The DpnI restriction enzyme cuts the wild type plasmid which has the methylated sites, in order to leave only the mutated (the amplified) one.

From 1 to 20µl of the PCR product digested with DpnI enzyme, were then transformed in *E. coli* DH5α competent cells following the heat shock protocol[5]. The remaining reaction was stored at -20°C.

The purified plasmid DNA was sent to GATC Biotech, a European Custom Sequencing Center (Eurofins Scientific, Luxembourg), to be sequenced with specific oligonucleotides, upstream and downstream our insert (table 4), to check if the mutation of interest was present and also to avoid the incidence of other sporadic mutations.

Name	**Sequence 5' → 3'**
CMV 30 forward	AATGTCGTAATAACCCCGCCCCGTTGACGC
CMV 24 reverse	TATTAGGACAAGGCTGGTGGGCAC

Table 4 – Oligonucleotide sequence upstream (CMV 30 forward) and downstream (CMV 24 reverse) the insert of interest, used for sequencing.

[5] Reference to 2.2.1 paragraph – 2.1.2 DH5α plasmid transformation

3.2 Cell culture techniques

3.2.1 Gene knockdown

In this work, gene knockdown technique was applied to different cell lines by exploiting various reagents in order to obtain an optimal silencing efficiency. In table 5 the siRNA sequences of the analyzed gene are reported. Details of knockdown protocols for various genes are included below.

Name	**Sequence 5' → 3'**
Fire-fly luciferase (siLUC) forward	UAAGGCUAUGAAGAGAUAC[dT][dT]
Fire-fly luciferase (siLUC) reverse	GUAUCUCUUCAUAGCCUUA[dT][dT]
TDP-43 (siTDP-43) forward	GCAAAGCCAAGAUGAGCCU[dT][dT]
TDP-43 (siTDP-43) reverse	AGGCUCAUCUUGGCUUUGC[dT][dT]
LCP1 (siLCP1) forward	GGACAUUUAGGAACUGGAU[dT][dT]
LCP1 (siLCP1) reverse	AUCCAGUUCCUAAAUGUCC[dT][dT]
EPDR1 (siEPDR1) forward	GCCAGAUGGCCCAACUGGA[dT][dT]
EPDR1 (siEPDR1) reverse	UCCAGUUGGGCCAUCUGGC[dT][dT]
SHANK1 (siSHANK1) forward	CUCUGUAGAGGUGAUUCGA[dT][dT]
SHANK1 (siSHANK1) reverse	UCGAAUCACCUCUACAGAG[dT][dT]
ITPR1 (siITPR1) forward	GGAAGAACCAGGAGUAUAU[dT][dT]
ITPR1 (siITPR1) reverse	AUAUACUCCUGGUUCUUCC[dT][dT]

Table 5 – siRNA sequences.

3.2.1.1 Knockdonw in HeLa cell line

HeLa cell are immortalized cell line derived from cervical cancer. In this work, this cell line was used for transient transfection experiments because they are quite amenable to different cellular treatments, like silencing and transfection, resulting in a high efficiency of the assay with a low level of non-specific death.

HeLa cell line silencing was performed to knockdown *TDP-43* gene using a siRNA against *Fire-fly luciferase* (siLUC) gene as a control. It was carried out in three days: at day one, 170000 HeLa cells were plated in p35 Petri dish with 1.5ml of D-MEM [6]media. At day two and three, two rounds of silencing were performed using 3µl of Oligofectamine™

[6] Reference to 2.8 paragraph – standard solutions

Transfection Reagent (Invitrogen, Carlsbad, California, USA), following the manufacture's instruction, with 80nM final concentration of siRNA (40µM) against *TDP-43* and *Luciferase*, in a final volume of 1.5ml of Opti-MEM [7]media.

Other treatment followed the silencing, and after 24 hours the cells were collected to test splicing capability of the mutants.

3.2.1.2 Knockdown in SH-Sy5Y ECACC (European Collection of Authenticated Cell Cultures, England) cell line

SH-Sy5Y (ECACC, England) neuroblastoma cell line gene silencing, was performed to test the effect of the downregulation of some genes in relation to TDP-43 expression and phosphorylation. This cellular model is less prone to treatments, but it is derived from neuroblastoma and it can recap neuronal pathways. Considering this, Oligofectamine™ Transfection Reagent (Invitrogen, Carlsbad, California, USA) is too weak for this cell line, accordingly the knockdown was carried out using Lipofectamine RNAiMAX reagent (Invitrogen, Carlsbad, California, USA) following the datasheet instructions. Basically, 800000 cells were plated and silenced at day one in p35 plates, using 9µl of Lipofectamine RNAiMAX reagent, 3µl of 40µM siRNA (against *LCP1*, *EPDR1*, *SHANK1*, *ITPR1*, and *Luciferase* as a control), and 150µl of Opti-MEM media, in a final volume of 1.5ml in D-MEM:F12. One knockdown round is enough to achieve a good silencing efficacy. After 48 hours, the cells were collected and prepared for the following tests, or to immunofluorescence analysis.

3.2.2 Cellular transfection

In order to obtain protein overexpression, cellular transfection with DNA plasmids was performed. In this work, five plasmids were used for the overexpression system:

- pTB-CFTR_Ex9 C155T co-transfected with the pFLAG-CMV4 TDP-43 siRNA resistant for the add back experiments, containing the minigene with the exon 9 of the *CFTR* (Pagani et al., 2003).

[7] Reference to 2.8 paragraph – standard solutions

- p-CMV4 plasmid used as a negative control in the RNA immunoprecipitation assay (**Fig.20**).

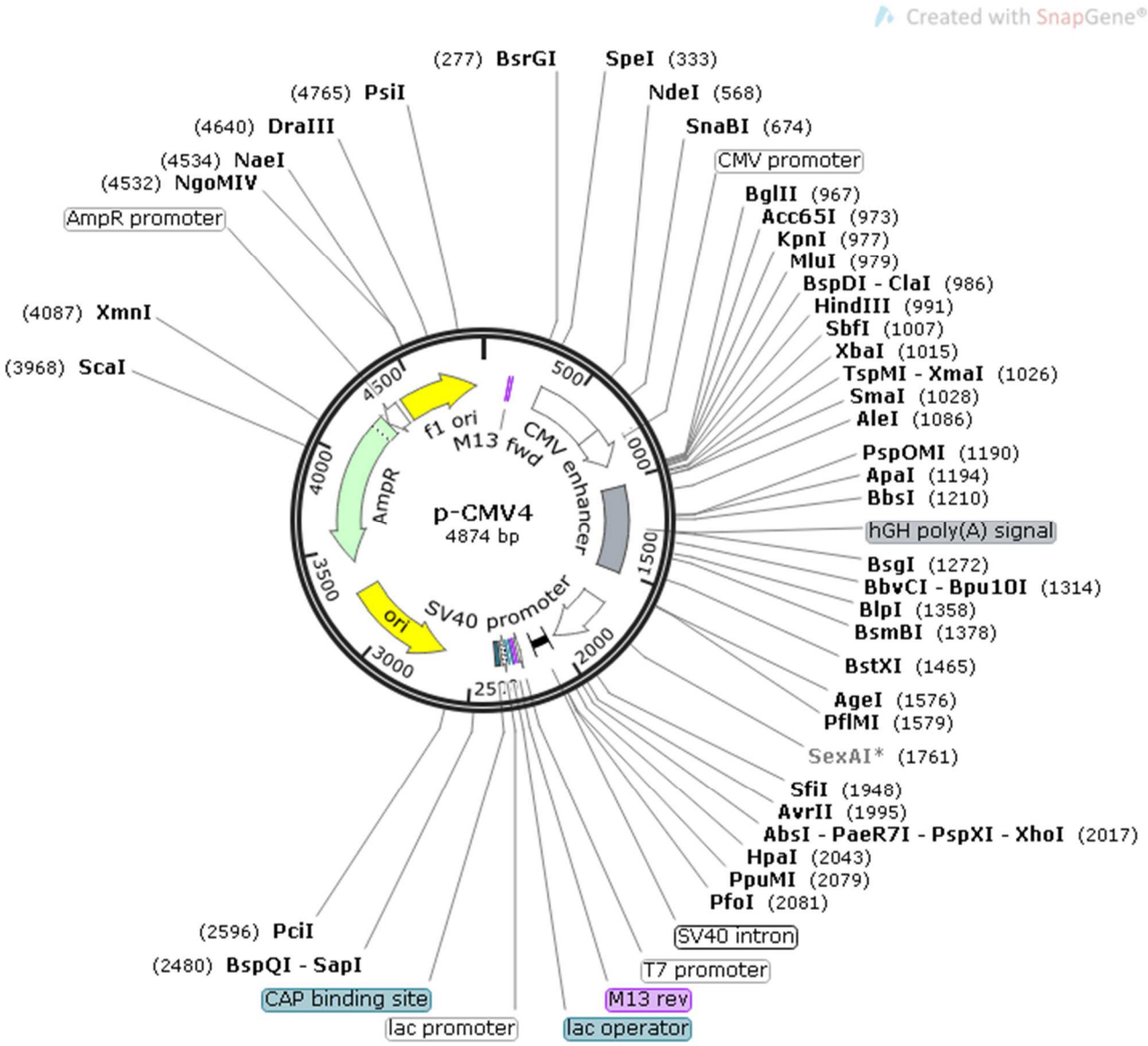

Figure 20 – p-CMV4 map.

- pFLAG-CMV4 TDP-43 siRNA resistant was used to overexpress TDP-43 wild type and mutated in the transient transfection experiments and for the RNA immunoprecipitation protocol. **Figure 21** represents the plasmid map.

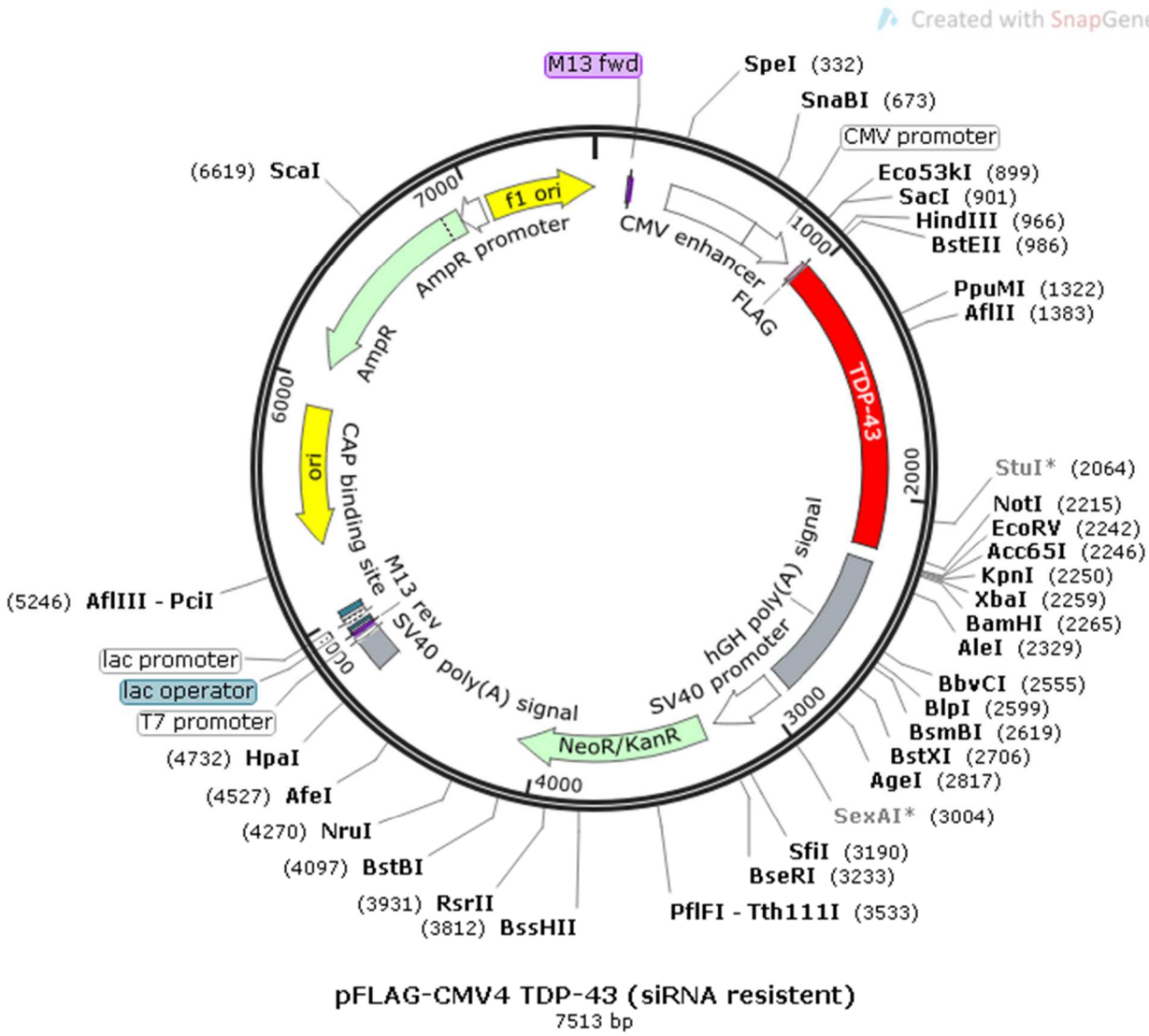

Figure 21 – pFLAG-CMV4 TDP-43 siRNA resistant map.

- p5cDNA FRT/TO flag TDP-43 was used in the stable clone creation, in order to overexpress stably TDP-43 wild type and the mutant form in the Hek293 Flp-In T-REx (Life Technology, Carlsbad, California, USA) cell line (**Fig.22**).

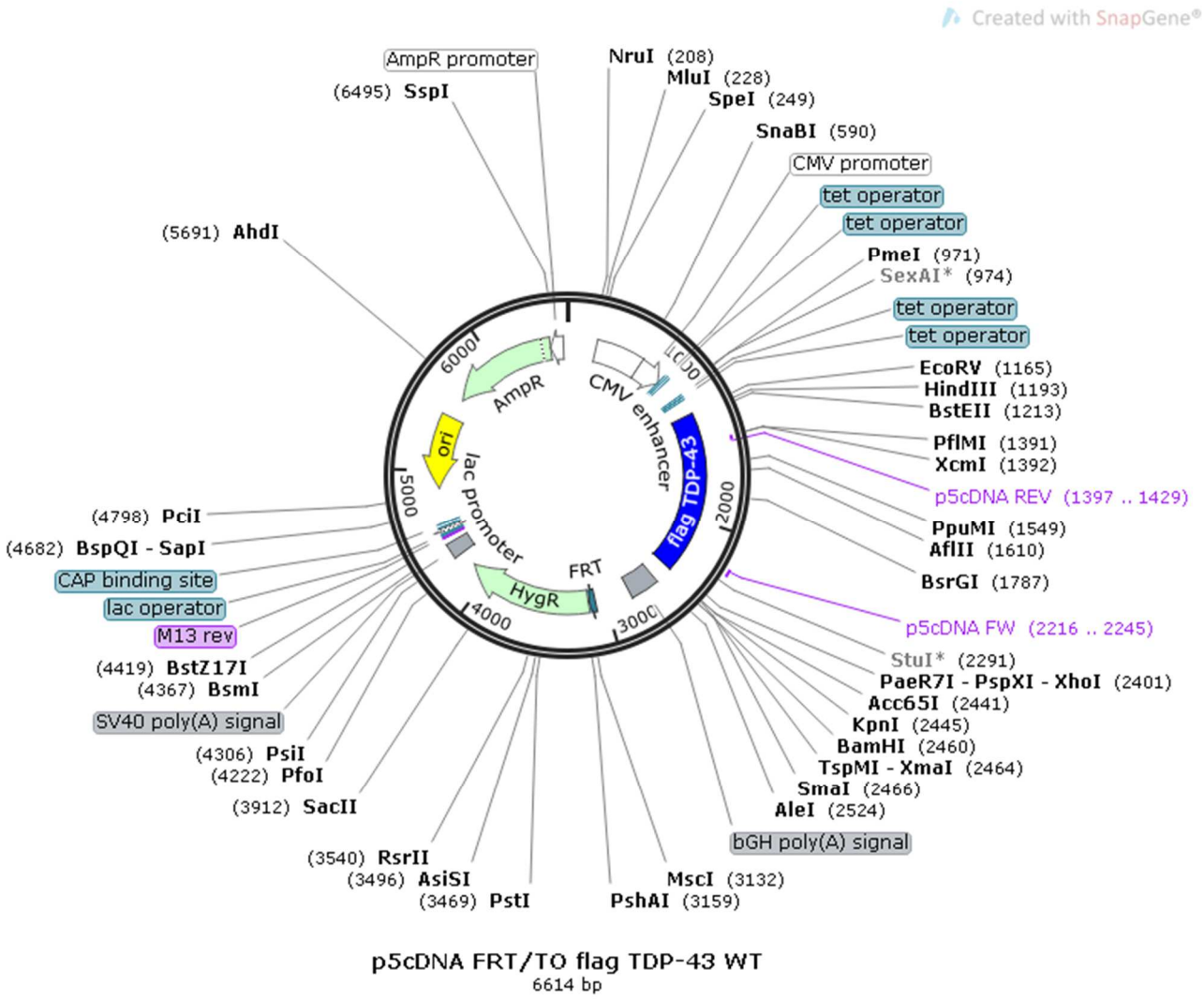

Figure 22 – p5cDNA FRT/TO flag TDP-43 map.

- pOG44 was necessary for the p5cDNA FRT/TO flag TDP-43 integration during the stable clone creation (**Fig.23**).

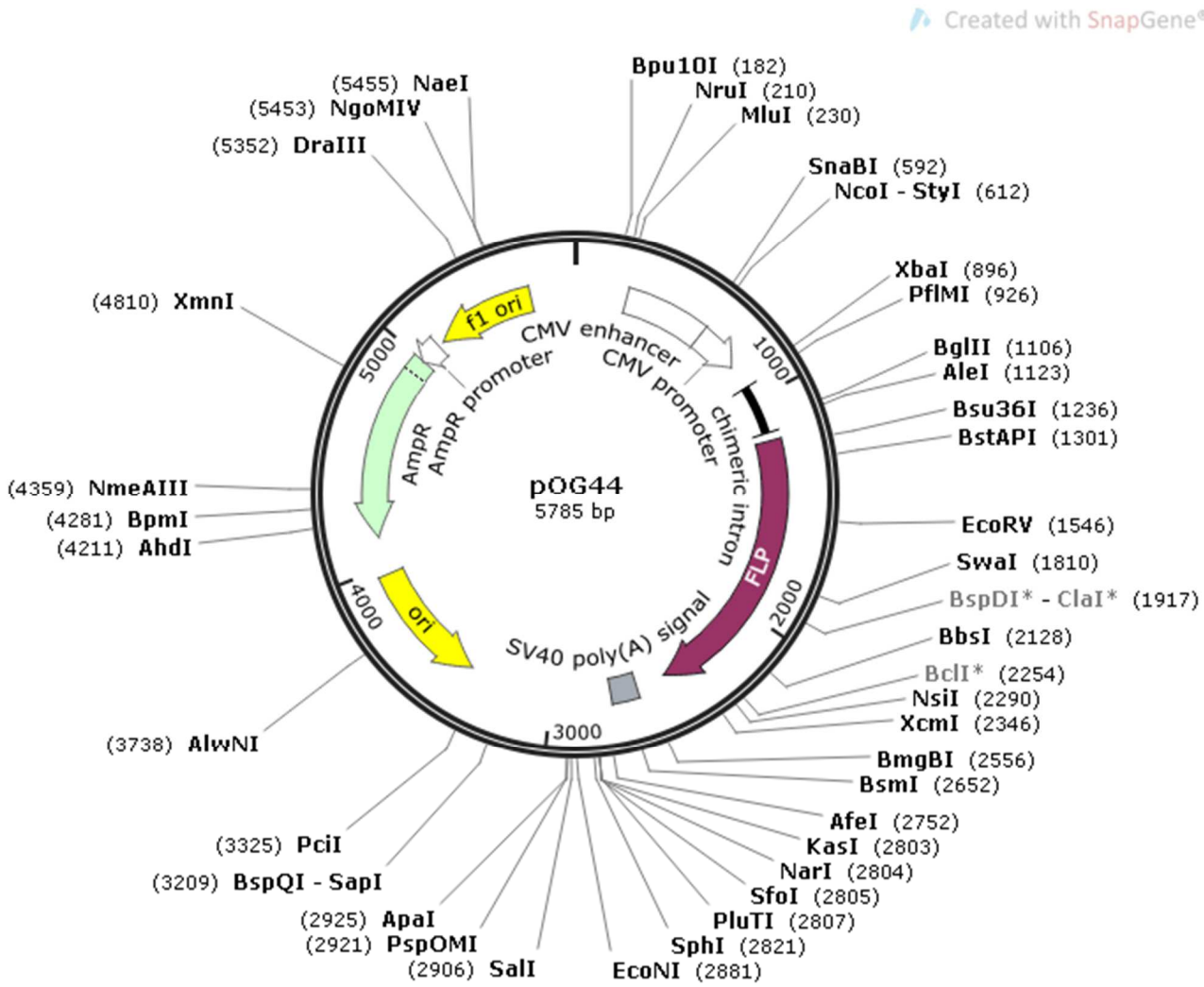

Figure 23 – pOG44 plasmid map.

3.2.2.1 Transfection in HeLa cell line and Hek293 Flp-In T-Rex (Life Technology, Carlsbad, California, USA) cell line

For the transient transfection experiments in HeLa cells and for the stable expression in Hek293 Flp-In T-Rex (Life Technology, Carlsbad, California, USA), the aforementioned plasmids were transfected with Effectene Transfection Reagent (Qiagen, Hilden, Germany), following the manufacture's instruction. Basically, the Effectene reagent is reacting in its own buffer (EC Buffer) with the Enhancer reagent forming micelles able to transport the DNA plasmid inside the cells. In table 6, the amount of reagents and plasmid are reported for the used plate.

	EC Buffer	Enhancer	Effectene	DNA plasmid

p35 (HeLa) final volume=1,5 ml D-MEM	150µl	4µl	5µl	0,5µg pTB-CFRT_Ex9 C155T
				1µg pFLAG-CMV4 TDP-43 siRNA resistant
p60 (Hek293) final volume=1,5 ml D-MEM	300µl	8µl	10µl	0,5µg pOG44
				1µg p5cDNA FRT/TO flag TDP-43

Table 6 – Effectene transfection reagents reported according to the plate volume.

First of all, the DNA plasmid was mixed together with the EC buffer and the enhancer, and this mix was left at room temperature 5 minutes. After that, the Effectene reagent was added and left 10 minutes at room temperature, and then the entire mix was administered to the cells.

3.2.2.2 Transfection in SHSy5Y ECACC cell line

The transient transfection in SHSy5Y ECACC cell line was performed for the RNA immunoprecipitation experiment, and it was carried out in p100 plates with the Lipofectamine 3000 reagent (Invitrogen, Carlsbad, California, USA). Like the Effectene reagent, also the Lipofectamine 3000 needs an enhancer for the reaction. Basically, two mix were prepared: one containing 500µl of Opti-MEM and 30µl of Lipofectamine 3000; the other one composed by 500µl of Opti-MEM, 16µg of DNA plasmid (p-CMV4 or pFLAG-CMV4 TDP-43 siRNA resistant), and 32µl of p3000, the enhancer of the reaction. Then the two solutions were mixed together and left 10 minutes at room temperature before place it in the cell media (D-MEM F-12, 9ml as final volume).

3.2.3 Generation of Constitutive Expression Cell Lines

The creation of a cell line that stably and constitutively expresses a gene/protein of interest can be a powerful tool for studying cellular processes regarding the overexpression of that protein or the consequences of a mutated form.

Hek293 Flp-In T-REx (Life Technology, Carlsbad, California, USA) cell line is designed for rapid generation of stable clones ensuring the homogenous expression of the gene/protein of interest due to the presence of a Flp Recombination Target (FRT) site. Exploiting this technology, a tetracycline inducible cell line was created by co-transfecting

the plasmid p5cDNA FRT/TO flag TDP-43, together with the pOG44. As reported in **Figure 21**, the p5cDNA FRT/TO plasmid is carrying the gene of interest, such as *TDP-43*, in frame with the flag tag, and it contains also the FRT homologous site to the one present in the cell line (Sauer, 1994). The presence of a homologous site is not enough to promote the stable integration of the gene of interest, and for this reason it is co-transfected with the pOG44 vector, that contains the Flp recombinase enzyme (O'Gorman et al., 1991). Moreover, the expression of the protein of interest is strictly controlled and it can only be detected upon tetracycline induction. Indeed, the T-REx system is based on the binding of tetracycline to the Tet repressor, releasing the promoter and, at least, leading to the constitutive expression of the gene of interest (Nelson et al., 1987; Boshart et al., 1985).

Basically, the creation of a constitutive expressing cell line takes few passages: first of all, 500000 Hek293 Flp-In T-REx cells were seeded in p60 plates, in D-MEM media containing Blasticidine S HCL (15µg/ml) (Gibco, Life Technology, Carlsbad, California, USA). The second day the cells were co-transfected with pOG44 and p5cDNA FRT/TO flag TDP-43 vectors. After 24 hours, the cells were detached with 2% trypsin-PBS[8], and plated in p100 plates. This step will allow to select mono-clones, ensuring a proper distance between the single selected cells. The day after, the D-MEM media containing the selection for the integration, such as Hygromycin (100µg/ml) (ThermoFisher Scientific, Waltham, Massachusetts, USA), was added. At this point, most of the cells died, and the single formed clones were collected and singularly plated first in 24-well plates, and then they were moved in p35. At this point, the stable clones are ready to be maintained in the double selection (blasticidine and hygromycin) or to be tested upon Anhydrotetracycline (1µg/ml) (Sigma-Aldrich, St. Louis, Missouri, USA) induction. In this work, the experiments on the stable clones were performed after 48 hours from the induction.

3.2.4 Sodium arsenate treatment

In order to induce cellular stress, the cells were treated with sodium arsenate following Colombrita and colleagues protocol (Colombrita et al., 2009). Briefly, the sodium arsenate was administrated in the cell media with the final concentration of 0.5mM, and it was left for 40 minutes in the incubator (37°C). After that, the media was removed, and cell were collected or processes for the immunofluorescence analysis.

[8] Reference to 2.8 paragraph – standard solutions

3.2.5 Toxicity study: Lactate Dehydrogenase (LDH) release toxicity assay

The LDH release assay, is a non-radioactive toxicity analysis that quantitatively measures the release of lactate dehydrogenase (LDH) derived from the cell lysis. In this work it was used the CytoTox 96® Non-Radioactive Cytotoxicity Assay (Promega, Madison, Wisconsin, USA).

Basically, 60000 cells were plated in 24-well plates in 500µl of media. After 24 hours, the cells were transfected using the Effectene method. 24, 48 and 72 hours later, the activity of LDH enzyme release by the cells was measured in relation to the toxicity of the treatment (silencing or transfection). From each well, were transferred 200µl in a tube and spun for 4 minutes at 250xg. From the supernatant, 40µL were taken and placed in triplicate in a 96-well plate. 40µL of substrate were added and the plate was left in dark for 30 minutes at room temperature. 40µL of stop solution were added in order to block the reaction. At this point the absorbance at 485nm was read due to the EnVision Multilabel Reader (PerkinElmer, Waltham, Massachusetts, USA).

The protocol is the same for each time-laps and it needs some controls:

- D-MEM, such as the medium culture without cells to test its background;
- D-MEM with cells, to test the basal toxicity without transfection;
- Maximum LDH Release Control, to test the maximum release of LDH when there is the apex of cell lysis. After 24 hours (and the same is for 48 and 72 hours) form the transfection, only in the Maximum LDH Release Control, were added 12.5µL of Lysis Buffer 10X (the final concentration must be 0.25X in 500µL) and incubated 40 minutes at 37°C.

3.2.6 Mitochondria marker: MitoTracker Red CMXRos kit (ThermoFisher Scientific, Waltham, Massachusetts, USA)

In order to track the mitochondria, the MitoTracker Red CMXRos kit (ThermoFisher Scientific, Waltham, Massachusetts, USA) was employed. This kit allows to specifically mark the mitochondria through a probe linked to red fluorescent dye. 250nM of MitoTracker Red CMXRos kit was added to the cell media, and it was left for 2 minutes. After this time, the

media was removed and the cells were prepared for the immunofluorescence assay. All the following steps were carried out in dark.

3.2.7 Multipotent stem cells derived from skin biopsies differentiated in neuronal cells

Multipotent stem cells derived from skin biopsies were cultured and differentiated by our collaborators at University Hospital *Santa Maria della Misericordia* in Udine (Italy), following their already published protocol (Dardis et al., 2016; Bergamin et al., 2013). Basically, the stem cells were enriched from patients' skin biopsies and also from already established skin fibroblast cultures at early passages, through 3 steps in selective medium composed of 60% DMEM/40% MCDB-201 (Sigma-Aldrich, St. Louis, Missouri, USA) together with 1 mg/ml Linoleic Acid-BSA (Sigma-Aldrich, St. Louis, Missouri, USA); 10-9 M dexamethasone (Sigma-Aldrich, St. Louis, Missouri, USA); 10-4 M Ascorbic acid-2 phosphate (Sigma-Aldrich, St. Louis, Missouri, USA); 1X Insulin transferrin-sodium selenite (Sigma-Aldrich, St. Louis, Missouri, USA); 2% fetal bovine serum (FBS), (STEMCELL Technologies, Vancouver, Canada), 10 ng/ml human PDGF-BB (Peprotech EC, London, UK); 10 ng/ml human EGF (Peprotech EC, London, UK) (Bergamin et al., 2013). The neuronal differentiation was performed by passing the cells in three different media: the first one, called N1, was composed by DMEM/HG with 10% FBS. After 24 hours it was replaced with the N2 fresh medium supplemented with 1% of B27 (Invitrogen, Carlsbad, California, USA), 10 ng/ml EGF (Peprotech EC, London, UK) and 20 ng/ml bFGF (Peprotech EC, London, UK). The cells were left for 5 days, and then they were incubated for 24/48 hours in N3 medium, composed by DMEM supplemented with 5 µg/ml insulin, 200 µM of indomethacin and 0.5 mM IBMX (all from Sigma-Aldrich, St. Louis, Missouri, USA) without FBS. The differentiation was determined by analyzing the expression of the neuron specific markers, such as NeuN and tubulin b3 (Dardis et al., 2016; Bergamin et al., 2013).

3.3 Propidium iodide cell cycle assay and flowcytometry analysis

500000 Hek293 Flp-In T-REx cells were plated in p35 with the D-MEM tetracycline selective medium. After 48 hours from the induction, the cells were collected and resuspended in 300µl of ice-cold PBS and 700µl of Ethanol (Honeywell, Charlotte, North Carolina, USA) were added. The cells were resuspended and kept at -20°C. After few hours, the cells were centrifuged 5 minutes at 500xg, and the supernatant was discarded. The pellet was carefully resuspended with 500µl of 0.1% of Nonidet P40 (ThermoFisher Scientific, Waltham, Massachusetts, USA) (NP40)-PBS supplemented with of RNase (Sigma-Aldrich, St. Louis, Missouri, USA) (10mg/ml), and propidium iodide (5µg/ml) (Sigma-Aldrich, St. Louis, Missouri, USA), and it was left 15 minutes in dark at room temperature. At this point the flowcytometry analysis was performed using FACS Calibur (Becton Dickinson, Franklin Lakes, New Jersey, USA). The gates were set based on physical parameters (side and forward scatted), and excluding/distinguishing the aggregates from the dividing cells (relation between area and breadth). The histogram representing the percentage of the events in the different phase of the cell cycle (G1, G2, S/M) was then created applying a third gate comparing the height and the signal intensity. In this way it was possible to distinguish the diploids (G1) from tetraploids (G2). The raw data were analyzed using FlowJoVX 64-bit software (FlowJo LLC Becton Dickinson, Ashland, Oregon, USA).

3.4 Immunohistochemical and immunocytochemical analysis

3.4.1 Immunohistochemical analysis on brain region derived from S375G patient

The immunohistochemical analysis on the S375G patient brain and spinal cord was carried out by our colleagues at University of Kansas School of Medicine, in Kansas City (USA). Basically, they harvested the brain and the spinal cord 24 hours after death. The right hemi-brain was sectioned fresh, while the left hemi-brain was fixed in 10% buffered formalin solution. For the neurohistopathological studies, they processed different 5 µm-thick formalin-fixed sections derived from multiple areas of the central nervous system, including middle frontal, primary motor, cingulate, temporal, insular, parietal and occipital cortex, hippocampus, caudate nucleus, putamen, globus pallidus, amygdala, thalamus, cerebellar cortex, dentate nucleus, midbrain, pons, medulla, cervical, thoracic, lumbar, and sacral levels of the spinal cord. They stained the sections with hematoxylin and eosin with Luxol Fast Blue, and they evaluated the presence of phosphorylated and non-phosphorylated TDP-43 using, respectively, phosphorylated TDP-43 antibody (pS409/410, monoclonal, Cosmo Bio, Tokyo, Japan), and non-phosphorylated TDP-43 antibody (polyclonal, Proteintech Group, Chicago, IL) (Newell et al., 2018).

3.4.2 Immunocytochemical analysis

primary antibody	host	dilution	media	company	secondary antibody	host	dilution	media	company
α-flag M2	mouse	1:200	2%BSA /PBS	Sigma-Aldrich (St. Louis, Missouri, USA)	α-mouse Alexafluor 594	donkey	1:500	2%BSA /PBS	Invitrogen (Carlsbad, California, USA)
α-TDP-43	rabbit	1:200	2%BSA /PBS	Proteintech EU (Manchester, UK)	α-rabbit Alexafluor 594	donkey	1:500	2%BSA /PBS	Invitrogen (Carlsbad, California, USA)
α-phospho TDP-43 (pS409/410)	rabbit	1:200	2%BSA /PBS	Cosmo Bio (Tokyo, Japan)	α-rabbit Alexafluor 594	donkey	1:500	2%BSA /PBS	Invitrogen (Carlsbad, California, USA)
α-AIF1	mouse	1:100	0,1M glycine/ PBS	Invitrogen (Carlsbad, California, USA)	α-mouse Alexafluor 488	donkey	1:600	1X PBS	Invitrogen (Carlsbad, California, USA)

Table 7 – Immunocytochemical analysis: pramary and secondary antibodies.

3.4.2.1 Standard immunofluorescence assay

According to the cellular type and the assay, on a cover glass (Corning, New York, USA) were plated:

- 300000 cells for HeLa and Hek293 Flp-In T-REx;
- 800000 cells for SH-Sy5Y ECACC.

Because Hek293 Flp-In T-REx and SH-Sy5Y ECACC are not prone to attach to the cover glass surface, it has been coated with poly-L-lysine solution at a final concentration of 0.01% (w/v) in H_20 (Sigma-Aldrich, St. Louis, Missouri, USA) for 20 minutes. After this incubation time, the poly-L-lysine was carefully removed and the cover glass was washed for three times with sterile water, and it was air-dried for 1 hour under a hood.

The immunofluorescence protocol was carried out after different assays were performed on the cell lines, like gene knockdown, protein overexpression, sodium arsenate treatment, tetracycline induction, etc. and it was carried out over two days. During day one, the cell media was removed and the cells were carefully washed one time with 2ml of 1X PBS. Then, the cells were fixed with 2ml of 3.2% para-formaldehyde (PFA) (Electron Microscopy Science, Hatfield, Pennsylvania, USA) in 1X PBS for 1 hours at room temperature. PFA was removed, and the slides were washed 3 times with 2 ml of 1X PBS. Cell permeabilization was performed with 2ml of 0.3%Triton (Sigma-Aldrich, St. Louis, Missouri, USA) in 1X PBS, left for 5 minutes in ice. Triton was removed and the slides were washed three times with 2ml of 1X PBS. In order to block non-specific sites, 1.5ml of 2%BSA/1XPBS were added to the slides for 20 minutes at room temperature. The slides were lifted up and incubated face down with 60 µL of the primary antibody (table 7) diluted in 2%BSA/1XPBS, and they were left overnight at 4°C in a dark humidified chamber. The day after, the slides were lifted up with 1ml of 1XPBS and they were washed twice with 2ml of 1XPBS. The slides were incubated face down with 60µL of the secondary antibody (table 7) diluted in 2%BSA/1XPBS for 1 hour in a dark humidified chamber. In the meantime, the SUPERFROST coverslip (ThermoFisher Scientific, Waltham, Massachusetts, USA) were cleaned with 100% isopropanol (Honeywell, Charlotte, North Carolina, USA). After the incubation time, the slides were picked up with 1ml of 1XPBS and they were washed twice with 2ml of 1X PBS. The slides were placed face down on the coverslip with 18µL of Vectashield with DAPI applied (Vector Laboratories Inc., Burlingame, California, USA). The slides were sealed with nail polish and stored in dark at 4°C.

The slides were analyzed with Nikon Elements AR 4.40.00 64-BIT confocal microscope (Nikon, Minato, Tokyo, Japan), and with LEICA epifluorescent microscope (Leica, Wetzlar, Germany).

3.4.2.2 Immunocytochemical assay: mitochondria and Apoptosis Inducing Factor 1 (AIF1) protein tracking

In order to detect the Apoptosis Inducing Factor 1 (AIF1) protein an optimized protocol was set-up. AIF1 is not ubiquitously expressed among various cells, but is normally localized in the mitochondria. The mitochondria structure was detected with the MitoTracker Red CMXRos kit (ThermoFisher Scientific, Waltham, Massachusetts, USA), while AIF1 protein with mouse α- AIF1 monoclonal antibody (Invitrogen, Carlsbad, California, USA) (table 7). After the incubation with the MitoTracker Red CMXRos kit[9], the media was removed and the cells, plated on the coverslip, were washed with 2ml of 1XPBS. The slides were fixed with 3.2% para-formaldehyde (PFA) (Electron Microscopy Science, Hatfield, Pennsylvania, USA) in 1XPBS for 20 minutes at room temperature, in dark. The PFA was removed, and the slides were washed three times with 2ml of 1XPBS. The cells were then permeabilized with 2ml of 0.3%Triton (Sigma-Aldrich, St. Louis, Missouri, USA) in 1XPBS, left for 5 minutes at room temperature in dark. Three washes with 1XPBS were followed. The block of non-specific sites was performed by incubating the slides with 0.1M glycine/PBS for few minutes. The slides were then incubated face down, in a dark humidified chamber, with 60µl mouse α- AIF1 monoclonal antibody (Invitrogen, Carlsbad, California, USA) (table 7), at 37°C overnight. The day after, the slides were recovered, washed three times with 1X PBS, and they were incubated with 60µl of secondary antibody (table 7). The incubation lasted for 30 minutes in a dark humidified chamber at 37°C. Three washes with 1X PBS were followed. The nuclei staining was performed with bisbenzimide H33342 trihydrochloride (Hoechst) (Sigma-Aldrich, St. Louis, Missouri, USA) (1µg/µl) diluted 1:1000 in 2ml of 1X PBS, left for 10 seconds. The slides were washed three times with 2ml of 1X PBS, and then three times with 2ml of sterile water. The slides were blocked with a drop of Mowiol mounting medium (Sigma-Aldrich, St. Louis, Missouri, USA) and nail polish.

[9] Reference to 2.2.6 paragraph – 2.2.6 Mitochondria marker: MitoTracker Red CMXRos kit (ThermoFisher Scientific, Waltham, Massachusetts, USA).

The slides were analyzed with LEICA epifluorescent microscope (Leica, Wetzlar, Germany).

3.4.2.3 Region of Interest (ROI) calculation

For the quantitative analysis, the Regions of Interest (ROIs) were selected from the gray scale, monochromatic images, using Fiji win-64 (ImageJ) software, and their fluorescence signals were measured in arbitrary units. For each condition, the average ratio between the cytoplasmic and nuclear signal, was plotted in a grouped graph with standard deviation and number of analyzed samples using GraphPad software (GraphPad Software, La Jolla California, USA).

3.5 Protein and Peptide analysis

3.5.1 Nuclear-cytoplasmic fractionation

For the nuclear-cytoplasmic separation, the NE-PER (Nuclear and Cytoplasmic Extraction Reagents) (ThermoFisher Scientific, Waltham, Massachusetts, USA) kit was employed. This kit allows a stepwise separation of cytoplasmic and nuclear extracts from mammalian cultured cells or tissue.

1-10 × 10^6 cells were seeded in p100 plates, two for each condition. After the treatment, the cells were collected in 5ml tubes and they were centrifuged 5 minutes at 500xg. The pellet was resuspended in 500µl of 1X PBS and the two replicates were combined in the same tube. The resuspended cells were transferred in 1.5ml tube and they were centrifuged 5 minutes at 500xg. The supernatant phase was discarded. The pellet was resuspended with the amount of CER I buffer necessary for the packed cell volume (table 8). The resuspended cells were vortexed 15 seconds at maximum speed, and they were left 10 minutes in ice. The CER II buffer was added and the sample was vortexed 5 seconds at maximum speed. It was left 1 minutes in ice and then it was centrifuged 5 minutes at 16000xg. The supernatant, such as the cytoplasmic fraction, was collected and stored at -80°C. In order to remove the remaining cytoplasmic fraction, the pellet was washed with 1X PBS and well resuspended. It was centrifuged 5 minutes at 16000xg. An additional step with CER I buffer was performed, then the sample was centrifuged at 16000xg 5 minutes, and the supernatant discarded. At this point the nuclear fraction can be extracted: the remaining pellet was resuspended with NER buffer, and it was vortex 15 seconds at maximum speed four times, leaving the sample at room temperature for 10 minutes between each vortex session. The sample was centrifuged 10 minutes at 16000xg, and the supernatant, such as the nuclear faction, was recovered. The nuclear fraction and the remaining pellet were stored at -80°C.

Packed cell volume (µl)	CER I (µl)	CER II (µl)	NER (µl)
10	100	5,5	50
20	200	11	100
50	500	27,5	250
100	1000	55	500

Table 8 - NE-PER Nuclear and Cytoplasmic Extraction reagents volumes according to packed cell volume.

The sample concentrations were measured with Bradford (Biorad, Hercules, California, USA) method[10], and 20µg of sample were loaded in a Sodium Dodecyl Sulphate (SDS) gel electrophoresis together with 4X NuPAGE LDS Sample Buffer (ThermoFisher Scientific, Waltham, Massachusetts, USA).

3.5.2 Solubility assay: soluble-insoluble fractionation

The solubility assay allows to detect the aggregative status of a protein by dividing the cell lysate in two fractions: supernatant, with soluble proteins, and pellet, containing the insoluble fraction.

The cells were seeded at 70% confluency in p100 plates, and they were collected and resuspended in 1mL of 10X RIPA buffer (Cell Signaling Technology, Danvers, Massachusetts, USA). After 2 minutes at room temperature, the sample was rotated for 30 minutes at 4°C. Following, it was centrifuged at 7000xg for 30 minutes at room temperature. The whole supernatant was transferred in a 1.5 ml tube, and it was sonicated in an ice-cooled sonicating bath (BioRuptor UCD-200, Diagenode, Belgium) for 5 minutes at high impulse (30 seconds on, 30 seconds off), obtaining the protein subcellular fraction. The protein concentration was calculated with Bradford (Biorad, Hercules, California, USA) method. At this point, 60µg of sonicated samples were mixed with 10µL of 4X NuPAGE LDS Sample Buffer (ThermoFisher Scientific, Waltham, Massachusetts, USA), representing the input; and then it was stored at -20°C. On the other hand, 600µg of lysate were mixed with 10X RIPA buffer (Cell Signaling Technology, Danvers, Massachusetts, USA) until they reach 500µL of final volume, and they were transferred in Beckman polycarbonate thick wall Centrifuge tube (Beckman Coulter, Brea, California, USA). The sample was ultra-centrifuged with the OptimaTM L-90K Ultracentrifuge (Beckman Coulter, Brea, California, USA) at the following conditions:

- 121968xg;
- 1 hour;
- 25°C;
- acceleration: SLOW;
- deceleration: SLOW.

[10] Reference to 2.5.3.3 paragraph – Bradford method

50µL, such as 1/10 of ultra-centrifuged sample, were added to 10µL of 4X NuPAGE LDS Sample Buffer (ThermoFisher Scientific, Waltham, Massachusetts, USA), representing the supernatant phase; and it was stored at -20°C. The left supernatant was collected in other tube and stored at -20°C. The remaining pellet was washed two times with 100µL of 10X RIPA buffer (Cell Signaling Technology, Danvers, Massachusetts, USA), and then it was resuspended with 100µL of urea buffer[11]. 10µL of the resuspended pellet fraction were mixed with 10µL of 4X NuPAGE LDS Sample Buffer (ThermoFisher Scientific, Waltham, Massachusetts, USA) and it was stored at -20°C. All the collected fractions were stored at -20°C.

The samples, mixed with 4X NuPAGE LDS Sample Buffer (ThermoFisher Scientific, Waltham, Massachusetts, USA), were ready to be loaded in a SDS PAGE gel, following a denaturation step.

3.5.3 Sodium Dodecyl Sulphate (SDS) - Polyacrylamide Gel Electrophoresis (SDS-PAGE) and Western Blot assay

3.5.3.1 Sample preparation: brain tissue

25mg of frozen formalin-fixed sections derived from multiple areas of the central nervous system, were cut and put in 230µl of 10X RIPA buffer (Cell Signaling Technology, Danvers, Massachusetts, USA), with 20µl of Protease Inhibitor Cocktail (25X) (Roche, Basel, Switzerland). The samples were sonicated two times in an ice-cooled sonicating bath (BioRuptor UCD-200, Diagenode, Belgium), 10 minutes each at high impulse (30 seconds on / 30 seconds off). Bradford (Biorad, Hercules, California, USA) colorimetric assay was performed to calculate the protein concentration, loading in the gel 10µg for each sample, together with 4X NuPAGE LDS Sample Buffer (ThermoFisher Scientific, Waltham, Massachusetts, USA). The samples were stored at -20°C.

[11] Reference to 2.8 paragraph – standard solutions

3.5.3.2 Sample preparation: cell lysate

For protein detection, the samples derived from cell culture were resuspended in 100µl of 1X PBS with 1X of Protease Inhibitor Cocktail (25X) (Roche, Basel, Switzerland). The cell lysate was obtained by sonicating the samples two times in an ice-cooled sonicating bath (BioRuptor UCD-200, Diagenode, Belgium), 5 minutes each, at high impulse (30 seconds on, 30 seconds off). At this point, the sample concentration was detected using Bradford (Biorad, Hercules, California, USA) colorimetric method, and from 10 to 20µg of samples were loaded in the SDS-PAGE gel, together with 4X NuPAGE LDS Sample Buffer (ThermoFisher Scientific, Waltham, Massachusetts, USA). The samples were stored at -20°C.

3.5.3.3 Sample preparation: concentration detection using Bradford colorimetric assay

Bradford colorimetric assay was used to detect protein concentration in order to load the same amount of sample for each condition. Protein assay Day Reagent Concentrated solution (Biorad, Hercules, California, USA) was diluted 1:5 in the cell resuspended media and 5µl of samples were added to a final volume of 1ml. The absorbance at 595nm was read with the D30 Eppendorf BioSpectometre (Eppendorf, Hamburg, Germany), and the final sample concentration was calculated basing on a standard curve created with scalar dilution of Bovine Serum Albumin (BSA) protein with a well-known starting concentration.

3.5.3.4 Sample preparation: denaturation

According to the experiment and to the protein that needs to be detected, 10 to 20µg of samples were loaded in the SDS-PAGE. Before loading them on the gel, the samples were denaturated together with 4X NuPAGE LDS Sample Buffer (ThermoFisher Scientific, Waltham, Massachusetts, USA) for 5 minutes at 85°C. A brief centrifuged was performed before loading the gel.

3.5.3.5 Sodium Dodecyl Sulphate - Polyacrylamide Gel Electrophoresis (SDS-PAGE)

Sodium Dodecyl Sulphate - Polyacrylamide Gel Electrophoresis (SDS-PAGE) is the most common electrophoretic technique employed to study proteins separation based on

their molecular weight. Combined with the Western Blot technique, the protein of interest can be detected with specific antibodies.

In this work, SDS PAGE was carried out using NuPAGE Bis-Tris 1.5mm precast gels (ThermoFisher Scientific, Waltham, Massachusetts, USA) 10% concentrated, and they were run with 1X NuPAGE MOPS SDS Running Buffer (20X) (ThermoFisher Scientific, Waltham, Massachusetts, USA). Gradient 4-12% NuPAGE Bis-Tris 1.5mm precast gels (ThermoFisher Scientific, Waltham, Massachusetts, USA) were used to better separate ITPR1, a high molecular weight protein. Together with the samples, Blue Protein Standard Broad Range (P7706S) (New England Biolabs, Ipswich, Massachusetts, USA), and SHARPMASS VII (EPS026500) (Euroclone S.P.A., Pero, Italy) were respectively loaded as molecular weight markers.

3.5.3.6 Western Blot assay

The western Blot technique provides the transfer of the separated proteins from the gel to a membrane in order to detect specific proteins using a couple of antibodies: the primary antibody, which will recognize the specific target; and the secondary antibody, that recognize the primary, and it is conjugated with a chemiluminescent molecule.

In this work the transfer from the gel to the membrane was performed with Power Blotter–Semi-dry Transfer System (ThermoFisher Scientific, Waltham, Massachusetts, USA), using Power Blotter Pre-cut Membranes and Filters, Nitrocellulose (ThermoFisher Scientific, Waltham, Massachusetts, USA). The blot lasted for 15 minutes, using a pre-programmed method (25V, 1.3A) for 1.5mm gels.

To control the correct transfer, the nitrocellulose membrane was stained with Pierce Reversible Protein Stain Kit for Nitrocellulose Membranes (ThermoFisher Scientific, Waltham, Massachusetts, USA), and the image was acquired with Alliance 9.7 Western Blot Imaging System (UVITEC, Cambridge, UK).

After the Pierce Reversible Protein Stain was removed, the membrane was blocked with 4% skimmed milk (Non-fat dry milk) or 3% Bovine Serum Albumin (BSA) (Sigma-Aldrich, St. Louis, Missouri, USA) in 1X PBS and 0.1%/0.01% Tween-20 (Sigma-Aldrich, St. Louis, Missouri, USA) (PBST), depending on the antibody (table 9). The blocking lasted for

around 1 hour. The primary antibody was incubated overnight at 4°C, and the day after three washes, of 5 minutes each, with PBST were performed.

primary antibody	host	dilution	media	blocking media	PBST	company
α-flag M2	mouse	1:1000	2%milk/PBST	4%milk/PBST	0,10%	Sigma-Aldrich (St. Louis, Missouri, USA)
α-TDP-43	rabbit	1:1000	2%milk/PBST	4%milk/PBST	0,10%	Proteintech EU (Manchester, UK)
α-phospho TDP-43 (pS409/410)	rabbit	1:1000	1,5%BSA/PBST	3%BSA/PBST	0,01%	Cosmo Bio (Tokyo, Japan)
α-AIF1	mouse	1:500	milk2%/PBST	4%milk/PBST	0,10%	Invitrogen (Carlsbad, California, USA)
α-ITPR1 (P3 Recptor 1)	rabbit	1:500	2%milk/PBST	4%milk/PBST	0,10%	Invitrogen (Carlsbad, California, USA)
α-tubulin	mouse	1:10000	2%milk/PBST	4%milk/PBST	0,10%	home made
α-P84	mouse	1:1000	2%milk/PBST	4%milk/PBST	0,10%	Abcam (Cambridge, UK)
α-CDK6	mouse	1:500	1,5%BSA/PBST	3%BSA/PBST	0,01%	Santa Cruz Biotechnology (Dallas, Texas, USA)

Table 9 – Primary antibodies, dilution and blocking media, and their final concentrations are reported.

The secondary antibody (table 10) was incubated for 2 hours at room temperature. 5 minutes washes with PBST were performed for three times. To detect the chemiluminescence, the membrane was incubated 2 minutes with ECL Luminata Classico Western HRP substrate (Merck Millipore, Burlington, MA, USA), and the images were acquired using Alliance 9.7 Western Blot Imaging System (UVITEC Limited, Cambridge, UK).

secondary antibody	host	dilution	media	blocking media	PBST	company
α-rabbit HRP	goat	1:2000	2%milk/PBST	4%milk/PBST	0,10%	Dako (Santa Clara, California, USA)
			1,5%BSA/PBST	3%BSA/PBST	0,01%	
α-mouse HRP	goat	1:2000	2%milk/PBST	4%milk/PBST	0,10%	

			1,5%BSA/PBST	3%BSA/PBST	0,01%	

Table 10 - Secondary antibodies, dilution and blocking media, and their final concentrations are reported.

Western Blot image quantification was carried out with Alliance 9.7 Western Blot Imaging Software (UVITEC Limited, Cambridge, UK).

3.5.4 Molecular Dynamic Simulation on peptides

The Molecular Dynamics simulations were performed by our colleagues at University of Castile-La Mancha, *Instituto Regional de Investigación Científica Aplicada*, in Ciudad Real (Spain). Briefly, the molecular dynamic simulation was based on the structure of NNSYSG peptide, that was modeled using ZipperDB database. They generated the S375G and S375E variants from the NNSYSG peptide taking advantage of PyMOL software. In all simulations, all the described structures were solved using TIP3P water molecules, pre-equilibrated at 1 atm and 300 K, and then individually submitted to 50-ns Molecular Dynamics simulations (Newell et al., 2018).

3.6 Nucleic acids analysis

3.6.1 DNA extraction and genetic analysis of the S375G patient's brain tissue

This was performed by our colleagues at University of Kansas School of Medicine, in Kansas City (USA). Genomic DNA was extracted from frozen brain tissue and the products were treated with ExoSAP-IT (USB, Cleveland, OH, USA). They were then amplified using the DTCS Quick Start Kit (Beckman Coulter, Fullerton, CA, USA), and the products were analyzed on a CEQ 8000 GeXP Genetic Analysis System (Beckman Coulter). A comparison between the resulting DNA with the known sequences (www.ncib.nlm.nih.gov) was carried out (Newell et al., 2018; Murrell et al., 1991).

3.6.2 RNA extraction

3.6.2.1 Sample preparation: brain tissue

In order to preserve the RNA tissue from freeze/thaw cycles, the frozen formalin-fixed sections derived from multiple areas of the central nervous system, were kept on dry ice; less than 50mg was cut. 700µl of QIAzol Lysis Reagent (Qiagen, Hilden, Germany) were added and the sample were homogenized with Utra-Turax T25 basic (IKA-WERKE GMBH & CO, Staufen im Breisgau, Germany) for 7 seconds. At this point, the RNA was extracted from the tissue.

3.6.2.2 Sample preparation: cell lysate

For RNA extraction, the cells were collected and the medium was removed. In order to better remove the culture medium, the cell pellet was washed with 1X PBS and centrifuged 5 minutes at 500xg, discarding the supernatant. At this point the cells were resuspended in 700µl of QIAzol Lysis Reagent (Qiagen, Hilden, Germany) and the RNA extraction was performed.

3.6.2.3 miRNeasy Mini Kit (Qiagen, Hilden, Germany)

In this work the RNA was extracted with the miRNeasy Mini Kit (Qiagen, Hilden, Germany), with some adjustment from the manufacturer's instructions. Briefly, the samples

(homogenized tissue or cell lysate) were transferred in 5PRIME Phase Lock gel tubes (Quantabio, Beverly, Massachusetts, USA), pre-centrifuged at 1500xg for 30 seconds, and the sample was left 5 minutes at room temperature. 140µl of chloroform (Sigma-Aldrich, St. Louis, Missouri, USA) were added; to mix the two reagents, the 5PRIME Phase Lock gel tubes were vigorously shaken and the samples were left 5 minutes at room temperature. To separate the phases and obtaining the aqueous/RNA supernatant, the samples were centrifuged at 4°C 10 minutes at 16000xg. The 5PRIME Phase Lock gel interposes the gel phase between the aqueous phase and the Qiazol one, containing what needs to be discarded. In this way, the supernatant is cleaner and it was easily collected and moved it into another collection tube where 1.5 volume of 100%ethanol (Honeywell, Charlotte, North Carolina, USA) was added. After this first separation, the RNA was extracted with the miRNeasy kit (Qiagen, Hilden, Germany): 700µl of the sample were pipetted on the RNeasy Mini spin column and it was centrifuge at 8000xg for 15 seconds at room temperature. The flow through was discarded. This step was repeated for the remaining sample. 700µl of buffer RWT were added upon the column and it was centrifuged at 8000xg for 15 seconds at room temperature. Again, the flow through was discarded. Two steps of washing with 500µl of Buffer RPE were performed, centrifuging the samples at 8000xg for 15 seconds at room temperature. The second centrifuge step was performed for 2 minutes at 8000xg, in order to remove any ethanol residues. The column was placed on 2ml another collection tube and it was centrifuged at full speed for 1 minute to eliminate RPE buffer residuals. At this point the RNA was eluted: the column was put on 1.5ml collection tube and 30µl of RNase-free water were added. The column was centrifuged at 8000xg for 1 minute and the RNA was eluted.

RNA concentration and the purification level were measured with D30 Eppendorf BioSpectometre (Eppendorf, Hamburg, Germany), using the Eppendorf µCuvette G1.0 (Eppendorf, Hamburg, Germany). The absorbance at 260nm was measured together with the ratio between the absorbance at 260/280nm (protein contamination) and at 260/230nm (reagents contamination).

3.6.3 Reverse transcription reaction: complementary DNA (cDNA) preparation

Starting from the extracted RNA, the complementary DNA (cDNA) was retrotranscribed with Moloney Murine Leukemia Virus Reverse Transcriptase (M-MLV RT)

(Invitrogen, Carlsbad, California, USA), in the presence of random primers (Sigma-Aldrich, St. Louis, Missouri, USA). Two mixes were prepared: the first one containing the RNA and the random primers with the concentrations reported in table 11. To reach the final volume of 20µl, sterile water was added. With this composition, the first mix was chilled at 85°C for 5 minutes, it was briefly centrifuged, and the sample was cooled in ice for 1 minute.

reagent	**final concentration (final volume=20µl)**
RNA	50ng/µl
random primers (100ng/ml) (Sigma-Aldrich, St. Louis, Missouri, USA)	1ng/µl

Table 11 – cDNA preparation: mix 1 containing random primers and RNA.

At this point, 20µl of the second mix were added. The second mix composition is reported in table 12.

reagent	**final concentration (final volume=20µl)**
5X M-MLV buffer	2X
Dithiothreitol (DTT) (100mM) Invitrogen (Carlsbad, California, USA)	20mM
Deoxynucleotide (dNTP) Solution Mix (2,5mM) (Rovalab, Teltow, Germany)	0,5mM
M-MLV (200 U/µl)	5 U/µl

Table 12 - cDNA preparation: mix 2 containing reverse transcription reaction reagents.

M-MLV reaction was carried out at 37°C for 1-2 hours. The samples were then stored at -20°C before using for gene expression or splicing analysis.

3.6.4 Pre-mRNA splicing analysis

Pre-mRNA splicing analysis was carried out by using the Polymerase Chain Reaction (PCR) technique, and it was performed in 50µl of final reaction volume, composed by 3µl of cDNA (or sterile water for the negative control sample) and 37µl of PCR mix (table 13). To reach the final volume, sterile water was added.

reagent	**final concentration (final volume=50µl)**

10X ThermoPol reaction Buffer (New England Biolabs, Ipswich, Massachusetts, USA)	1X
Deoxynucleotide (dNTP) Solution Mix (2,5mM) (Rovalab, Teltow, Germany)	0,2mM
Primer forward (100ng/µl)	3ng/µl
Primer reverse (100ng/µl)	3ng/µl
Taq Biolabs 5 U/µl (New England Biolabs, Ipswich, Massachusetts, USA)	0,02U/µl

Table 13 – PCR reaction mix.

The pre-mRNA splicing was tested for the cDNA extracted from the HeLa cells, knockdown for *TDP-43* and transient transfected with mutant TDP-43 plasmids (addback experiment); and from the stable cell lines expressing constitutively TDP-43 mutated forms. For the HeLa cells, the pre-mRNA splicing assay was performed on the minigene containing the exon 9 of the *CFTR* gene. The minigene technique allows to recreate a splicing event when transfected into cells. In this work, the minigene system is carrying CFTR exon 9 and a small portion of intron 8 and 9, including a mutation in a splicing enhancer element in order to obtain a 50/50 ratio of exon inclusion/skipping. On the other hand, the pre-mRNA splicing analysis was carried out using one of the best characterize endogenous TDP-43 target, such as *DNA Polymerase Delta Interacting Protein 3* (*POLDIP3*) gene. In table 14 are reported the primer sequences.

Name	**Sequence 5' → 3'**	
α2-3	CAACTTCAAGCTCCTAAGCCACTGC	pTB-CFTR_Ex9 C155T
BRA2	CACCAGGAAGTTCCTTAAATCA	
POLDP3ex2	GCTTAATGCCAGACCGGGAGTTGGA	POLDIP3
POLDP3ex4	TCATCTTCATCCAGGTCATATAAATT	

Table 14 – Pre-mRNA splicing primer sequences.

The two experiments required different PCR protocols in order to optimize the fragments amplification (table 15) and they were carried out with MiniAmp Plus Thermal Cycler (Applied Biosystem, Foster City, California, USA).

target	**temperature**	**time**	**cycles**
pTB-CFTR_Ex9 C155T	95°C	2 minutes	
	94°C	45 seconds	35
	54°C	45 seconds	
	72°C	45 seconds	
	72°C	10 minutes	
	4°C	∞	
POLDIP3	94°C	2 minutes	

	94°C	30 seconds	35
	56°C	1 minute	
	72°C	45 seconds	
	72°C	10 minutes	
	4°C	∞	

Tabella 15 – Pre-mRNA splicing protocols.

PCR products were then run with the QIAxcel DNA Screening Kit (Qiagen, Hilden, Germany), providing the separation of the nucleic acid basing on size, using a capillary filled with a precast agarose gel. Before starting, the cartridge was immerged in the QX Wash Buffer (Qiagen, Hilden, Germany) for 20 minutes. For the running, the instrument requires two different markers to separate correctly the samples and to identify the size of the DNA fragments: the QX Alignment Marker 15 bp/3 kb (Qiagen, Hilden, Germany), that establishes the range in which identify the bands; and the QX DNA Size Marker 50 bp – 1.5 kb (Qiagen, Hilden, Germany), that gives information about the fragment size. The size marker must be included in the range of the alignment marker and together create the reference marker. At this point, 15µl of sample were loaded in the QX 0.2 ml 12-Tube Strips (Qiagen, Hilden, Germany) and the run was performed using the AM420 method. The QIAxcel DNA Screening Kit (Qiagen, Hilden, Germany) output generate a gel image, for the qualitative analysis, and the electropherogram, by which it is possible to quantify the signal intensity calculating the Area Percentage of the electropherogram peaks. The obtained data were then analyzed with GraphPad software (GraphPad Software, La Jolla California, USA).

3.6.5 Gene expression analysis: real time quantitative PCR (qPCR)

Gene expression analysis was performed on cDNA prepared from:

- S375G patient brain samples in order to study *TDP-43* expression, using the hippocampal TDP-43 as the internal control. To normalize the results, *Glyceraldehyde-3-phosphate Dehydrogenase* (*GAPDH*) was used as the housekeeping gene;
- Multipotent stem cells, differentiated in neurons derived from NPC patients and healthy controls, in order to validate RNA sequencing data, especially regarding the following genes: *Cadherin 18* (*CDH18*), *Doublecortin Like Kinase 1* (*DCLK1*), *DEP Domain Containing MTOR Interacting Protein* (*DEPTOR*), *Cell Adhesion Associated, Oncogene Regulated* (*CDON*), *Leucine Rich Repeat Containing G Protein-Coupled Receptor 4* (*LGR4*), *Inositol 1,4,5-Trisphosphate Receptor Type 1* (*ITPR1*), *Lymphocyte Cytosolic Protein 1* (*LCP1*), *SH3 And Multiple Ankyrin Repeat Domains 1* (*SHANK1*), *Ependymin*

Related 1 (*EPDR1*), and *TDP-43*. *Glyceraldehyde-3-phosphate Dehydrogenase* (*GAPDH*) and *Hypoxanthine Posphoribosyltransferase 1* (*HPRT1*) expression was not changing between the NPC and healthy samples, so they were employed as housekeeping genes to normalize the results.

- On SH-Sy5Y to test the expression of *ITPR1*, *LCP1*, *SHANK1*, and *EPDR1* genes, upon their knockout, using the siLUC as the relative control. *Glyceraldehyde-3-phosphate Dehydrogenase* (*GAPDH*) and *Hypoxanthine Posphoribosyltransferase 1* (*HPRT1*) were used as housekeeping genes.
- And on SH-Sy5Y cell line after the RNA immunoprecipitation experiment, in order to test the following gene enrichment: *Cadherin 18* (*CDH18*), *Doublecortin Like Kinase 1* (*DCLK1*), *DEP Domain Containing MTOR Interacting Protein* (*DEPTOR*), *Cell Adhesion Associated, Oncogene Regulated* (*CDON*), *Leucine Rich Repeat Containing G Protein-Coupled Receptor 4* (*LGR4*), *Inositol 1,4,5-Trisphosphate Receptor Type 1* (*ITPR1*), *Lymphocyte Cytosolic Protein 1* (*LCP1*), *SH3 And Multiple Ankyrin Repeat Domains 1* (*SHANK1*), and *Ependymin Related 1* (*EPDR1*). *Glyceraldehyde-3-phosphate Dehydrogenase* (*GAPDH*) was used as housekeeping gene.

In table 16 are reported the forward and reverse primer sequences employed for the gene expression analysis. The primer sequence was generated using PrimerBank online tool (https://pga.mgh.harvard.edu/primerbank/). All the forward and reverse primer sequences are placed on different exons; therefore, no DNase treatment was performed in order to eliminate possible presence of genomic DNA.

Name	**Sequence 5' → 3'**	
GAPDH forward	CGCTCTCTGCTCCTCCTGTT	**Housekeeping genes**
GAPDH reverse	CCATGGTGTCTGAGCGATG	
HPRT1 forward	TGACACTGGCAAAACAATGCA	
HPRT1 reverse	GGTCCTTTTCACCAGCAAGCT	
TDP-43 forward	ATCTGGTGGTATGTTGTCAACTATCC	**Target genes**
TDP-43 reverse	GAACTTCTCCAAAGGTACTAAAATACTC	
LCP1 forward	GATCAGTGTCCGATGAGGAAATG	
LCP1 reverse	CCAGATCACCTGTAGCCATCA	
EPDR1 forward	GTCCAGGAGTGGTCGGACA	
EPDR1 reverse	ACACCGAGGGGTCTTTAATACC	

SHANK1 forward	TGGACCCCAATTACCATGACT	
SHANK1 reverse	CATGCGGCCTTATGCAGTG	
ITPR forward	GCGGAGGGATCGACAAATGG	
ITPR1_rev	TGGGACATAGCTTAAAGAGGCA	
CDON forward	AAAGCTGAGGTGCGCTATAAAA	
CDON reverse	AAGAAGGACGACTCACAAGGA	
LGR4 forward	TCGAGGGCTGAGTGCTTTG	
LGR4 reverse	ATGCCGTAACTGAACAAGTCC	
DCLK1 forward	GCTGATTTGACCCGAACTCTG	
DCLK1 reverse	AGCCACATACATAACTCTCTCCT	
DEPTOR forward	TTAGCAGACCGGGGCATTATT	
DEPTOR reverse	GAAGGTGCCGTCATCCTTTCT	
CDH18 forward	CAAAAGGGGATGGGTATGGATC	
CHD18 reverse	CCCGTGGTATCGTCAATGATAAA	

Table 16 – Quantitative Real Time PCR primer sequences.

For the first two, the gene expression was validated using CFX96 Touch Real-Time PCR Detection System (Biorad, Hercules, California, USA); for the SH-Sy5Y knockdown and RNA immunoprecipitation experiments, the QuantStudio 5 Real-Time PCR System, 96-well, 0.1 mL block (ThermoFisher Scientific, Waltham, Massachusetts, USA) machine was used. The two instruments required different protocols and different master mix reagent, the best for the quantitative Real Time PCR run optimization (table 17).

Machine	Temperature	Time	Steps	Cycles	Master mix reagent
CFX96 Touch Real-Time PCR Detection System (Biorad, Hercules, California, USA)	95°C	3 minutes	Polymerase Activation		SYBR Green Master Mix (Biorad, Hercules, California, USA)
	95°C	10 seconds	Denaturation	45	
	60°C	30 seconds	Annealing/Elongation		
	95°C	10 seconds	Melting Curve Profile		
	65°C	1 minute			
	95°C-5°C	---	Dissociation		
QuantStudio 5 Real-Time PCR System,	50°C	2 minutes	UDG attivation		PowerUp™ SYBR™ Green Master Mix
	95°C	2 minutes	Polymerase Activation		

96-well, 0.1 mL block (ThermoFisher Scientific, Waltham, Massachusetts, USA)	95°C	1 second	Denaturation	35	(Applyed Biosystems, Foster City, California, USA)
	60°C	30 seconds	Annealing/Elongation		
	95°C	15 seconds	Melting Curve Profile		
	65°C	1 minute			
	95°C	15 seconds	Dissociation		
	5°C	0,15°C/sec			

Table 17 – Quantitative Real Time PCR protocols and related master mix reagents.

To perform the gene expression analysis, 4µl of diluted cDNA (1:5 for the S375G patient brain regions; 1:10 for the other two experiments, in sterile water) was added to 6µl of reagents mix, composed by: the master mix reagent containing the DNA polymerase, the dNTPs mix, and the DNA intercalant agent that binds the nucleic acid in a non-specific manner, emitting a proportional fluorescence to the quantity of the amplified DNA; the forward and reverse primer, specific for the target gene or the housekeeping gene; and sterile water to reach the final volume (table 18).

Reagent	**Final Concentration**
Master mix reagent SYBR Green Master Mix (Biorad, Hercules, California, USA) or PowerUp™ SYBR™ Green Master Mix (Applyed Biosystems, Foster City, California, USA)	diluted 1:2
Primer forward (20µM)	0,5µM
Primer reverse (20µM)	0,5µM

Table 18 – Quantitative Real Time PCR reagents mix.

The expression levels were calculated exploiting different methods:

- For the S375G patients *TDP-43* expression, the comparative C_T methods was applied (Schmittgen and Livak, 2008), in which the $2^{-\Delta\Delta CT}$ was calculated. This method was applied in order to correct the higher heterogeneity between the different cut sections. Also, for the RNA immunoprecipitated samples was used this method, in order to better calculate the mRNA enrichment.
- For the RNA sequencing validation on multipotent stem cells, differentiated in neurons, derived from NPC patients and healthy controls, the homogeneity between the different samples was higher (supported also by the RNA sequencing results), therefore, CFX Maestro Software for CFX Real-Time PCR Instruments (Biorad, Hercules, California, USA) was exploited where the normalized expression (ΔΔCq) was calculated by the

software. The obtained data were then plotted in grouped table with GraphPad software (GraphPad Software, La Jolla California, USA).

- For the SH-Sy5Y knockdown samples, the Thermo Fisher Connect Cloud, Relative Quantification qPCR app (ThermoFisher Scientific, Waltham, Massachusetts, USA) was employed for the relative quantification (Rq) analysis. As per company suggestion, the software is merging together the independent experiments and it analyzes the Rq, upon indication of the normalization parameters, such as the housekeeping genes and the internal reference control (siLUC for example). The data were then plotted in a grouped table with GraphPad software (GraphPad Software, La Jolla California, USA).

3.6.6 RNA sequencing analysis of differentially expressed genes

Before sending the samples for the RNA sequencing analysis, the RNA extracted from multipotent stem cells, differentiated in neurons, derived from NPC patients and healthy controls were tested for their quality in terms of purification and integrity, using the QIAxcel RNA QC Kit v2.0 (Qiagen, Hilden, Germany). The instrument provides the RNA Integrity Score (RIS) that indicate the quality of the extracted RNA basing on the quality of 28s and 18s ribosomal RNA. This number should be higher than 7 for the RNA sequencing protocol optimization. According to this, 1µl of RNA sample were diluted 1:1 with the QX Denaturation buffer (Qiagen, Hilden, Germany) and the sample was denaturated at 70°C for 2 minutes. The same treatment was performed also for the QX RNA size marker 200-6000bp (Qiagen, Hilden, Germany). 8µl of QX Dilution buffer (Qiagen, Hilden, Germany) were added, and the sample was run in the QX RNA cartridge (Qiagen, Hilden, Germany) together with the QX RNA size marker 200-6000bp (Qiagen, Hilden, Germany) and the QX RNA size marker 15bp (Qiagen, Hilden, Germany). 5µg of the samples with RIS number higher than 7 and with optimal values of 260/280 and 260/230 absorbance, were send to Novogene (Novogene Co., Ltd, Beijing, China) for the sequencing.

Novogene (Novogene Co., Ltd, Beijing, China) performed both the sequences as well as the bioinformatic analysis concerning the clusterization, gene ontology (GO) analysis and Kyoto Encyclopedia of Genes and Genomes (KEGG) enrichment.

Basically, they purified the mRNA from total RNA using poly T oligos attached to magnetic beads, and then it was randomly fragmented using a fragmentation buffer. Secondly, a NEB library was prepared (**Fig.24**): the first strand cDNA was synthesized using

random hexamer primers and M-MuLV Reverse Transcriptase (RNase H-). The second strand cDNA synthesis was performed using DNA Polymerase I and RNase H. After adenylation of 3' ends of DNA fragments, NEBNext Adaptor (New England Biolabs, Ipswich, Massachusetts, USA) with hairpin loop structure was ligated to prepare for hybridization. The cDNA fragments were then purified with AMPure XP system (Beckman Coulter, Beverly, USA) of 150~200 bp in length and they were obtained by PCR amplification.

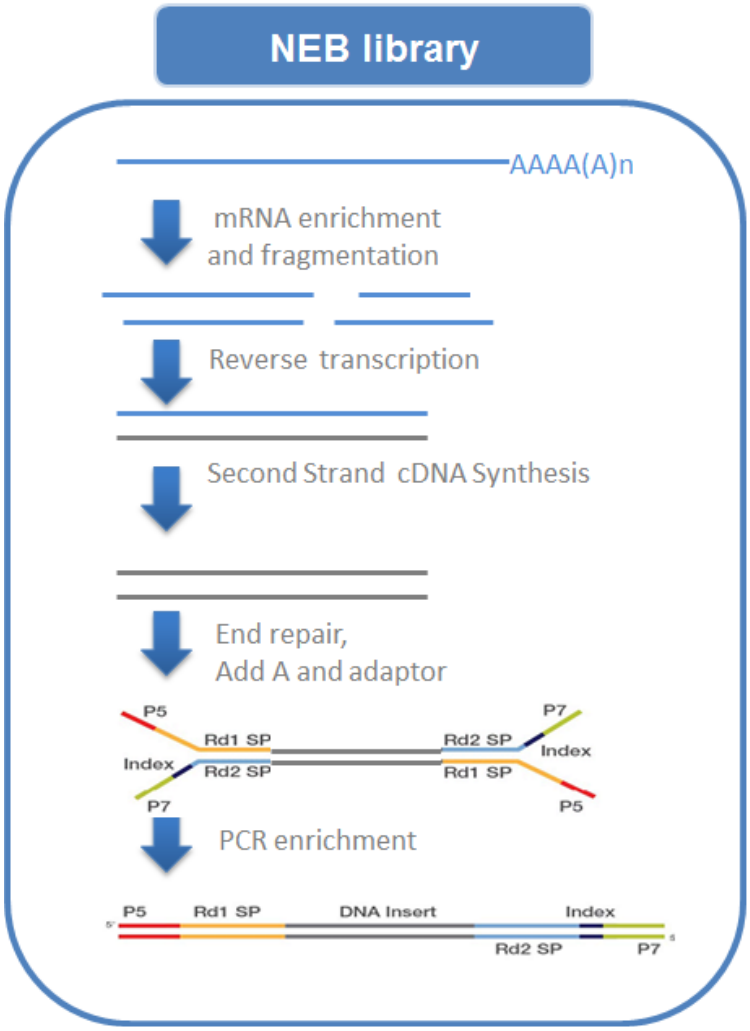

Figure 24 – NEB library proposed by Novogene.

A library quality assessment was performed and the samples were sequenced using the Illumina technology (**Fig.25**). We chose a paired end analysis improving the capability to identify the relative positions of various reads in the genome. In contrast with the single end analysis that reads the fragment from one end to the other, the paired end performs to reading steps in the opposite directions. As a depth of coverage, we decided for 60mln of reads per samples, in order to cover also low-abundant transcripts. We choose these stricter parameters for two reasons: first of all, the samples that we sequenced were directly derived

from humans (skin biopsies) and this depth of coverage with the paired end analysis allowed us to flatten the difference between the same samples' category (controls or patients), and to detect small perturbations between the patients and the controls. Moreover, as I will later explain, we were interested in the differentially expressed genes, but this type of analysis could allow us to go in deeper and also to check for the different alternative splicing events.

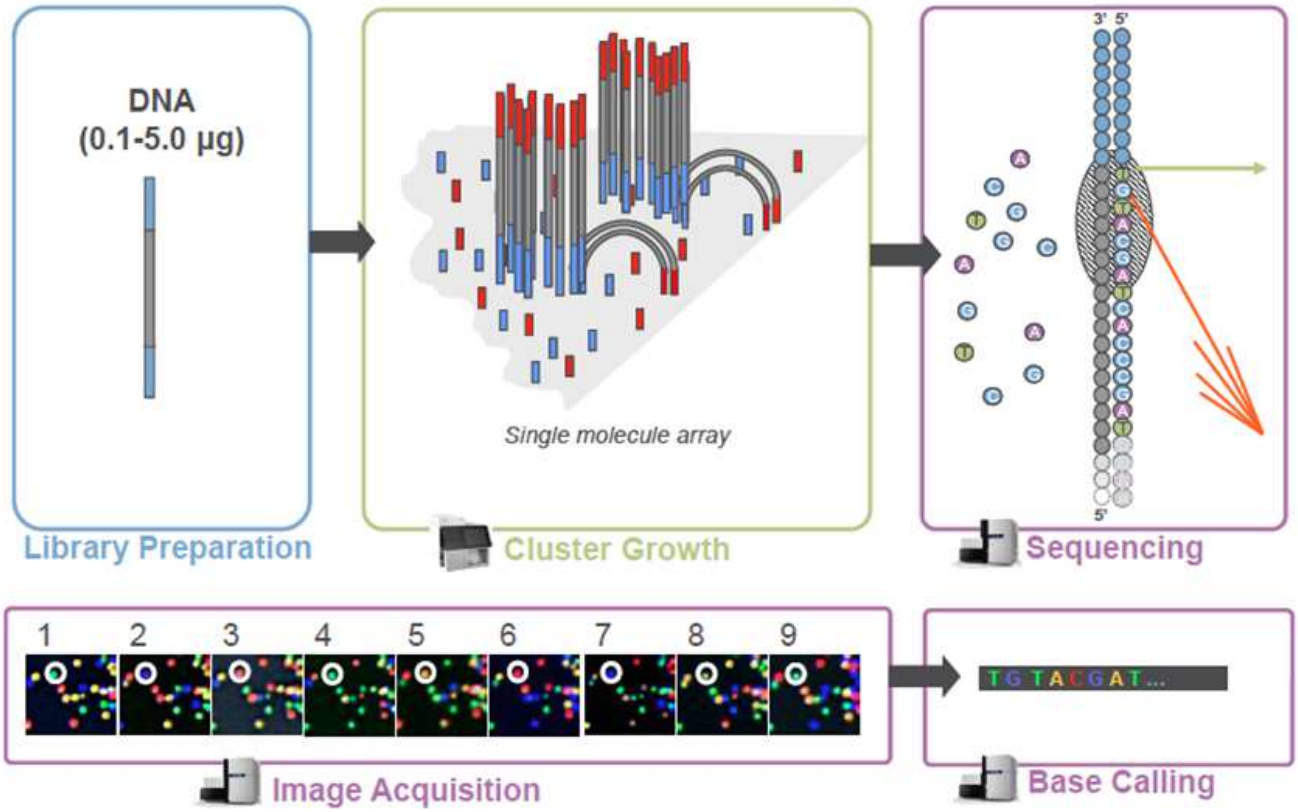

Figure 25 – Illumina sequencing scheme (Novogene report).

The bioinformatic analysis was carried out: a quality check of the sequencing was performed by calculating the error rate distribution, such as the sequencing error rate related to the base quality values of the Illumina machine; and the GC content to detect potential AT/GC separation, such as when G and C, A and T are not in an equal rate.

Also, the obtained data were filtered by removing the reads containing adaptors; eliminating the reads containing a number of bases that cannot be determinate higher than 10%; and they cut out the reads with a quality score of over 50% bases of the read is less than 5. Finally, the clean reads were mapped on the reference genome: Novogene aligned the paired-end clean reads to the reference genome using STAR (v2.5) software, that exploits the method of Maximal Mappable Prefix (MMP) generating a precise mapping result for junction reads.

In order to quantify the gene expression level, HTSeq v0.6.1 software was used to count the read numbers mapped for each gene, and the Reads Per Kilobase of exon model per Million mapped reads (FPKM) was calculated basing on the length of the gene and the reads count mapped to this gene.

Differential expression analysis was performed with edgeR package, and the threshold of differential expression genes was applied: 0.7<Fold Change (FC)>1.3 and p-value adjusted (pAdj)<0.05.

The Venn diagrams were prepared using the function Venn Diagram in R based on the gene list for different group.

Cluster Analysis of differential expression genes was used to estimate expression pattern of differential expression genes under different experimental conditions. Hierarchical clustering analysis was carried out with the log10(FPKM+1) of union differential expression genes of all comparison groups under different experimental conditions.

Gene Ontology (GO) enrichment analysis of differentially expressed genes was implemented by the cluster Profiler R package, in which gene length bias was corrected. GO terms with corrected pAdj less than 0.05 were considered significantly enriched by differential expressed genes.

KEGG database is a resource for understanding high-level functions and utilities of the biological system (http://www.genome.jp/kegg/). Novogene used cluster Profiler R package to test the statistical enrichment of differential expression genes in KEGG pathways. KEGG terms with padj < 0.05 are significant enrichment.

3.6.7 RNA immunoprecipitation (RNA-IP) assay

2800000 SH-Sy5Y ECACC cells were seed in p100 plate (three plates for the target plasmid and one for the negative control) with D-MEM:F12 cultured medium, in order to achieve 70-80% of confluence the day after. The second day, the cells were transfected with pFLAG-CMV4 TDP-43 vector using Lipofectamine 3000 reagent [12] (Invitrogen, Carlsbad, California, USA), and with p-CMV4 plasmid without the insert. After 24 hours, the cells were collected: the three plates transfected with the target protein were merged and the samples

[12] Reference to 2.2.2.2 paragraph – SHSy5Y ECACC cell line

were centrifuged at 500xg for 5 minutes. The supernatant was discarded and the cells were resuspended in: 3ml of ice-cold 1X PBS for the negative control, and 6ml of ice-cold 1X PBS, for the target protein that were then divided it in 3 tubes (2ml per tube). The samples were centrifuged at 500xg for 5 minutes and the supernatant was discarded. One pellet from the target transfection and the pellet transfected with the negative control, were tested with SDS-PAGE and Western Blot techniques in order to check the transfection efficacy.

The last two pellets, transfected with the target protein underwent to the RNA immunoprecipitation assay, performed with the Imprint® RNA Immunoprecipitation Kit (Sigma-Aldrich, St. Louis, Missouri, USA).

The first step is the cell lysis: in this work, the Mild Lysis Buffer (Sigma-Aldrich, St. Louis, Missouri, USA) was employed because it is a nonionic detergent and it leaves the nuclei intact. According to the cell number, different volumes of reagents were used for the pellet resuspension, following table 19:

Reagent	**Volume for 0.5-2x10^6 cell range**	**Volume for ≥2x10^6 cell range**
Mild Lysis Buffer (Sigma-Aldrich, St. Louis, Missouri, USA) or Harsh Lysis Buffer (Sigma-Aldrich, St. Louis, Missouri, USA)	100µl	200µl
Protease Inhibitor Cocktail (Sigma-Aldrich, St. Louis, Missouri, USA)	1µl	2µl
Dithiothreitol (DTT) (100mM) Invitrogen (Carlsbad, California, USA)	0,05µl	0,1µl
Ribonuclease Inhibitor 40U/µl (Sigma-Aldrich, St. Louis, Missouri, USA)	0,4µl	0,8µl

Table 19 – RNA-IP lysis reagents volume, according to cell range.

After the resuspension, the samples were incubated in ice for 15 minutes, and then they were centrifuged 10 minutes at 16000xg at 4°C. The supernatant was collected and its volume was measured. 10% of the lysate supernatant was removed, corresponding to the "10% Input", such as the initial control. The "10% Input" was stored at -80°C.

In the meantime, the preparation of the Protein A Magnetic Beads (Sigma-Aldrich, St. Louis, Missouri, USA) was performed: the magnetic beads were resuspended and 0.02ml were quickly transferred to each 1.5ml microcentrifuge tube. 0.1ml of RIP Wash Buffer (Sigma-Aldrich, St. Louis, Missouri, USA) were added, and the beads were briefly vortexed. The tubes were placed on a magnetic separator support in order to ease the

supernatant separation and the beads collection. This wash step was repeated. At this point the beads are ready for the bridging antibody pre-binding. The tubes were briefly centrifuged and the beads were resuspended in 0.1 ml of RIP Wash Buffer (Sigma-Aldrich, St. Louis, Missouri, USA) and they were transferred in 0,5ml microcentrifuge tubes. 1µl of bridging antibody (in this work IgG from mouse serum, Sigma-Aldrich, St. Louis, Missouri, USA), and they were incubated for 30 minutes at room temperature in rotation. After this time, the tubes were briefly centrifuged and the magnetic beads-bridging antibody complex were resuspended in 0.1 ml of RIP Wash Buffer (Sigma-Aldrich, St. Louis, Missouri, USA) and they were transferred in 1.5ml tubes. The tubes were placed on a magnetic separator and the supernatant was discarded. 0.5ml of RIP Wash Buffer (Sigma-Aldrich, St. Louis, Missouri, USA) were added, and the samples were briefly vortexed. Again, the supernatant was discarded employing the magnetic support. This wash step was repeated one again. At this point the specific antibody prebinding was performed: one was hybridizing with the target-specific antibody, such as α-flag M2, Invitrogen, Carlsbad, California, USA; and the other with a negative control antibody, such as the Anti-mouse IgG antibody produced in rabbit (Sigma-Aldrich, St. Louis, Missouri, USA). The beads were resuspended in 0.1 mL of RIP Wash Buffer (Sigma-Aldrich, St. Louis, Missouri, USA) and they transferred in 0,5ml microcentrifuge tubes. 5µl of specific antibody were added, and the beads were incubated in rotation for 30' at room temperature. Then, the tubes were briefly centrifuged. The magnetic beads-specific antibody complex was resuspended with 0.1 ml of RIP Wash Buffer (Sigma-Aldrich, St. Louis, Missouri, USA) and they were transfer in 1.5ml tubes. The supernatant was discarded. 0.5ml of RIP Wash Buffer (Sigma-Aldrich, St. Louis, Missouri, USA) were added and the samples were briefly vortexed and centrifuged. The supernatant was discarded and the wash step was repeated with 0.2ml of RIP Wash Buffer (Sigma-Aldrich, St. Louis, Missouri, USA). Now the beads are ready for the immunoprecipitation step. In table 20, are reported the employed volumes for the IP-buffer preparation, with the final volume of 0.5ml for each sample.

Reagent	Volume
RIP Wash Buffer (Sigma-Aldrich, St. Louis, Missouri, USA)	1000µl
Protease Inhibitor Cocktail (Sigma-Aldrich, St. Louis, Missouri, USA)	10µl
Ribonuclease Inhibitor 40U/µl (Sigma-Aldrich, St. Louis, Missouri, USA)	4µl

Table 20 – IP-buffer preparation mix.

The supernatant was discarded from the beads and the immunoprecipitation reaction was set and it was composed by prebound beads, the IP Buffer, and the cell lysate. The mix was incubated overnight in rotation at 4°C. The day after, the samples were briefly centrifuged and 10% of the supernatant was removed, representing the Negative Control Reaction supernatant, called “Negative Control RNA-IP Input”. This sample was stored at -80°C. The remaining supernatant was discarded and washing step followed. 1ml of RIP Wash Buffer (Sigma-Aldrich, St. Louis, Missouri, USA) was added and the samples were gently vortexed. The RNA-IP reaction was transferred into a fresh 1.5ml tube that was quickly spun down and the supernatant was removed. This wash step was repeated five times, moving the sample always in a fresh 1.5ml tube. After this, the samples were resuspended in 200µl of RIP Wash Buffer (Sigma-Aldrich, St. Louis, Missouri, USA). The 10% Input sample was recovered and lift up to a final volume of 200µl using RIP Wash Buffer (Sigma-Aldrich, St. Louis, Missouri, USA).

At this point, enriched RNA was purificated: 500µl of EuroGold Trifast (Euroclone, Milan, Italy) were added and the samples were incubated for 5 minutes at room temperature. 100µl of chloroform (Sigma-Aldrich, St. Louis, Missouri, USA) were summed and the samples were incubated for 3 minutes at room temperature. They were then centrifuged at 16000xg for 15 minutes at 4°C. The supernatant aqueous phase was collected and it was placed in a new collection tube. 6µl of RNA-glycogen 5mg/ml (final concentration 0.05µg/µl) (ThermoFisher Scientific, Waltham, Massachusetts, USA), 60µl of 5M ammonium acetate (Honeywell, Charlotte, North Carolina, USA), and 600µl of isopropanol (Honeywell, Charlotte, North Carolina, USA) were added. The samples were vortexed and then they were stored at -80°C for 2-3h, to precipitate the RNA. After the -80°C incubation, the samples were thawed in ice, and then they were centrifuged at 16000xg for 10 minutes at 4°C. The supernatant was removed and the pellet was washed once with 500µl of 80% ethanol (Honeywell, Charlotte, North Carolina, USA) solution. They were centrifuged at 16000xg for 10 minutes at 4°C, the supernatant was discarded and the pellet was air-dried at 37°C for few minutes. Then it was resuspended in 20µl sterile water and the concentration, the purification, and the quality of the extracted RNA was tested with D30 Eppendorf BioSpectometre (Eppendorf, Hamburg, Germany), using the Eppendorf µCuvette G1.0 (Eppendorf, Hamburg, Germany). The absorbance at 260nm was measured together with the ratio between the absorbance at 260/280nm (protein contamination) and at 260/230nm (reagents contamination). The samples were stored at -80°C.

The RNA extracted was retrotranscribed in cDNA and the abundance of possible TDP-43 target genes was evaluated by quantitative Real-Time PCR.

3.7 Statistical analysis

The statistical analysis was performed on three independent experiments, using GraphPad software (GraphPad Software, La Jolla California, USA). An unpaired t-test or a multiple comparison Anova test with Bonferroni correction were carried out, and the statistical test performed for each experiment is reported in the captions.

3.8 Standard solutions

- **1X PBS** (Phosphate Buffer Saline): 137mM NaCl; 2.7mM KCl; 10mM Na_2HPO_4; 2mM KH_2PO_4 pH 7.4
- **LB medium** (Luria-Bertani medium): 10g Bacto Tryptone; 5g Yest Extract; 10g NaCl pH 7.5 → per liter.
- **TB**: (Terrific Broth) medium: 1.2% peptone, 2.4% yeast extract, 72 mM K2HPO4, 17 mM KH2PO4 and 0.4% glycerol
- **1X TSS** (Transformation & Storage Solution): 10%PEG 4000 (5g); 35mM $MgCl_2$ (1.75 mL $MgCl_2$ 1M); 35mL LB (without antibiotics); lead to pH 6.5 with HCl 0.5M; filter with 0.22µm membrane; DMSO 2.5ml → 50ml.
- **D-MEM**: Dulbecco's Modified Eagle's Medium, composed by High Glucose 1X; L-glutamine; Phenol Red; Sodium Pyruvate (Gibco, Life Technology, Carlsbad, California, USA). With fetal bovine serum 10% (Life Technology, Carlsbad, California, USA) and antibiotic antimycotic solution 1% (Sigma-Aldrich, St. Louis, Missouri, USA).
- **Opti-MEM**: Opti-MEM® Reduced-Serum Medium with L-glutamine and Phenol Red (Gibco, Life Technology, Carlsbad, California, USA). Lack of Bovine Serum.
- **D-MEM:F12**: Dulbecco's Modified Eagle's Medium/Nutrient Mixture F-12 Ham, composed by L-glutamine, 15mM HEPES, and sodium bicarbonate, liquid, sterile-filtered (Sigma-Aldrich, St. Louis, Missouri, USA). With fetal bovine serum 15% (Life Technology, Carlsbad, California, USA) and antibiotic antimycotic solution 1% (Sigma-Aldrich, St. Louis, Missouri, USA).

4 RESULTS

4.1 Characterization of a TDP-43 mutation in an ALS case that might affect phosphorylation sites in the C-terminal region of this protein.

4.1.1 Clinical case: TDP-43 S375G unpublished variant associated with ALS

This work started with the study of a clinical case in collaboration with the Department of Pathology & Laboratory Medicine of the University of Kansas School of Medicine (Kansas City, USA). In this work, Kathy Newell and Dino Ghetti studied the brain and spinal cord of a 26-year-old woman clinically diagnosed with ALS at the very early age of 22, and with a history ALS in distant relatives. Neuropathologic evaluation showed the upper and lower motor neuron impairment with an immunoreaction for the phosphorylated TDP-43 (**Fig.26**) (Newell et al., 2018).

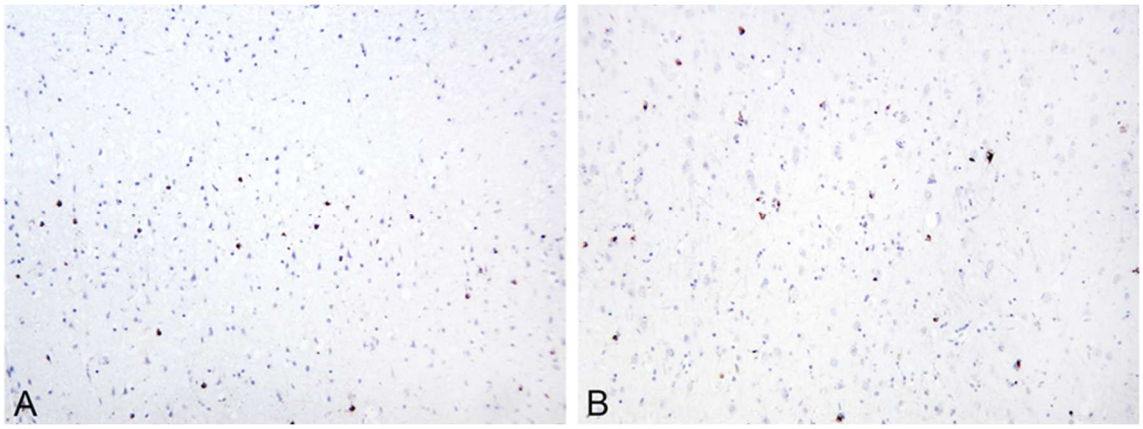

Figure 26 – phosphoTDP-43 density and distribution of immunoreactive neurons and glia of the motor cortex. In panel A are shown the upper cortical layers; in panel B the lower cortical levels. 10X original magnification (Newell et al., 2018). *Figure in collaboration with Kathy Newell.*

An autopsy was carried out on samples derived from central nervous system frozen regions: the primary motor cortex, neurons, and glial cells were positively stained for intracytoplasmic inclusions, immunolabelled with TDP-43 antibodies (**Fig.27**).

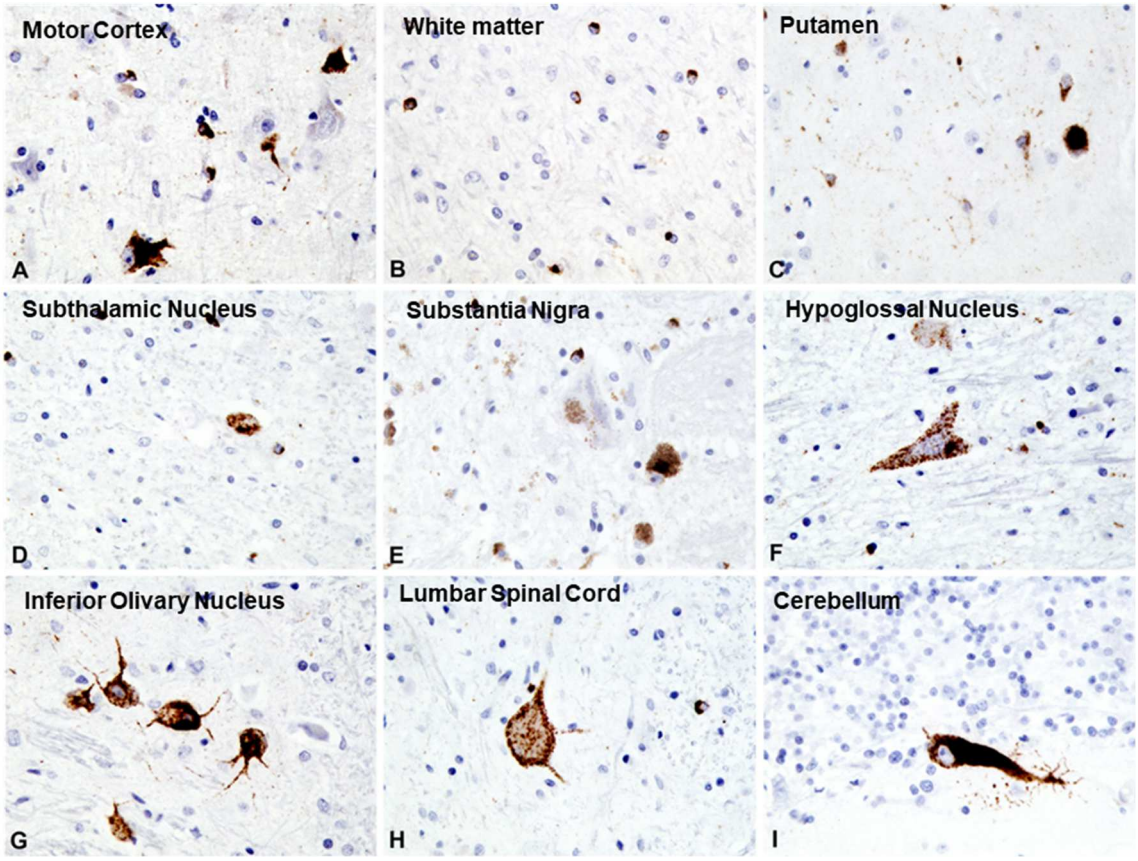

Figure 27 – phosphoTDP-43 density and distribution of different brain areas. 40X original magnification (Newell et al., 2018). *Figure in collaboration with Kathy Newell.*

Due to the availability of a high number of brain regions from this ALS case, it was possible to compare the expression levels of phosphoTDP-43 (pTDP-43) in neuronal and glia cells, and compare it with the total TDP-43 mRNA expression in order to determine whether phosphoTDP-43 (pTDP-43) levels were correlated with total TDP-43 expression levels (Newell et al., 2018). **Figure 28** shows that results revealed prominent differences in the analyzed brain regions. As expected, most of the pTDP-43 staining was concentrated in the areas affected by the disease, such as the primary motor cortex and the spinal cord, while pTDP-43 absence was detected in the hippocampus (**Fig.28A**). In contrast, however, TDP-43 total mRNA expression levels were constant in all the analyzed regions with few exceptions, especially in the dentate nucleus (cerebellum) where expression levels were considerably higher than in the other tissues (**Fig.28B**). These mRNA expression data were confirmed by Western blot analysis (**Fig.28C**) (Newell et al., 2018). Taken together, the analysis revealed that there is no simple correlation between the amount of pTDP-43 and total TDP-43 expression in different brain regions (Newell et al., 2018). In fact, this observation suggests that altered phosphorylation is not a simple reflection of relative TDP-

43 expression levels in different brain regions but may be a consequence of pathological mechanisms that are active only in selected brain areas.

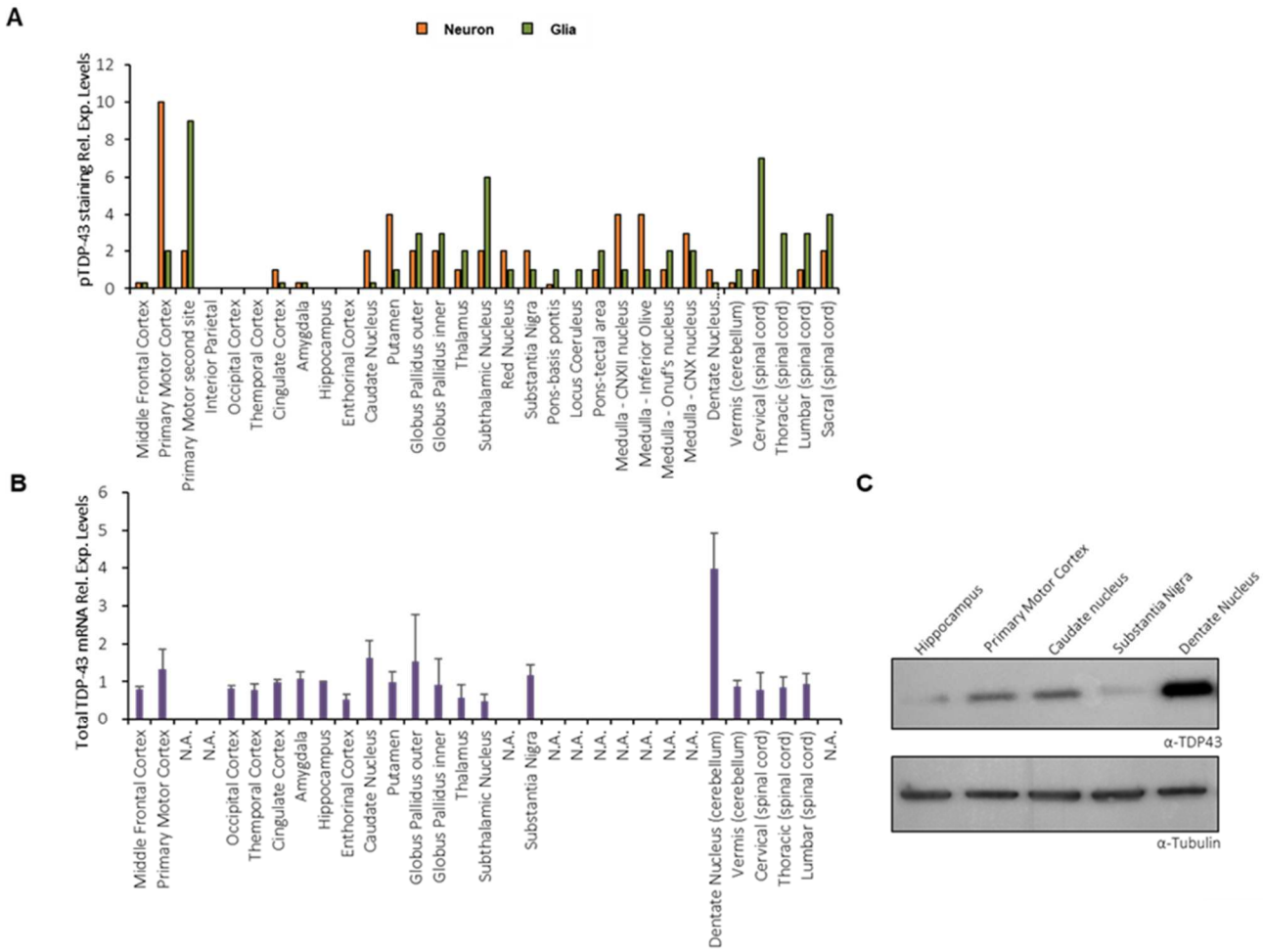

Figure 28 – pTDP-43 amount in glial and neuronal cells versus total TDP-43 expressed. A) in this panel the pTDP-43 amount, found in different brain regions of the patient, was plotted in a graph. B) total TDP-43 expressed levels were detected by quantitative Real Time PCR on different brain regions derived from the patient. Hippocampus was used as the internal standard sample. C) western blot analysis on brain regions stained with α-TDP43 antibody. Tubulin was used as standard loading control (Newell et al., 2018).

At the time of discovery, it was still unclear the reason for this early onset of disease. In fact, little information was available about her siblings that could help identify disease segregation and familiarity. Both parents were healthy and without clinical history of neurological disorders. The same was for the patient's older kin, even though some occurrence of ALS in distant relatives was documented. In particular, one of the parent's cousin was diagnosed with ALS after the fifth decades of age. Also, the other parent had a great uncle who was clinically diagnosed with ALS. Moreover, a grandmother was reported to have died with late onset Alzheimer. Nonetheless, there was no direct link to disease, leaving uncertain the classification of this patient as a familial or sporadic case.

To start addressing this issue at the molecular level, we performed a molecular genetic analysis on extracted DNA from frozen brain tissue. No *C9ORF72* expansion, or sequence alterations in *SOD1*, *ANG*, *FIG4*, and *FUS* genes were reported; however, a novel S375G (AGT>GGT) change was identified in a mutational hot-spot of *TDP-43* gene, the C-terminal region of the protein (**Fig.29**) (Newell et al., 2018).

Figure 29 – TDP-43 S375G variant located in the CTD (Newell et al., 2018). *Figure in collaboration with by Kathy Newell.*

Bioinformatics analyses performed on this mutation using well known prediction programs such as SIFT, PolyPhen-2, SNAP, etc. failed to predict an effect of this mutation on protein functionality. However, considering the severity of the disease in this patient, I tested the effects of this variant on TDP-43 localization, pre-mRNA splicing activity, and toxicity, in parallel with the effects on neighboring disease-associated mutations. Moreover, this variant was hypothesized to potentially affect a potential post-translational modification site, with the deletion of a phosphorylation site in the C-terminal domain of TDP-43 protein (Kametani et al., 2016; Hasegawa et al., 2008).

4.1.2 Characterization of S375G variant and of the adjacent G376D, N378D, and Y374X TDP-43 disease-associated mutants.

4.1.2.1 Splicing capability

As described in the introduction section, TDP-43 is mostly known for its involvement in splicing. Based on this, I first tested the splicing capability of S375G comparing it to neighboring disease-associated mutations (G376D, N378D, and Y374X). The splicing assay was performed in transient transfected HeLa cells with a minigene containing the CFTR exon 9 (C155T) following the knockdown of the endogenous *TDP-43*. As reported **in Figure 30**, the change in CFTR exon 9 inclusion was measured following the addition of flagged-

siRNA-resistant wild type TDP-43 (WT), an RNA-binding impaired mutant (F4L) as a negative control, and the mutant variants. After a reverse transcriptase PCR amplification, using minigene-specific primers, the levels of CFTR exon 9 inclusion (Ex 9+) were measured by QIAxcel DNA Screening Kit (**Fig.30A**). The results from three biological triplicates are reported in **Figure 30B**: no difference in splicing pattern between the WT and S375G variant, as in the other neighboring mutations, was detected (Newell et al., 2018). In panel C of **Figure 30** is reported the silencing and transfection efficiency, measured by Western Blot.

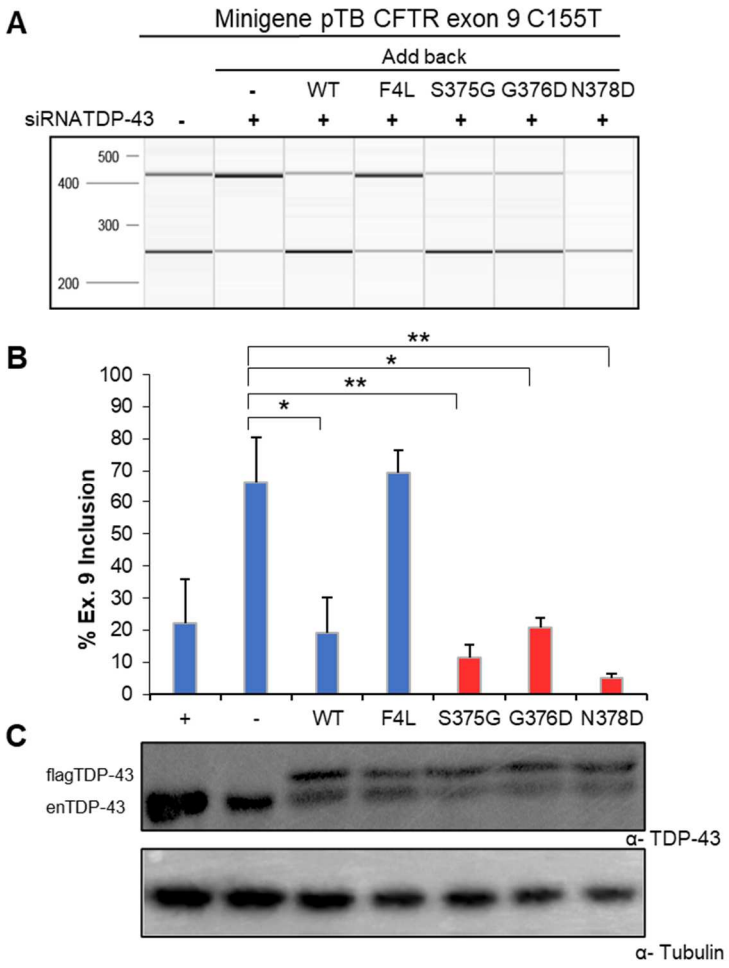

Figure 30 – Addback splicing assay. A) QIAxcel capillary electrophoresis gel image reporting CFTR exon 9 splicing for the WT, F4L; and the TDP-43 mutant forms. The samples were silenced with the siLUC, as a control (-), and with the siTDP-43 (+). In all the samples the minigene containing the CFTR exon 9 was transfected, while the different TDP-43 forms were added-back in all the TDP-43 silenced samples, except for the negative control (Add-back "–"). B) Statistical quantification analysis of the gel image. Unpaired t-test was performed using GraphPad software (GraphPad Software, La Jolla California, USA); C) Western blot image stained with α-TDP-43 antibody detecting flag-tag TDP-43 (the transfected one) and endogenous silenced TDP-43. Tubulin was used as internal standard loading control. The "+" sample is showing the endogenous TDP-43 in the siLUC sample; the "-" is still the endogenous silenced TDP-43. The WT, F4L, S375G, G378D, and N378D represent the added-back TDP-43 forms in the TDP-43 knockdown cells (Newell et al., 2018).

The same experiment was repeated for TDP-43 Y374X nonsense mutation, in order to understand if the lack of the last 33 residues was somehow impairing the splicing capability of the protein. As shown in **Figure 31**, the Y374X stop-codon mutation was still preserving the splicing capability of the protein compared to the WT (**Fig.31A** and **31B**). As above, a Western blot analysis was performed to confirm the silencing and the transfection. As shown in **Figure 31C**, the flag-TDP-43 Y374X band was not present. The reason for this apparent discrepancy is that it is not possible to distinguish the endogenous TDP-43 from the flagged one because this truncated mutant protein migrates together with the unflagged endogenous protein (Newell et al., 2018).

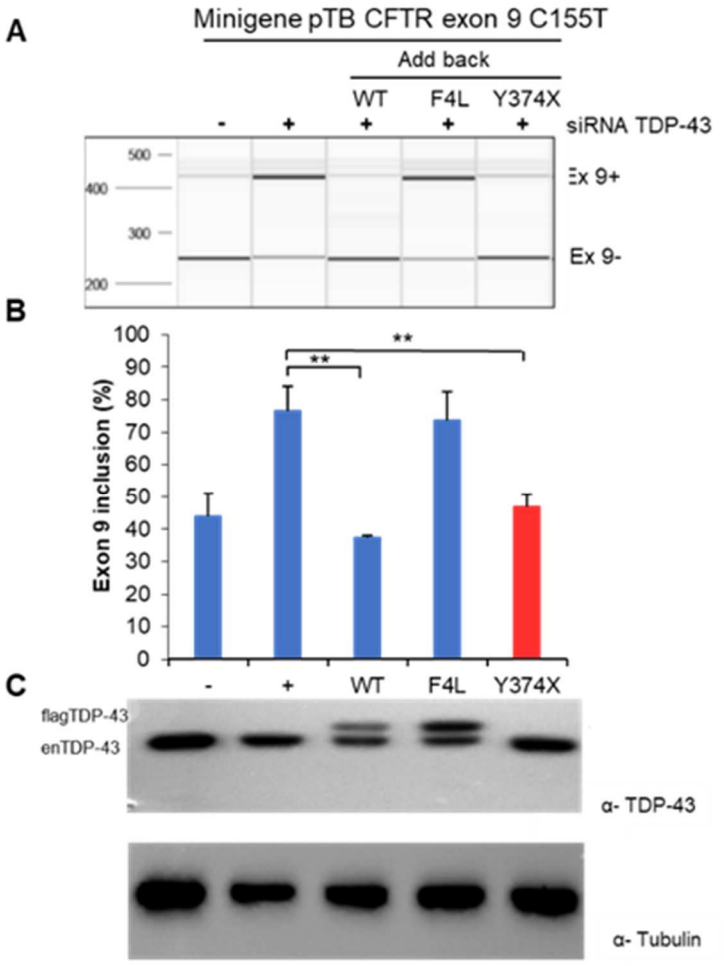

Figure 31 – TDP-43 Y374X nonsense mutation addback analysis. A) QIAxcel capillary electrophoresis gel image reporting CFTR exon 9 splicing. The samples were silenced with the siLUC, as a control (-), and with the siTDP-43 (+). In all the samples the minigene containing the CFTR exon 9 was transfected, while the different TDP-43 forms were added-back in all the TDP-43 silenced samples, except for the negative control. B) Statistical quantification analysis of the gel image. Unpaired t-test was performed GraphPad software (GraphPad Software, La Jolla California, USA); C) Western blot image stained with α-TDP-43 antibody detecting the transfected flag-TDP-43 and silenced endogenous TDP-43. Tubulin was used as internal standard. The "-" sample represent the negative control silenced with the siLUC and the total endogenous TDP-43 was stained. In the "+" sample the cells were just silenced for TDP-43 without any added-back

form, and the silenced TDP-43 was stained. The WT, F4L, and Y374X shows the TDP-43 staining of the added-back forms in the cells silenced for the endogenous TDP-43. (Newell et al., 2018).

4.1.2.2 Immunolocalization analysis

Secondly, I investigated whether the S375G substitution could affect the intracellular localization of TDP-43 in comparison with the wild-type protein or with respect to TDP-43 localization occurring in disease-associated mutations G376D and N378D, that had been previously described by other authors but not well characterized (Newell et al., 2018; Buratti, 2015).

The subcellular distribution of all the TDP-43 mutants was investigated in transient transfected HeLa cell line with flag-tagged TDP-43 forms mentioned also in the previous paragraph. As reported in **Figure 32**, the wild-type TDP-43 was predominantly nuclear, with a lower abundance in the cytoplasm, due to the continuous shuttling of the protein between the two compartments. While the G376D and N378D substitutions did not significantly affect the distribution of TDP-43, which remained prominently nuclear, in the S375G variant the distribution of TDP-43 was significantly more nuclear than in any other mutants (**Fig.32A** and **32B**). This result was also confirmed by the western blot separation of the nuclear-cytoplasmic fraction (**Fig.32C**) (Newell et al., 2018).

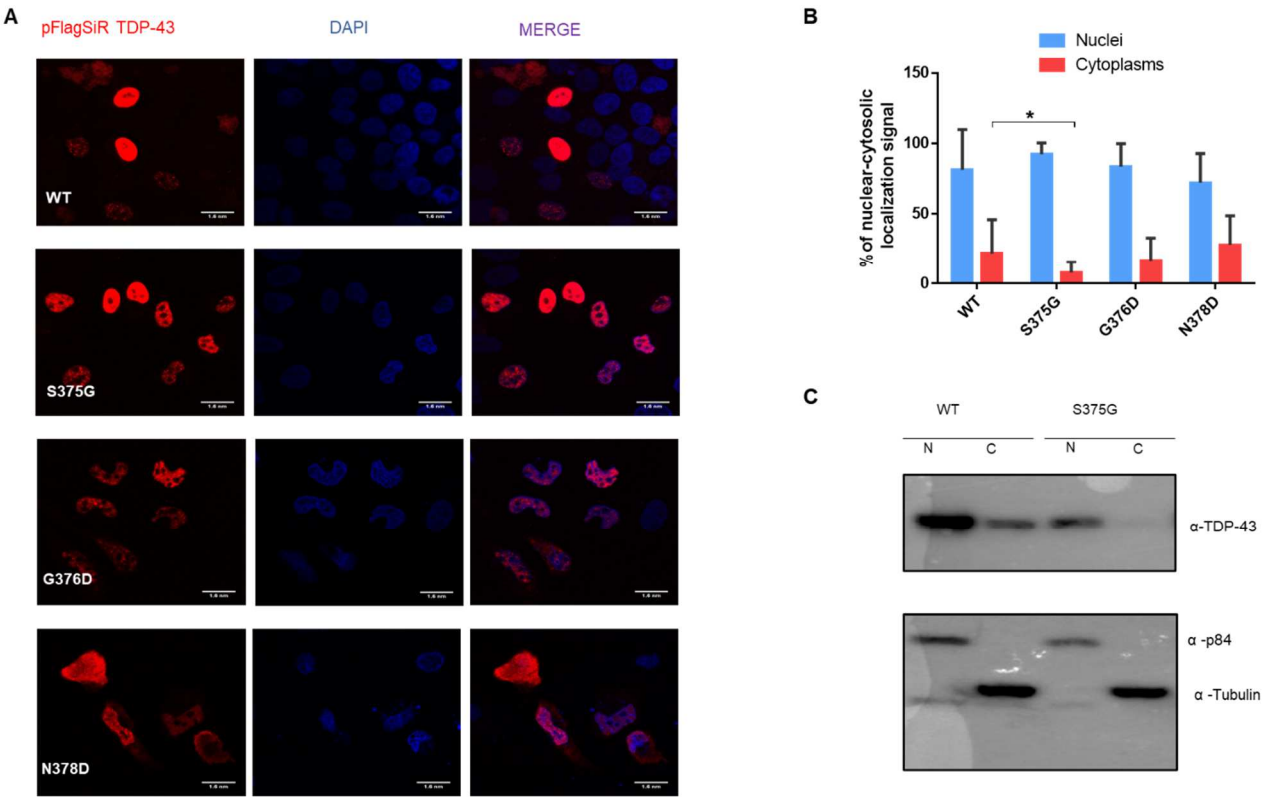

Figure 32 – pFlagSiRTDP-43 subcellular localization. A) Immunofluorescence localization: flag-TDP-43 WT, S375G, G376D, N378D transfected plasmids were detected with α-flag antibody, nuclei were stained with DAPI. B) Quantification of nuclear-cytoplasmic staining intensity for WT flag-TDP-43, S375G, G376D and N378D was performed by measuring the Region of Interest (ROI). Unpaired t-test was performed using GraphPad software (GraphPad Software, La Jolla California, USA). C) Nucleus-cytoplasmic (N/C) distribution of transiently transfected HeLa cells with flag-tagged wild-type TDP-43 and flag-tagged S375G mutant. The detection of p84 and tubulin was performed as control for nuclear/cytoplasmic contamination of the two fractions (Newell et al., 2018).

The intracellular localization was also performed for the Y374X mutant. As reported in **Figure 33**, however, the absence of the last 33 residues did not impair the sub-cellular localization compared to WT (Newell et al., 2018).

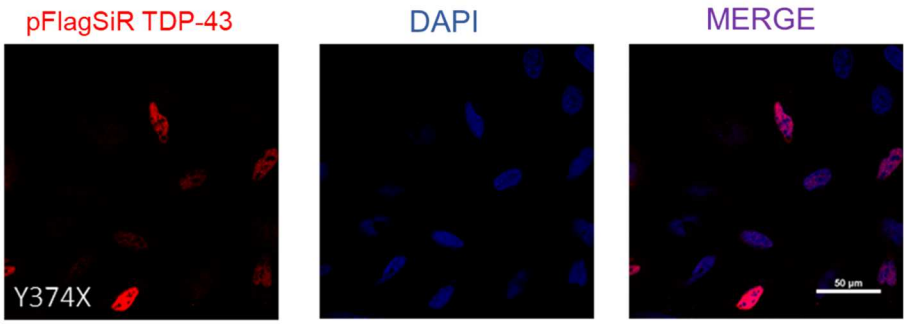

Figure 33 – Y374X TDP-43 mutant immunolocalization (Newell et al., 2018).

4.1.2.3 TDP-43 mutants' cellular toxicity: LDH release assay

According to the previous results, I therefore examined whether the S375G, G376D, N378D, and Y374X substitutions could increase cellular toxicity in relation with WT protein. To perform this analysis, HeLa cells were transiently transfected with the flagged TDP-43 vectors: after 24-, 48-, and 72-hours lactate dehydrogenase (LDH) levels were measured. The LDH levels in the cell medium levels after 24 hours did not show any difference between the mutants, compared to cells transfected with wild-type TDP-43 (**Fig.34A**). On the other hand, the expression of the S375G caused a strong significant cytotoxicity after 48 hours that was similar to that of the other mutants (**Fig.34B**) and even stronger than some if we consider that the N378D mutant showed a toxic effect only after 72 hours (**Fig.34C**). In all transfected cells, Western blot analysis against total TDP-43 showed that the flagged wild-type and mutant proteins were expressed at similar levels after 48 hours post-transfection (**Fig.34D**) (Newell et al., 2018). Taken together, these results have suggested that, although TDP-43 functional properties in the regulation of pre-mRNA splicing were not affected, this mutation still had the ability to alter the nuclear cytoplasmic balance of this protein. As a

consequence, this novel S375G mutation displayed a toxicity that was comparable, and even somewhat greater, than neighboring disease-associated mutations. What these results did not explain, however, was the reason why this change could affect the cellular distribution of TDP-43.

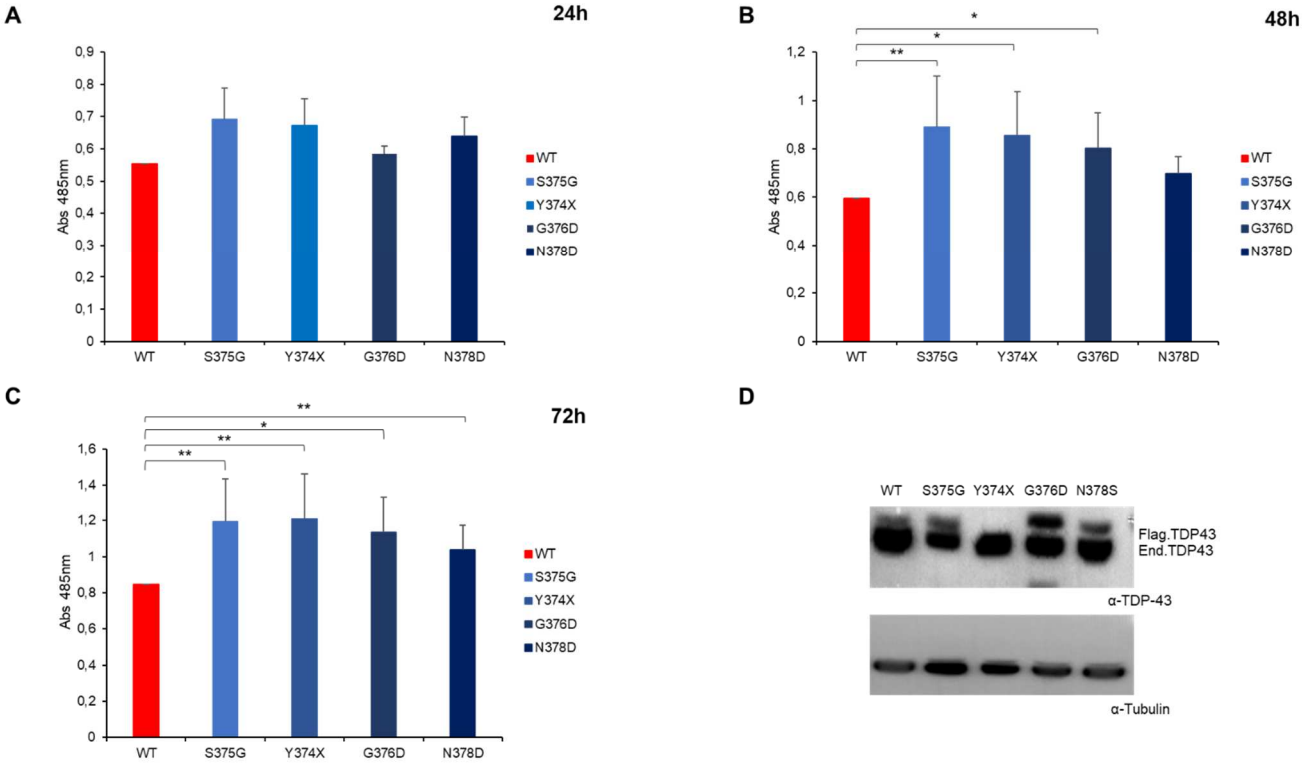

Figure 34 - LDH release. Levels were measured 24 hours (A), 48 hours (B) and 72 hours (C) after cells transfection with the specific constructs. Multiple comparison one-way Anova test with Bonferroni's correction was performed using GraphPad software (GraphPad Software, La Jolla California, USA). D) Western blot analysis of flagged TDP-43 protein expression after 48 hours to show comparable expression of all mutants in our cell line. Tubulin was used as the internal standard loading control (Newell et al., 2018).

4.1.2.4 Functional effects of mimicking post-translational phosphorylation at the S375 position

According to the literature (Kametani et al., 2016; Hasegawa et al., 2008), the most likely hypothesis for the change introduced by this replacement of Serine with a Glycine could be to prevent the eventual phosphorylation of position 375. Therefore, to test the potential effects of phosphorylation at this position I prepared a phosphomimic mutant of TDP-43 where the Serine in position 375 was mutated with a Glutamic Acid (S375E) (Newell et al., 2018).

I then tested both the immunolocalization and the splicing capability of this phosphomimic mutant protein like we did for the S375G mutation (**Fig.35**). Immunohistochemistry analysis showed that, contrarily to the S375G variant, the localization of the S375E mutant protein is not confined to the nucleus, but is present in the cytoplasm (**Fig.35A**), while the toxicity of the S375E substitution was comparable to that of the S375G variant. I also performed an add-back experiment to correlate the mislocalization with CFTR exon 9 splicing and I observed no alteration emerged comparing to the wild-type TDP-43 (**Fig.35C**). These results suggested that the amount of TDP-43 persisting in the nucleus is sufficient to drive correct splicing of the transfected minigene (within the limits of this transient assay) (Newell et al., 2018).

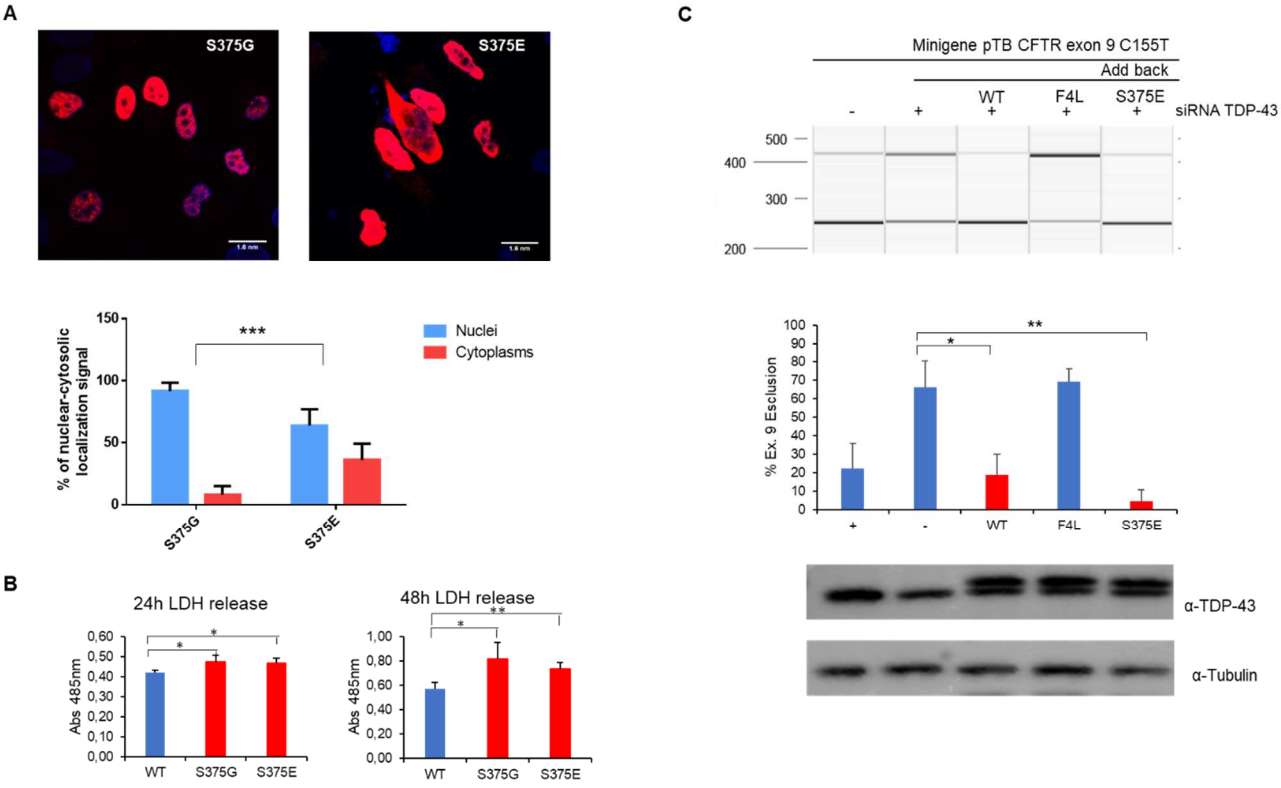

Figure 35 - S375E phosphomimic analysis. A) Immunofluorescence analysis of the pFlagSiRTDP-43 S375G and S375E. The mutant TDP-43 was detected with an α-flag antibody (red) and the nuclei were stained with DAPI. A ROI quantification is also reported showing a significant difference between the amount of protein present in the cytoplasm of the transfected cells. Unpaired t-test was performed using GraphPad software (GraphPad Software, La Jolla California, USA). B) LDH release assay. Multiple comparison one-way Anova test with Bonferroni's correction was performed using GraphPad software (GraphPad Software, La Jolla California, USA). C) Add-back assay performed with QIAxcel, testing exon 9 splicing with the S375E phosphomimic. A western blot analysis was performed to detect the efficiency of Silencing and the presence of the transfected protein (Newell et al., 2018).

Neurodegenerative disorders are characterized by cellular stress and looking at the effects of these two mutations on the cellular distribution of TDP-43 it was therefore

interesting to see what happens if the cells are stressed following transfection. For this reason, I induced cell stress by treating HeLa cells with sodium arsenate (Colombrita et al., 2009). Upon this condition, the S375E phosphomimic showed an even stronger cytoplasmic localization than WT, whereas the S375G seemed to remain mostly unaffected and still predominantly localized in the nucleus (**Fig.36**) (Newell et al., 2018).

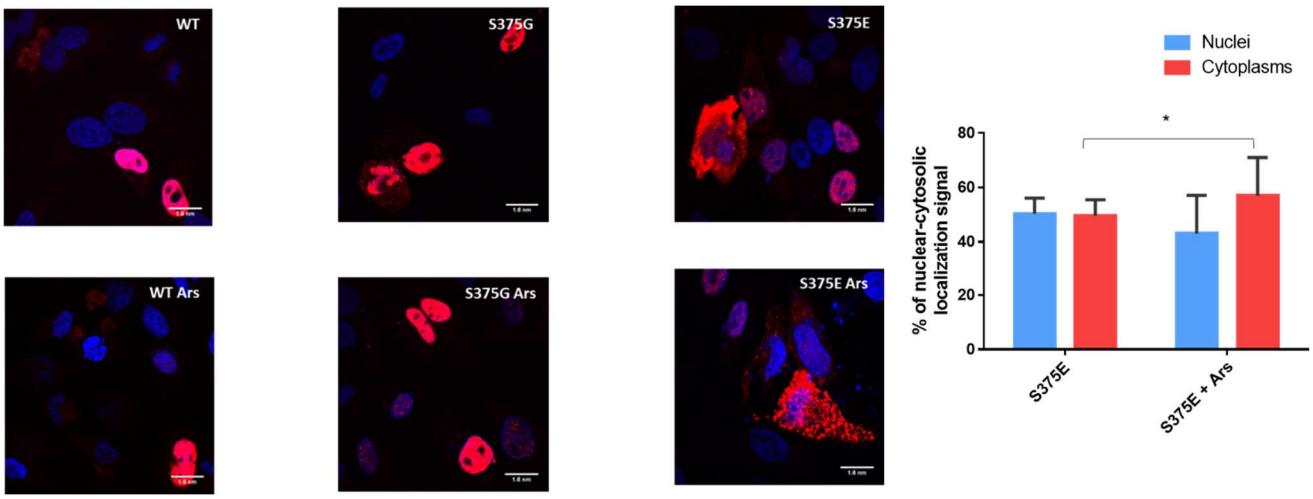

Figure 36 - S375G and S375E immunolocalization under sodium arsenate stress conditions. In red are detected the transfected WT, S375G and S375E using an α-flag antibody. The nuclei are stained with DAPI (blue). Unpaired t-test was performed using GraphPad software (GraphPad Software, La Jolla California, USA) (Newell et al., 2018)

4.1.2.5 Analysis of the effects of other sites in TDP-43 CTD that have been shown to undergo phosphorylation

Based on these results, I therefore decided to consider the neighboring residues to S375 in the C-terminal tail of the protein in order to understand if the capability to balance the nuclear-cytoplasmic amount of the protein was specific for the region or whether this ability to affect TDP-43 localization was a specific property of the 375 residue (Newell et al., 2018).

In particular, to perform this analysis I decided to consider two paper from Hasegawa's group that were published in 2008 and 2016 and analyzed the potential phosphorylation sites in vitro and in two patients in vivo by mass spectrometry (Kametani et al., 2016; Hasegawa et al., 2008).

Following the literature (Buratti, 2015), I therefore combined the potential phosphorylation sites with the described disease associated variant, reported in table 21.

Residues	*In vitro* phosphorylation	*In vivo* ALS P1	*In vivo* ALS P2	Mutations	References
S 2	√	X	X		
Y 4	√	X	X		
T 25	√	X	X		
T 88	√	X	X		
S 91	√	X	X		
S 92	√	X	X		
T 116	√	X	X		
S 183	√	X	X		
S 242	√	√	√		
S 273	√	X	X		
S 292	√	X	√	**S292N**	(Zou et al., 2012; Xiong et al., 2010)
S 305	√	√	√		
S 317	X	√	√		
S 332	X	X	√	**S332N**	(Corrado et al., 2009)
S 333	X	X	√		
S 342	√	X	X		
S 347	√	X	X		
S 350	√	X	X		
S 369	√	X	X		
S 373	X	X	√		
S 375	√	√	√	**S375G**	
S 377	√	X	X		
S 379	√	X	√	**S379C / S379P**	(Chiang et al., 2012; Ticozzi et al., 2011; Corrado et al., 2009)
S 387	√	√	√	**S387delinsTNP**	(Solski et al., 2012)
S 389	√	√	√		
S 393	√	√	√	**S393L**	(Praline et al., 2012; Origone et al., 2010; Corrado et al., 2009)
S 395	√	√	√		
S 403	√	√	X		
S 404	√	√	√		
S 407	√	X	√		
S 408	√	X	√		
S 410	√	X	√		

Table 21 - TDP-43 potential phosphorylation sites and disease-associated mutations already described in literature.

Using these criteria, I was therefore able to extend my functional analyses to other sites (highlighted in yellow in table 21) localized in TDP-43 C-terminal domain. As a consequence, I then prepared four different phosphomimic flag-tag, siRNA-resistant, TDP-

43 plasmid, mutating the Serine (S) residue with a Glutamic acid (E) (Newell et al., 2018). As shown in **Figure 37**, all of these changes were single residue mutation except for the S387-95E which included four different mutation sites (S387, S389, S393, S395) because the Serine residues of interest were one next to the other (Newell et al., 2018).

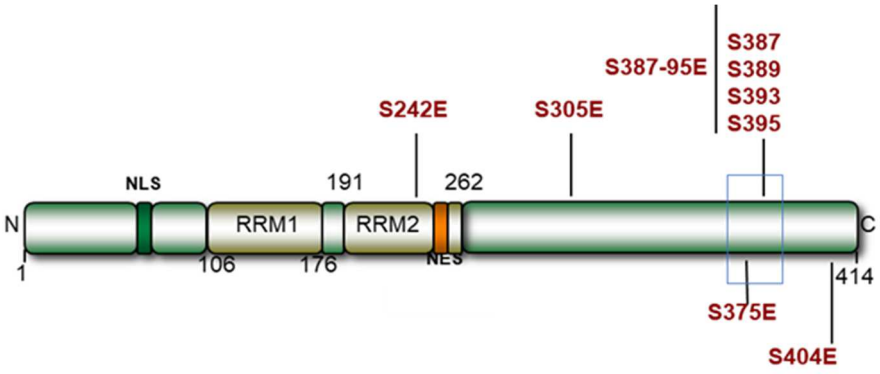

Figure 37 - TDP-43 phosphomimic analyzed residues.

In **Figure 38** are reported the immunohistochemical data obtained on transfected HeLa cells of all these mutants. After analyzing the immunofluorescence images (**Fig.38A**) and from the ROI graph (**Fig.38B**), it is clear that the only phosphomimic plasmid able to reproduce the phenotype of the S375E was the S387-95E, composed by four different mutated sites (Newell et al., 2018). Taken together, these results have suggested that the capability to balance TDP-43 amount in the nucleus or in the cytoplasm can be specifically connected to S375 potential phosphorylation and that phosphorylation events in the S375 surrounding region could contribute in controlling TDP-43 intracellular redistribution (Newell et al., 2018).

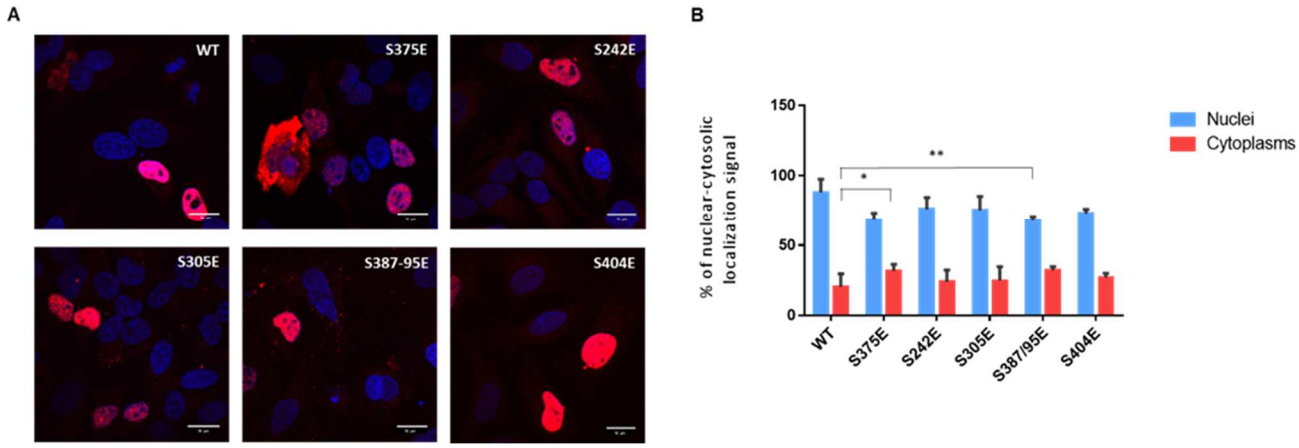

Figure 38 - TDP-43 CTD phosphomimic analysis. A) immunolocalization of TDP-43 phosphomimic in CTD. B) Nuclear-cytoplasmic localization derived from ROI analysis. Multiple comparison one-way Anova test with Bonferroni's correction was performed using GraphPad software (GraphPad Software, La Jolla California, USA) (Newell et al., 2018).

4.1.2.6 Molecular dynamic (MD) simulation: propensity of β-sheet formation in TDP-43 371-376 CTD segment upon S375G and phosphomimic S375E substitutions

The results obtained by the phosphomimic mutants could not explain, however, why a phosphorylation event at this site is capable of affecting TDP-43 localization. To further characterize this point, we decided to focus on the structural integrity of the WT sequence comparing to the S375G and the S375E mutants. In particular, I decided to focus on inter-molecular interactions that might be occurring in this region between different TDP-43 molecules. Thanks to the help of our collaborators in Spain (University of Castile-La Mancha, *Instituto Regional de Investigación Científica Aplicada* (IRICA), Ciudad Real, Spain; and Instituto de Química Física "Rocasolano", Consejo Superior de Investigaciones Científicas, Madrid, Spain) we performed structural investigations of the TDP-43 C-terminal region that includes the S375 residue. First of all, three segments of the CTD containing the residue of interest were selected for peptide synthesis: N_{371}-NSYSG$_{376}$ for the WT protein; N_{371}-NSYGG$_{376}$ for the variant S375G; and N_{371}-NSYEG$_{376}$ for the phosphomimic S375E. On these segments, our collaborators performed molecular dynamic simulations and, as shown in **Figure 39**, a measure was obtained at three different time points (**Fig.39A**) as well as the Cα–Cα intra-β-sheet distances were measured throughout the course of the simulations (**Fig.39B**). As shown in this figure, both WT and S375G exhibited a high structural stability, which we interpret as the ability to S375G to maintain inter-protein contacts similar to those of the WT sequence. On the other hand, S375E showed an

instability assembly due to the presence of strong electrostatic repulsions which are promoting structure dissociation (Newell et al., 2018).

Taken together, these results suggest that phosphorylation of S375 might mediate a key aspect of TDP-43 assembly and nuclear localization, meaning that the lack of S375 phosphorylation induced by the mutation can promote TDP-43 self-association and therefore its nuclear retention (Newell et al., 2018).

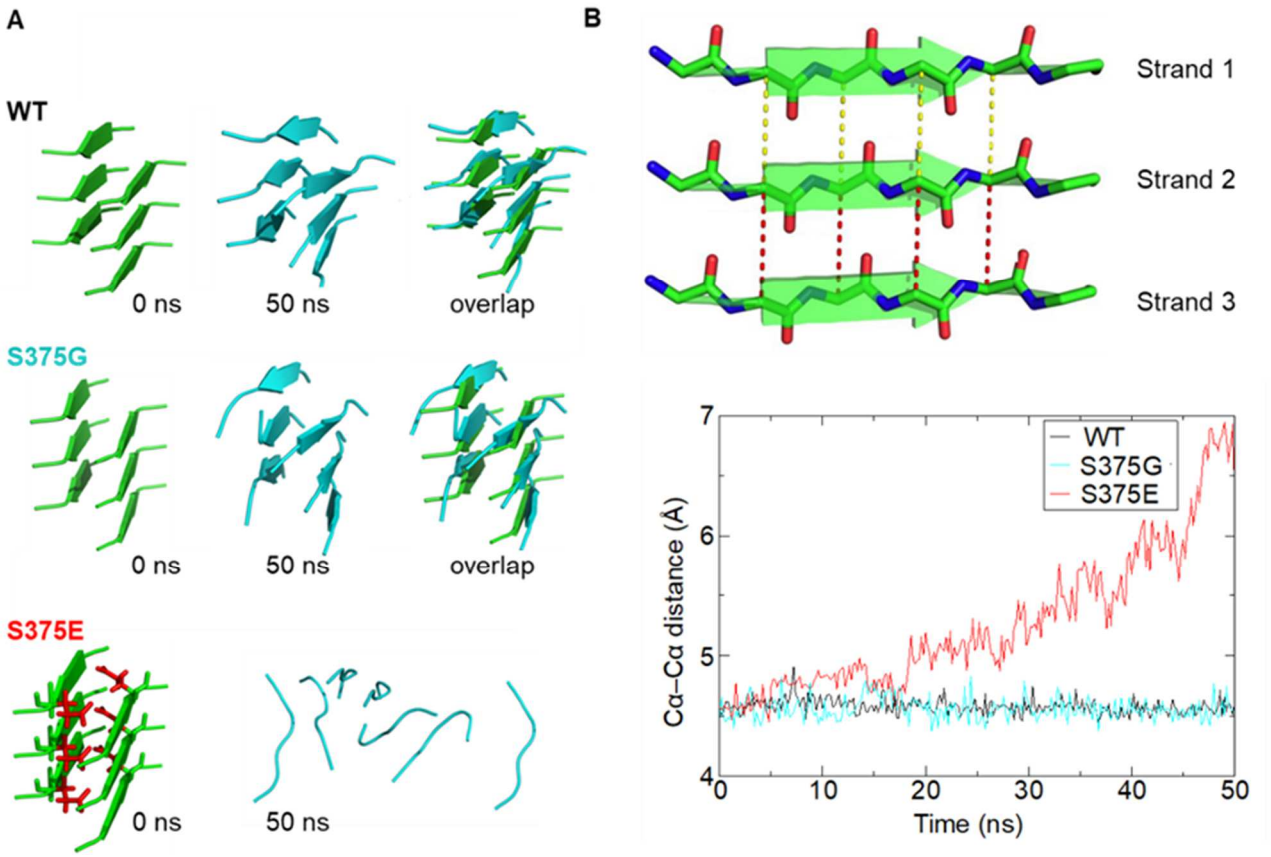

Figure 39 – Molecular dynamic simulation analysis. A) The molecular dynamic trajectories were followed at 0 (green) and after 50ns (blue). From the overlap of the starting and the finishing sequence, the WT and the S375G remained assembled during the simulation time; instead, the phosphomimic S375E variant was disassembled. B) Cα- Cα inter-β-strands and intra-β-sheet measurements. Each of these distances was calculated at each data point of the simulation, and they were all averaged and plotted (lower part of the panel). Whereas WT and S375G inter-strand distances remained constant over time (blue and violet curves), S375E (red) increased as a result of disassembly (Newell et al., 2018). *Figure in collaboration with Miguel Mompean.*

4.1.3 Creation of a stable cell line expressing S375G and S375E

The problem with transient transfections is that the relatively low efficiency of cells producing the transfected protein and time limitations do not allow to fully appreciate what could be the functional differences introduced by these mutations. Therefore, based on the results obtained with the transient transfection experiments, I decided to create a stable cellular model in which the flag-tag, siRNA resistant S375G and the S375E variants could be expressed constantly following induction (together with a stable cell line stably expressing wild-type TDP-43).

As discussed in detail in the Material and Methods section, I prepared these different stable clones in the Hek293 Flp-In T-REx (Life Technology, Carlsbad, California, USA) cell line where the exogenous protein can be inducible expressed upon addition of Tetracycline to the cell media. Following these results, I tested all the prepared stable clones for what concern the protein expression. As reported in **Figure 40**, in the flag-tag siRNA resistant TDP-43 WT two clones, on five prepared, did not work; all the clones prepared for the S375G have a good expression; all the S375E clones are fine, with the exception for the S375E1 clone 2 in which the expression is also present in the Tet off (-) sample, maybe due to small amount of Tet in the serum (reported also in the datasheet troubleshooting).

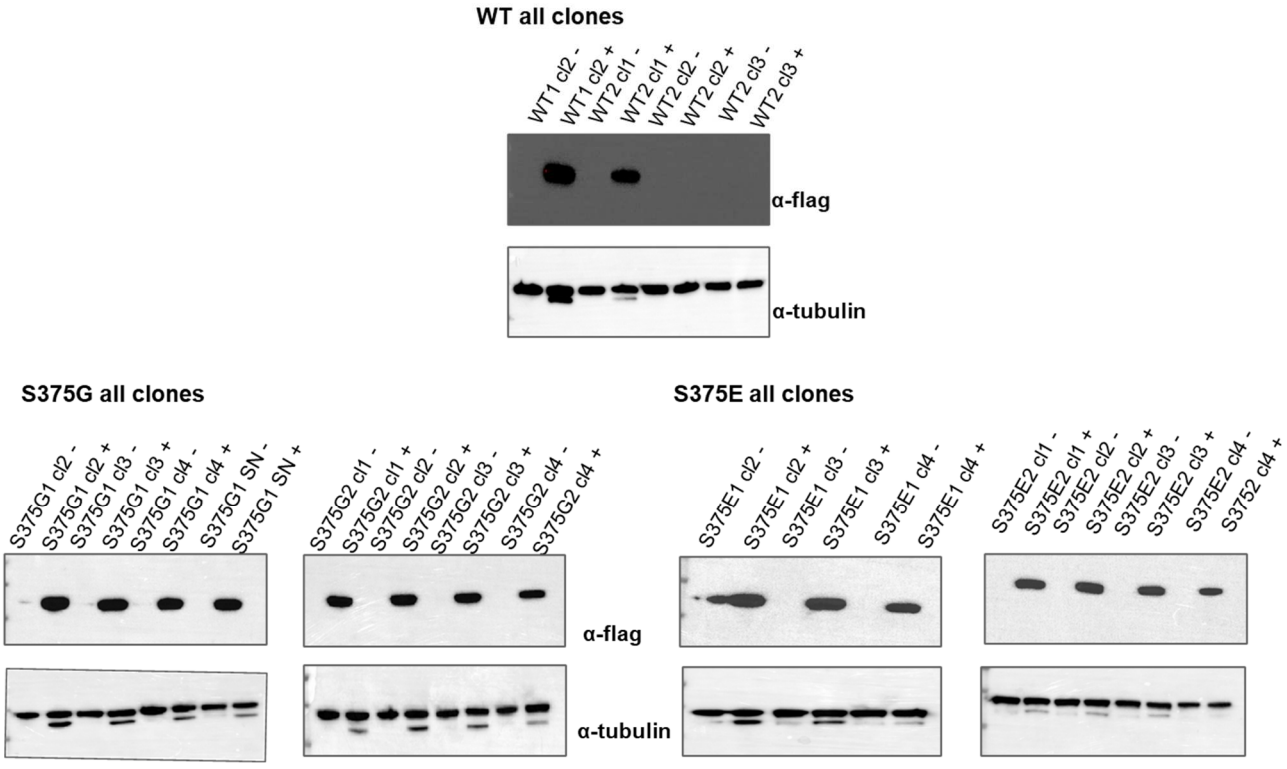

Figure 40 - Western blot analysis of all the stable clones prepared. The stable protein was detected with α-flag antibody and the tubulin was used as internal standard: the band under the tubulin is the flag antibody because they are detected with the same secondary antibody.

Subsequential selection of the positive clones, WT1-Clone1, S375G2-Clone1, and S375E2-Clone4 were employed for all the following assays due to their similar expression levels. **Figure 41** show the levels of protein expression at 24, 48 and 72 hours after induction for all three cell lines expressing TDP-43, WT, S375G and S375E. As shown in this figure, expression remained stable for all three different time laps and for all further experiments I induced the clones for 48 hours.

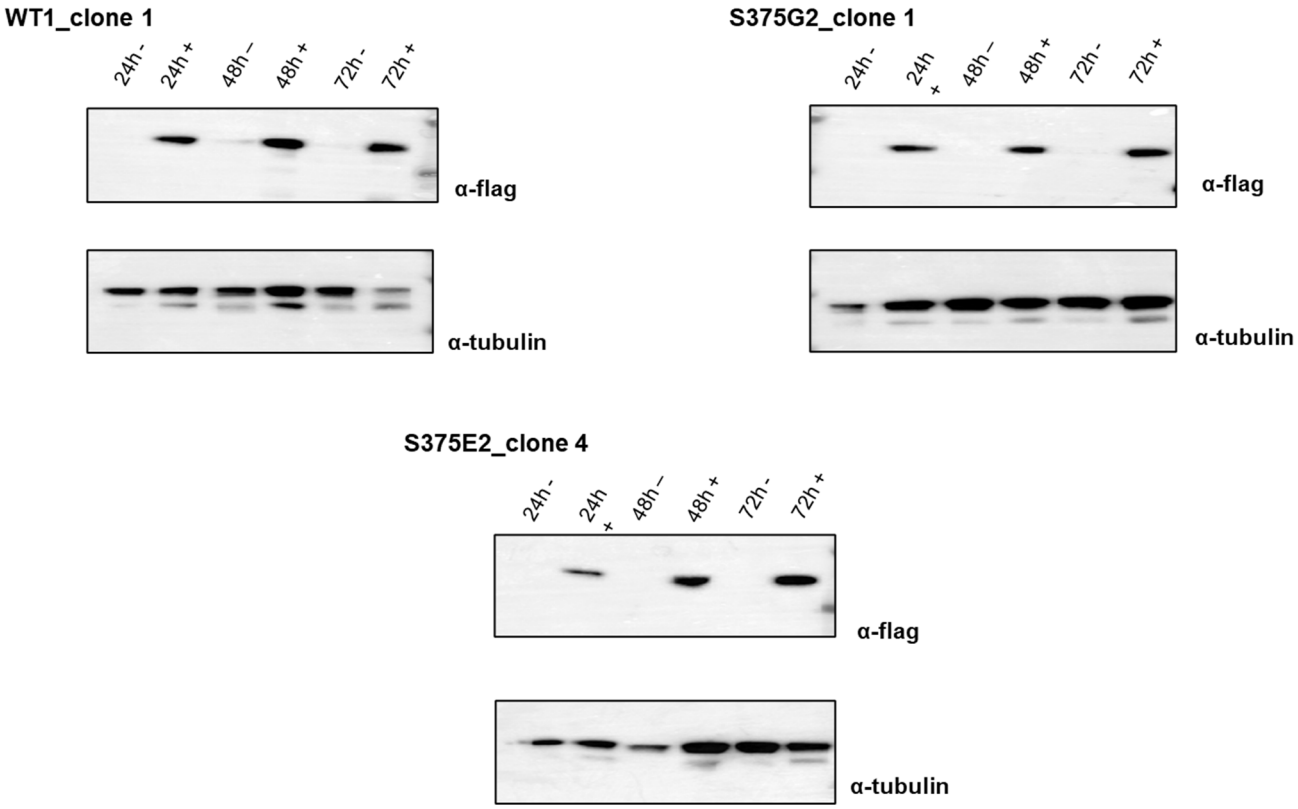

Figure 41 - Western blot analysis testing stable clones' expression at three different time points: 24, 48 and 72 hours. The expression of the stable allele upon tetracycline induction, was detected with α-flag antibody, specific for the recognition of the stable protein only. Tubulin was used as a standard loading control.

First of all, although in transient transfection I observed no effects of these mutations on TDP-43 splicing ability, I decided to look again at the splicing capability of the various TDP-43s in the stable clones (because of its presumably greatest sensitivity). In particular, because all cells are producing the exogenous protein upon induction, there was no reason to transfect the CFTR minigene as a reporter system. Instead, I decided to look at *POLDIP3* as an endogenous target gene in all three cell lines (**Fig.42**). The reason this gene was chosen is because it is one of the most well characterized endogenous targets from the point of view of TDP-43 splicing properties. In this gene, in fact, the inclusion of exon 3 is completely dependent on the binding of TDP-43 to a UG-rich region downstream from the 5'ss (Fiesel et al., 2012). In normal conditions, TDP-43 splicing activity results in about 80% of exon 3 inclusion and approximately 20% of exon 3 exclusion. As shown in **Figure 42**, the S375G mutant and the S375E phosphomimic cell lines were behaving exactly as the WT in terms of keeping the same inclusion/exclusion ratio of exon 3, thus confirming the previous results obtained with the CFTR exon 9 mini gene in the transient transfection experiments (Newell et al., 2018).

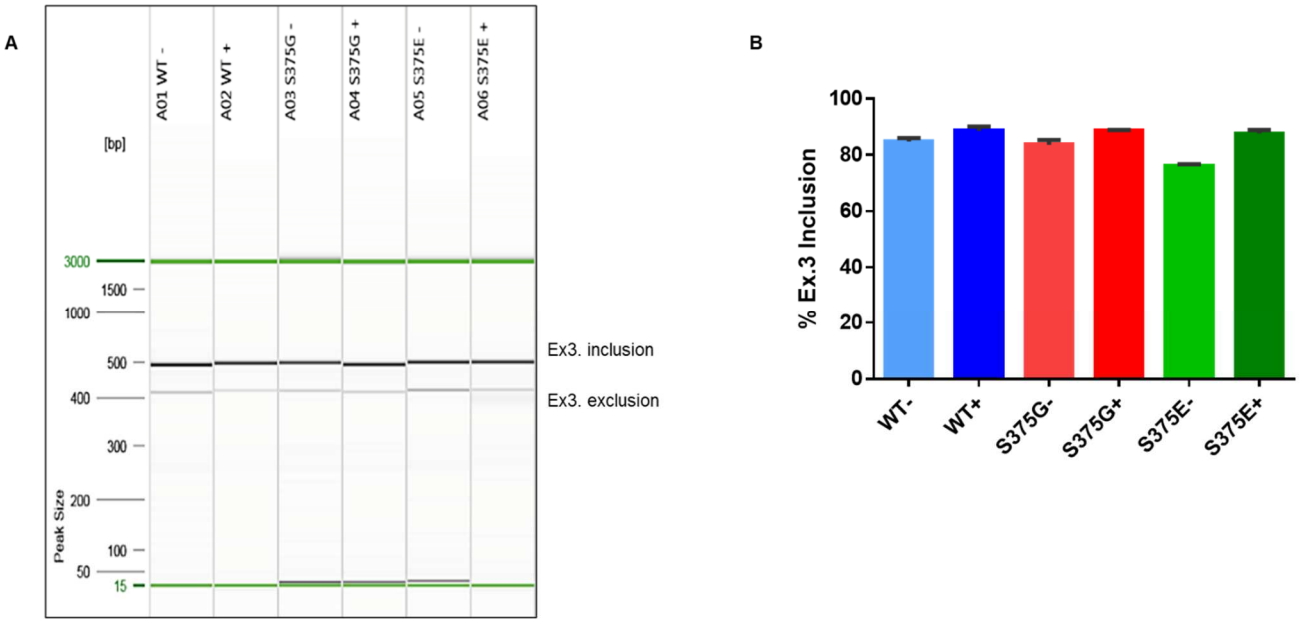

Figure 42 - POLDIP3 gene splicing analysis. A) Qiaxcel capillary electrophoresis gel image. B) Statistical analysis of POLDIP3 exon 3 inclusion performed with multiple comparison one-way Anova test with Bonferroni's correction using GraphPad software (GraphPad Software, La Jolla California, USA).

The availability of these stable clones also represented a powerful tool that could clarify some involved processes bypassing the limits of a transient transfection. For example, they are suitable to examine eventual alterations in TDP-43 autoregulation levels or the presence of this protein in the soluble or insoluble fraction.

Following this idea, I first studied the behavior of the S375G mutant and the S375E phosphomimic in the autoregulation process of endogenous TDP-43. As previously mentioned in the Introduction, TDP-43 is able to bind to a specific region in the 3'UTR of its pre-mRNA and trigger the skipping of intron 7 that contains one of the major polyadenylation sites of its mRNA (pA1). Loss of this polyadenylation site forces the use of another suboptimal polyA site (pA2) and this leads to nuclear retention and degradation of the transcript. In fact, one of the first observations we did when expressing TDP-43 in a stable manner was that the induced exogenous protein was capable of "switching-off" expression of the endogenous gene (Budini and Buratti, 2011). It was therefore interesting to see if the S375G and S375E clones were capable of downregulating the endogenous gene as well as the WT TDP-43 protein. As shown in **Figure 43**, however, all stable alleles were able to inhibit expression of the endogenous TDP-43 in a similar manner and no statistical differences were reported in autoregulation activity of the mutated TDP-43 form comparing to the WT.

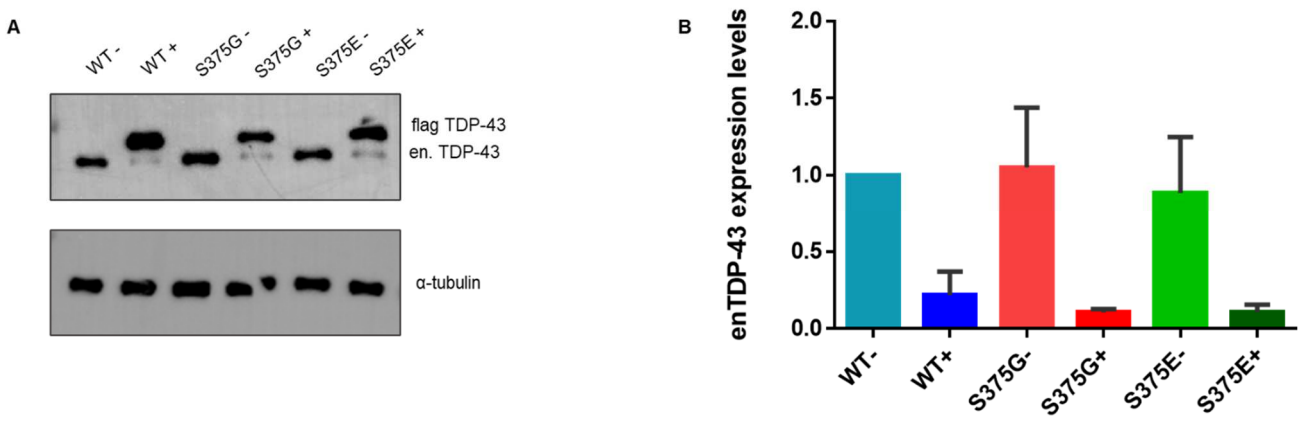

Figure 43 - S375G and S375E stable alleles autoregulation on the endogenous TDP-43. A) Western Blot analysis performed against total TDP-43. Tubulin was used as a loading control. B) Statistical analysis of endogenous TDP-43 expression levels performed with multiple comparison one-way Anova test with Bonferroni's correction using GraphPad software (GraphPad Software, La Jolla California, USA).

As autoregulation was not impaired, I then decided to study the presence of the mutated proteins in the soluble/insoluble fraction, something that would have been difficult to study in transient transfection because of the lower expression. However, all the stable proteins were present both in the soluble as in the insoluble fraction even though they are mainly soluble (**Fig.44**). Therefore, also for the solubility assay, no significant differences could be reported for S375G and S375E compared to WT.

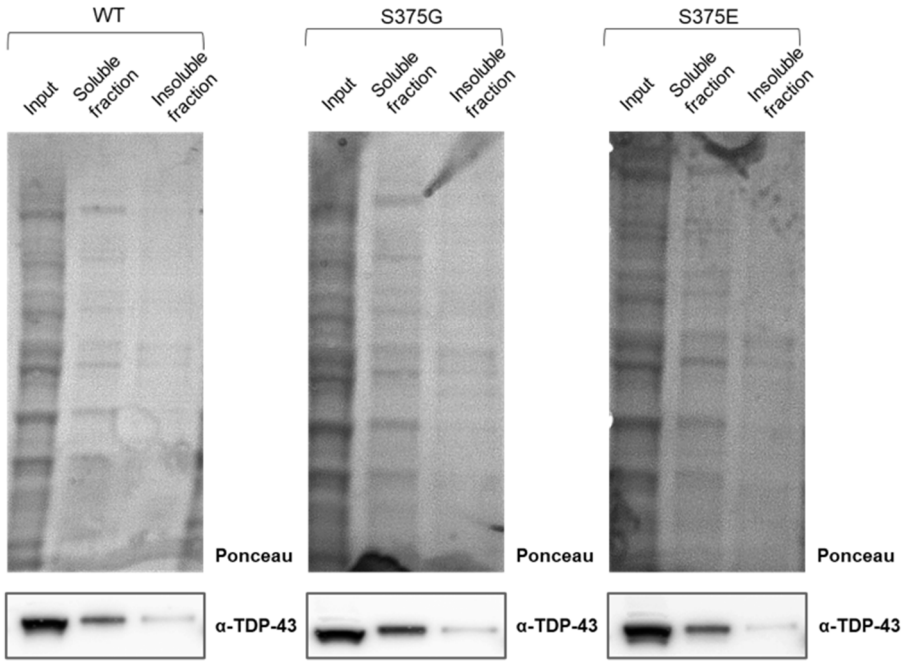

Figure 44 - Western Blot analysis of the solubility assay performed on the stable clones. The membranes were stained against the total TDP-43. I used the Pierce Reversible Protein Stain Kit for Nitrocellulose Membranes (ThermoFisher

Scientific, Waltham, Massachusetts, USA) as a loading control. Please note that the Pierce Reversible staining kit does not allow any quantification.

The same assay was also repeated upon sodium arsenate treatment, in order to check if the protein solubility could have changed in cell stress conditions. However, upon induced stress conditions, both mutated forms of TDP-43 remained mainly soluble as the WT (**Fig.45**).

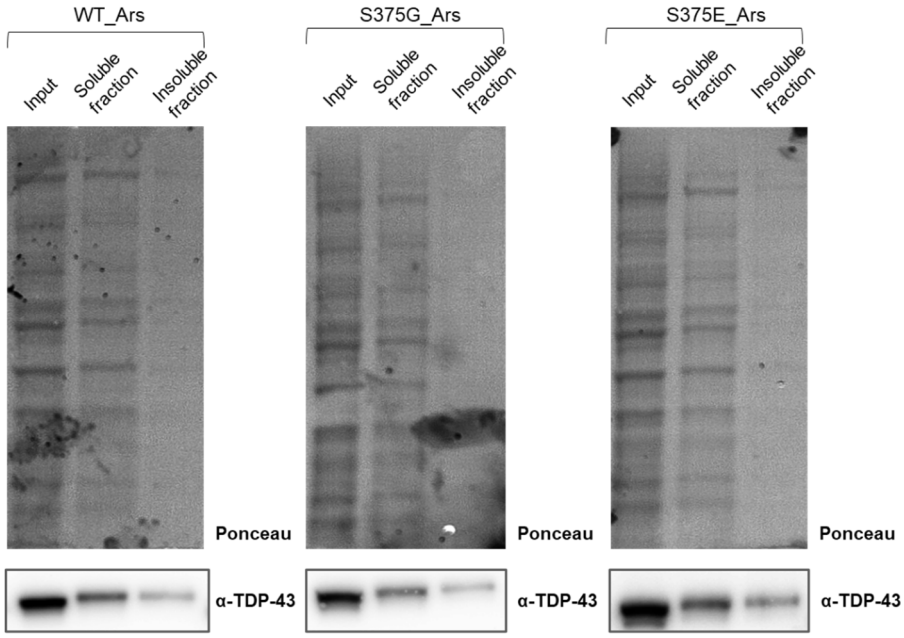

Figure 45 - Western Blot solubility assay of the stable clones upon arsenate treatment. The membranes were stained against the total TDP-43. I performed the Pierce Reversible Protein Stain Kit for Nitrocellulose Membranes (ThermoFisher Scientific, Waltham, Massachusetts, USA) as a loading control. Please note that the Pierce Reversible staining kit does not allow any quantification.

Considering that the autoregulation and the solubility assay yielded negative results, I then tested the stable clones for the immunolocalization of the mutants in order to see if there were more distinguishing features that were not observed in previous transient expression experiments (Newell et al., 2018). Interestingly, as shown in **Figure 46**, I noticed that in the S375G and the S375E stable clones there seemed to be an abundance of nuclei with a non-canonical shape (highlighted with white circle in **Figure 46**), similar to dividing/apoptotic cells. This outcome had not been noticed in the transient transfection experiments probably because in transient transfections only a minority of cells were actually transfected by the plasmids. Importantly, this difference was particularly present for the phosphomimic S375E mutant that showed a higher number of non-canonical nuclear shape (around 20%) compared to the S375G (9%) and to the WT (6%).

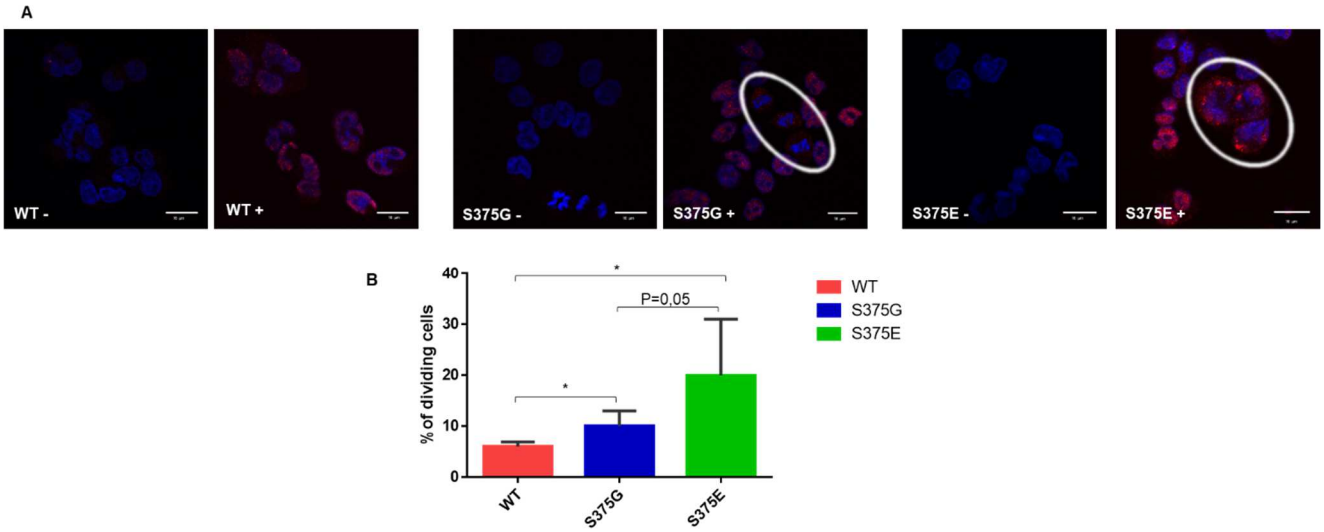

Figure 46 – Stable clones immunolocalization analysis. A) Immunofluorescence images are reported for all the stable clones with and without tetracycline induction. Here I reported the merged images between the nuclei (DAPI channel in blue); and the Alexa-Fluor 594 (red) detecting the anti-flag TDP-43 (such as the stable alleles expression). B) Statistical analysis of the percentage of non-canonical nuclear shape was performed with unpaired t-test using GraphPad software (GraphPad Software, La Jolla California, USA).

This immunolocalization experiment was also performed upon induced cell stress conditions, after treating the stable clones with sodium arsenate. In stress conditions, the number of non-canonical nuclear shape increased in both the mutant forms (S375G around 20%, and S375E around 30%), but it was constantly higher for the phosphomimic variant (**Fig.47**).

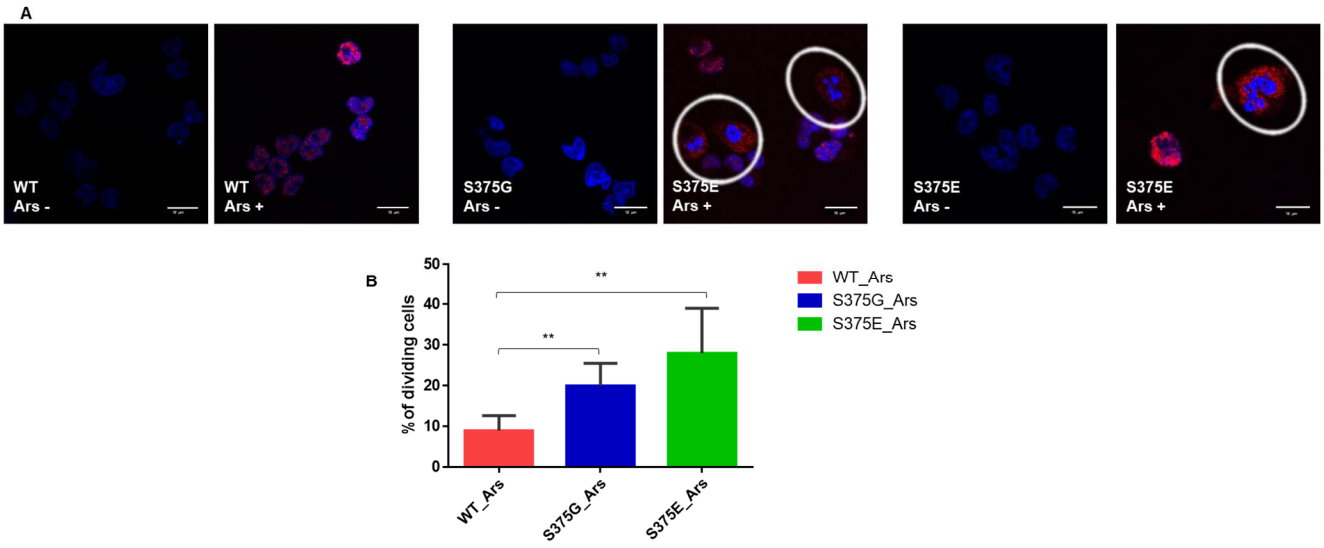

Figure 47 - Immunolocalization analysis upon sodium arsenate treatment. A) Immunofluorescence images are reported for all the stable clones with and without tetracycline induction. Here I reported the merged images between the DAPI channel (blue), staining the nuclei; and the Alexa-Fluor 594 (red) detecting the anti-flag TDP-43 (such as the stable

alleles expression). B) Statistical analysis of the percentage of non-canonical nuclear shape was performed with unpaired t-test using GraphPad software (GraphPad Software, La Jolla California, USA).

Following this interesting result, I tested if the S375G mutation and especially if the phosphomimic mutant S375E could affect cell cycle.

It is in fact known through the literature that TDP-43 is involved in mRNA stability of Cyclin Dependent Kinase (CdK6), an important regulator of cell cycle progression in the restriction point (Youhna M Ayala et al., 2008). To investigate the possible impairment of the cell cycle and Cdk6 involvement in this observed increase of cell division I performed a Western Blot analysis against Cdk6. As shown in **Figure 48**, however, no differences were reported between the WT and the S375G/S375E mutant forms in Cdk6 expression levels.

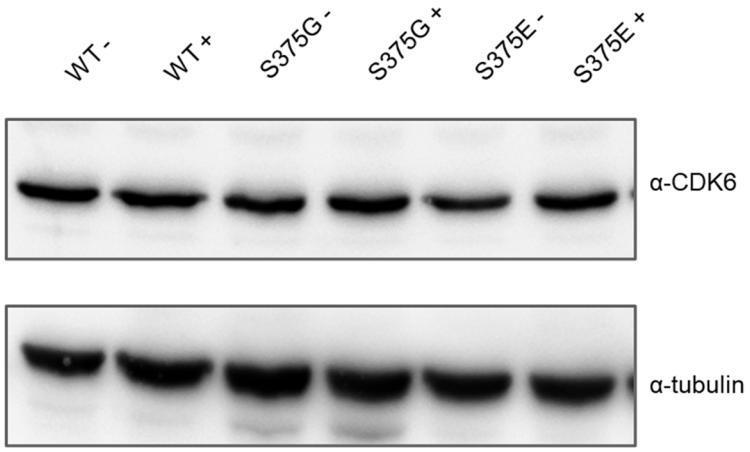

Figure 48 - Western Blot against CdK6. Tubulin was performed as a standard loading control.

In parallel, in order to check if this observation was due to an impairment of the cell cycle, a flow cytometry (FACS) analysis was performed using propidium iodide staining. As shown in **Figure 49**, the G2 phase in the S375G and S375E seemed to be significantly impaired, possibly due to involvement of apoptosis.

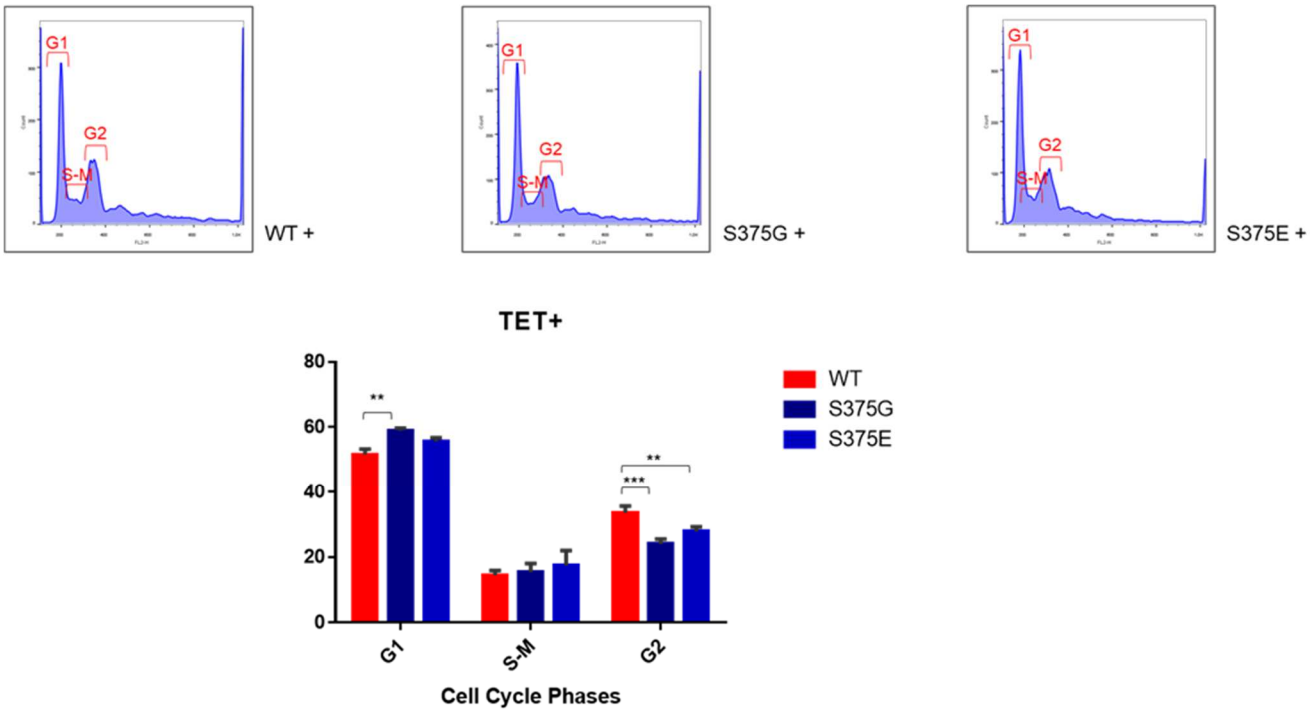

Figure 49 - Cell cycle analysis performed with flow cytometry and propidium iodide staining. In the upper part of the figure the cell cycle trend was reported for each clone stably expressing the TDP-43 form (WT, S375G, S375E mutants). The results were plotted in a grouped table and a multiple comparison one-way Anova test was performed using GraphPad software (GraphPad Software, La Jolla California, USA)

In literature, TDP-43 ctd fragmentation was already described to be linked with caspase apoptosis, but is still unknown if the caspases are activated intrinsically as a result of aberrant TDP-43 aggregation or other mechanisms are occurring (Yamashita et al., 2014).. Moreover, it is already known that TDP-43 neurotoxicity can trigger the mitochondria pathway (Braun et al., 2011). In particular the Apoptosis-inducing factor 1 (AIF1), a mitochondrial protein, was described to be consistently involved in neuronal death (Shibata et al., 2009; Krantic et al., 2007; Candé et al., 2002). Upon a lethal signal or a strong and persistent cellular stress, AIF1 protein translocate, via the cytosol, to the nucleus where it binds to DNA and provokes caspase-independent chromatin condensation (Candé et al., 2002). For this reason, AIF1 protein expression and sub-cellular localization was studied. As shown in **Figure 50** panel A, AIF1 expression was found to be increased in the S375G and in the S375E expressing clones. This data was also consistent with the immunolocalization experiment in which the AIF1 expression was more robust in the mutants. Moreover, also AIF1 sub-cellular localization was changing, following the hypothesis of mitochondria-related apoptosis. As reported in **Figure 50B**, in the WT expressing clone, AIF1 (in green) mainly localized with the mitochondria signal (red). This co-localization was also present for the S375G mutant, even if a part of the protein was

present also in the nucleus. This result was even more evident for the phosphomimic S375E mutant.

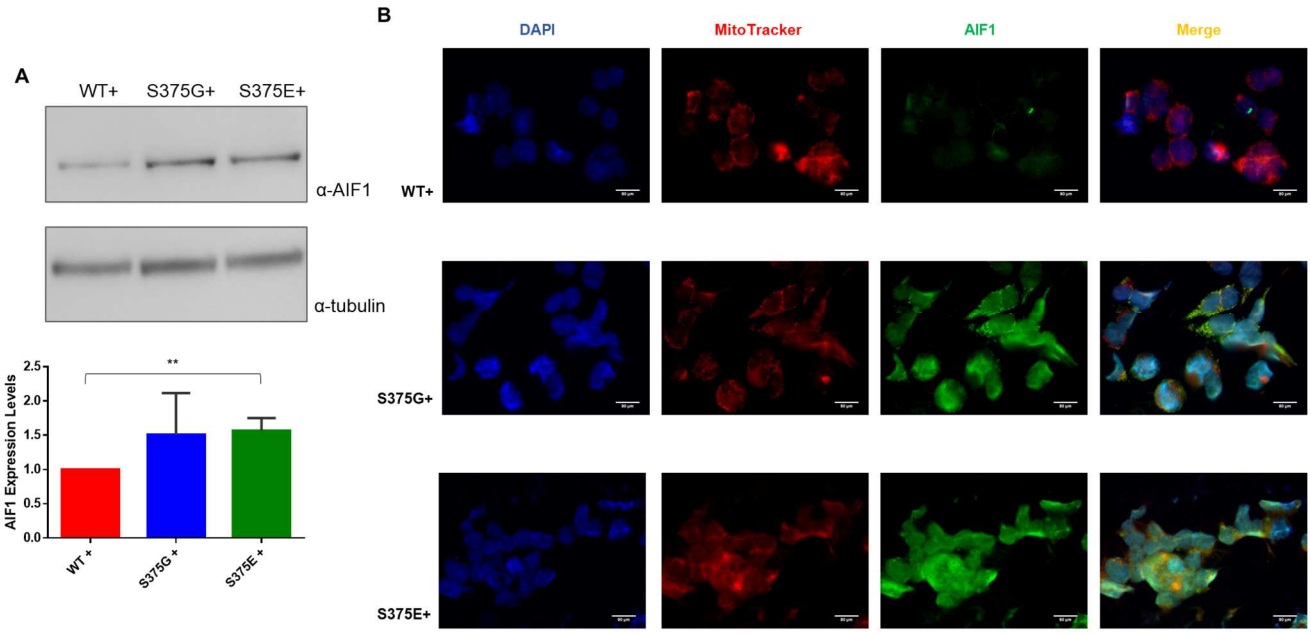

Figure 50 – AIF expression and immunolocalization analysis on stable cell line expressing WT, S375G, and S375E TDP-43. A) Western blot analysis of AIF1 expression in the stable clones (upper panel) and its quantification and statistical analysis (lower panel) performed with unpaired t-test using GraphPad software (GraphPad Software, La Jolla California, USA). Tubulin was employed as a standard loading control B) immunolocalization analysis of AIF1 protein. In blue are stained the nuclei with Hoechst; in red mitochondria signal was performed with MitoTracker Red CMXRos kit (ThermoFisher Scientific, Waltham, Massachusetts, USA); in green AIF1 signal was stained with α-mouse Alexafluor 488. The merged channels are also reported.

In the future, in order to better identify all the changes in gene expression mediated by these mutants we plan to perform RNA sequencing analysis. This will allow us, for the first time, to pinpoint exactly all the genes that are misregulated in the presence of a disease-associated mutation that changes only one aminoacidic out of the 414 which compose TDP-43. Of course, as this mutation has only been described in one individual, it is unlikely that the results will represent the basis for a therapeutic approach that might be specific just for this change. However, my hope that RNA sequences study will allow to identify pathways and genes that could mediate the toxicity of TDP-43 in neuronal cells irrespective of the presence or not of the mutation. In the future, in fact, my aim will be to test these genes/pathways for their ability to rescue the toxic effects of TDP-43 also in cells from sporadic patients where the protein is almost always in the wild-type condition.

4.2 Involvement of TDP-43 in neurological defects of Niemann-Pick type C: new therapeutic target for the disease

As already discussed in the introduction, RNA binding proteins like TDP-43 can be involved in the appearance of the neuronal degeneration features in lysosomal storage disorders (Janas et al., 2016; Jellinger, 2009; Potashkin and Meredith, 2006). A clear example of this is represented by the case of Niemann-Pick type C (NPC) where it was reported by Andrea Dardis and colleagues that TDP-43 can be found mislocalized and hyperphosphorylated in the cytoplasm in different models (Dardis et al., 2016). Following their conclusions, I further extended and characterized the differentially expressed genes occurring in NPC disease due to TDP-43 mislocalization. As for the S375G mutation, the aim of this work has been to characterize the cellular events that become misregulated upon aberrant phosphorylation and localization of TDP-43. In turn, this will hopefully be able to provide novel targets for therapeutic intervention and biomarker analysis.

4.2.1 RNA sequencing analysis on human NPC disease model

To reach our goal, we sent for RNA sequencing to Novogene (Novogene Co., Ltd, Beijing, China), eight RNA samples derived from neuronal cells differentiated from human multipotent adult stem cells isolated from the skin (hSKIN-MASCs) of NPC patients and healthy controls (**Fig.51**). These cells were differentiated to human neuronal cells using a protocol employed in a previous work by Dardis's lab and described in detail in the Material and Methods section (Bergamin et al., 2013). As shown in **Figure 51**, the differentiated neuronal cells from healthy individuals (left) and NPC patients (right) already displayed a different phenotype, with NPC cells showing larger cytoplasmic regions and less neurite growth.

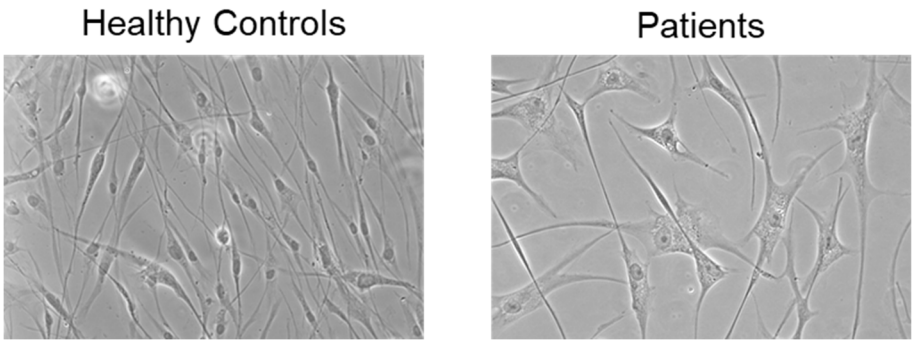

Figure 51 – Multipotent stem cells isolated from skin biopsies reprogrammed in neurons, in this figure are reported the healthy controls and the patients. Figure in collaboration with Stefania Zampieri and Andrea Dardis.

The samples' details, sent for the RNA sequencing analysis, are reported as follows in table 22.

Sample	**Mutations**		**Concentration**
CTR-1	WT	WT	1171,18
CTR-2	WT	WT	728,06
CTR-3	WT	WT	894,15
CTR-4	WT	WT	875,74
PT_1	-p.I1061T c.3182 T>C	-p.I1061T c.3182 T>C	1121,83
PT_2	-p.I1061T c.3182 T>C	-p.I1061T c.3182 T>C	616,65
PT_3	-p.I1061T c.3182 T>C	-p.I1061T c.3182 T>C	725,14
PT_4	- p.M1142T c.3424T>C - p.L648H c.1943T>A	-p.C100S c. 298T>A	586,89

Table 22 – Controls (CTR) and patients (PT) details in terms of allele mutations and sample concentration.

Before sending the RNA, I performed a quality control analysis using the QIAxcel® RNA QC Kit (QIAGEN) (**Fig.52**).

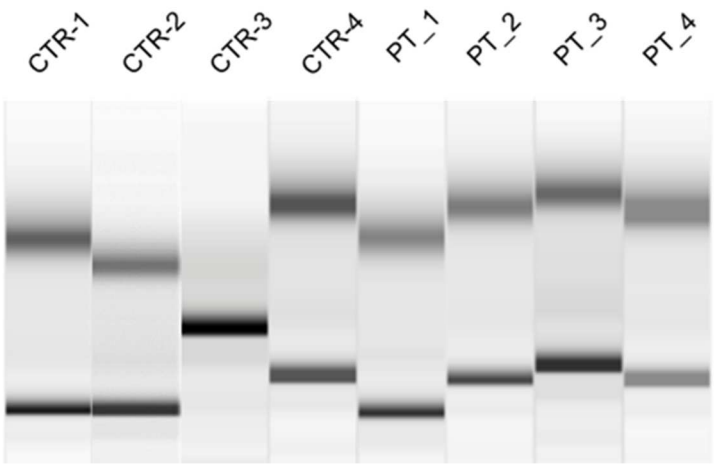

Figure 52 – RNA quality check. Qiaxcel gel image of the RNA run.

As reported in **Figure 53**, a cluster analysis was performed between the two groups in order to estimate the expression pattern of differential expressed genes and it confirmed that the gene profile of the differentiated neurons from the patients were very different from each other. As supported by the Venn diagram (**Fig.53B**), a total of 799 genes were differentially expressed between NPC patients and healthy controls out of the more 12.000 that were tested in the RNA sequence analysis.

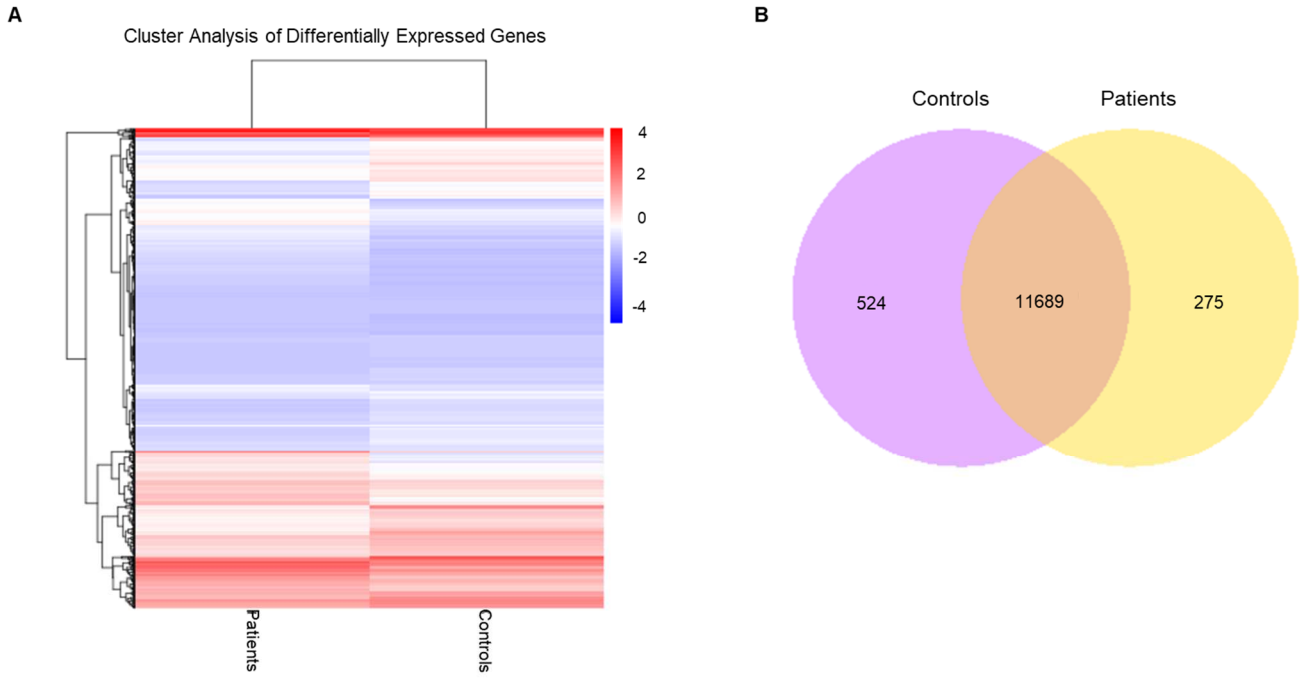

Figure 53 – Gene expression analysis of differentially expressed genes. A) Cluster analysis of differential expressed genes: in blue are represented the genes with low expression, in red the highly expressed genes. B) Venn diagram

representing the number of different expressed genes between the two groups. The overlapping region is showing the number of genes that are commonly expressed (Novogene report).

These genes were then sorted for the p-value adjusted (pAdj<0.05) and for the fold change (FC>1.3 for the up-regulated genes; FC<0.7 for the down regulated genes). They were then plotted in a Volcano plot (**Fig.54**) showing that approximately 300 genes were found up-regulated, and 500 genes were down-regulated.

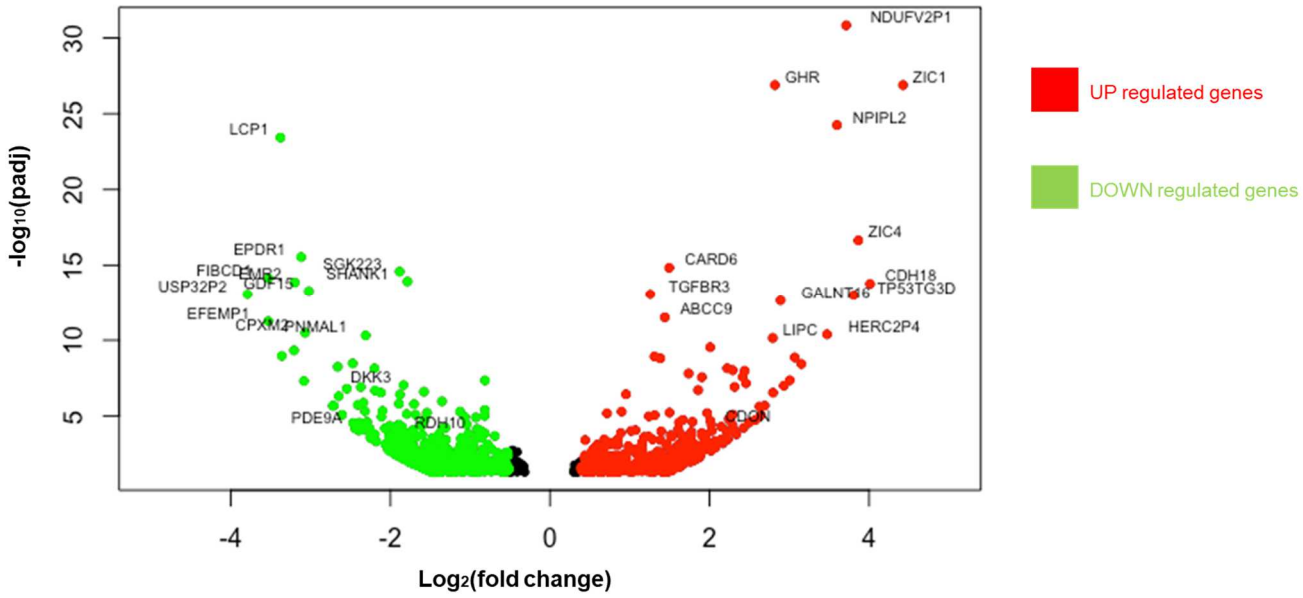

Figure 54 – Volcano plot representing the 799 differentially expressed genes. In green are reported the down-regulated genes, and in red the up-regulated targets.

A more detailed analysis was carried out in order to better understand the cellular system involved, the genes potentially associated in diseases, and the involved pathways.

As shown in **Figures 55** and **56**, a Gene Ontology (GO) and a Kyoto Encyclopedia of Genes and Genomes (KEGG) enrichment analysis were carried out. This analysis showed that many GO terms referred to genes involved in metabolic pathways (**Fig.55**), a result that is consistent with NPC pathogenesis. Moreover, the GO analysis also detected genes linked to locomotor behavior, confirming the hypothesis of a neurological impairment similar to ALS or motoneuron disease with NPC (**Fig.55**).

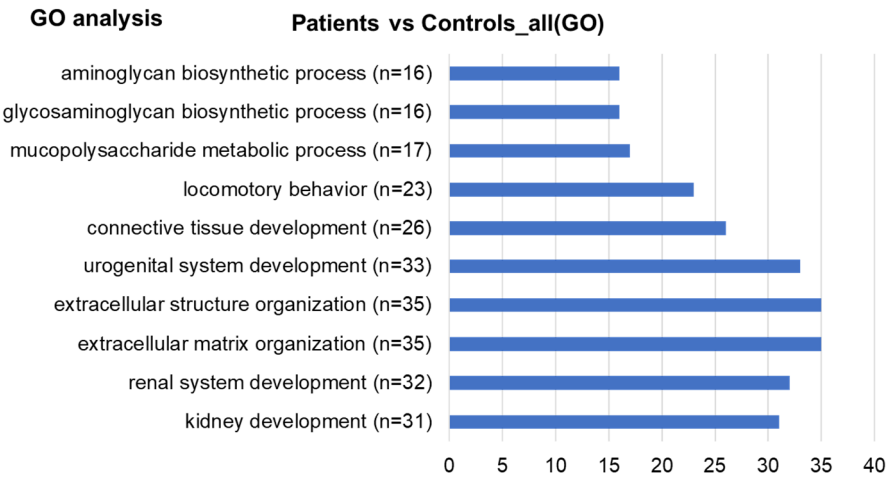

Figure 55 – GO enrichment analysis. The number of counts were plotted considering the p-value adjusted (Novogene report).

These results were also confirmed by the KEGG analysis, in which the main term to be represented was axon guidance, again in agreement with the neuronal degeneration observed in the disease (**Fig.56**).

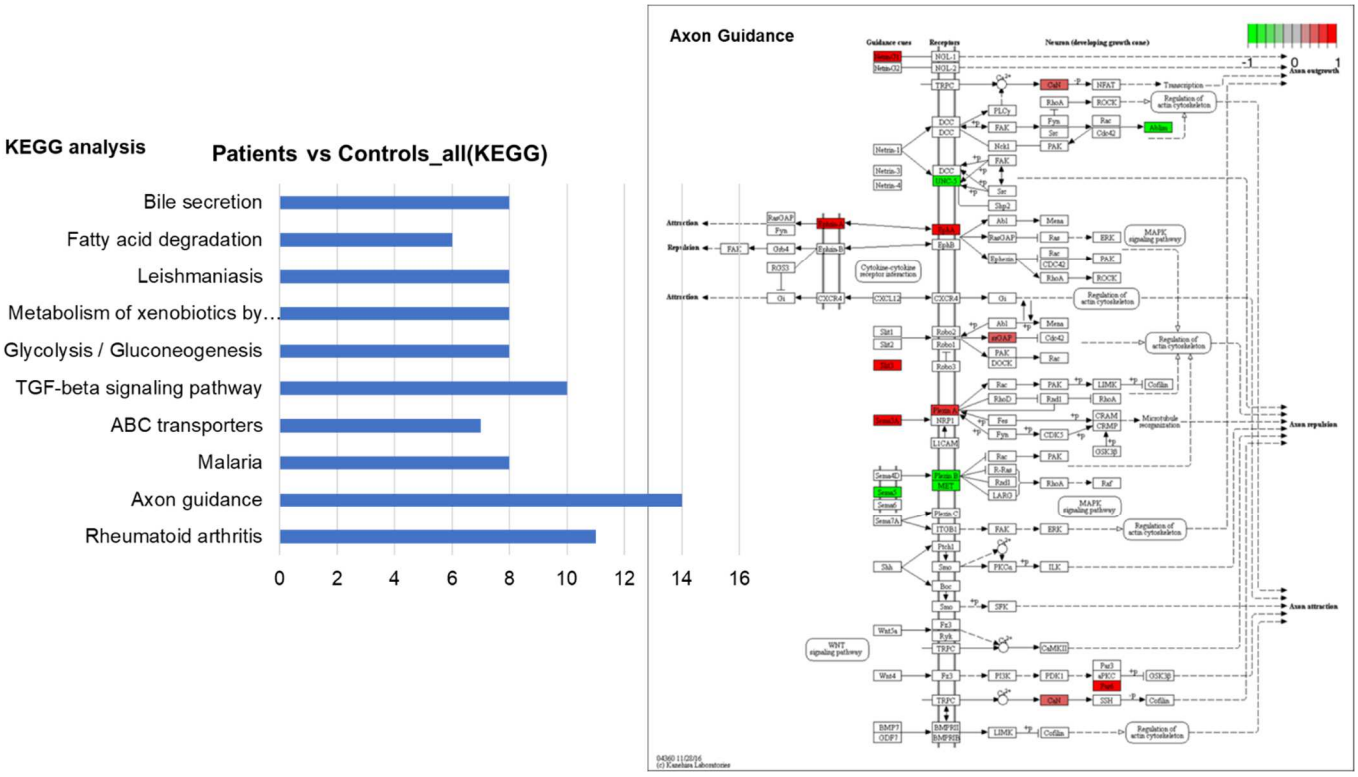

Figure 56 – KEGG enrichment analysis. The number of counts were plotted considering the p-value adjusted (right part of the panel). A deeper analysis on axon guidance term was reported (Novogene report).

Clearly, many of these deregulated gene expressions were due (directly or indirectly) to the absence of the NPC1 protein. Therefore, it would be incorrect to think that they become misregulated simply because TDP-43 in NPC is mislocalized to the cytoplasm

and aberrantly phosphorylated. Then, in order to find a relationship between the Niemann Pick type C disease and TDP-43 mis-localization and hyperphosphorylation, we decided to merge the data emerged from the NPC RNA sequencing with the data obtained from a previous RNA sequencing analysis carried out in our lab on SHSy5Y cells silenced for TDP-43 (**Fig.57**) (Cappelli et al., 2018). As a comparison with the NPC analysis, the data shown in **Figure 57** give the result of this previous analysis where 3533 genes were differentially expressed between the cells silenced for TDP-43 and the control (siLUC); around 33% of the genes were down regulated, and the 67% were up regulated. From this analysis, it emerged that many genes involved in different pathways, especially related to neurodegeneration, as well as to inflammation, became dysregulated (Cappelli et al., 2018; Appocher et al., 2017).

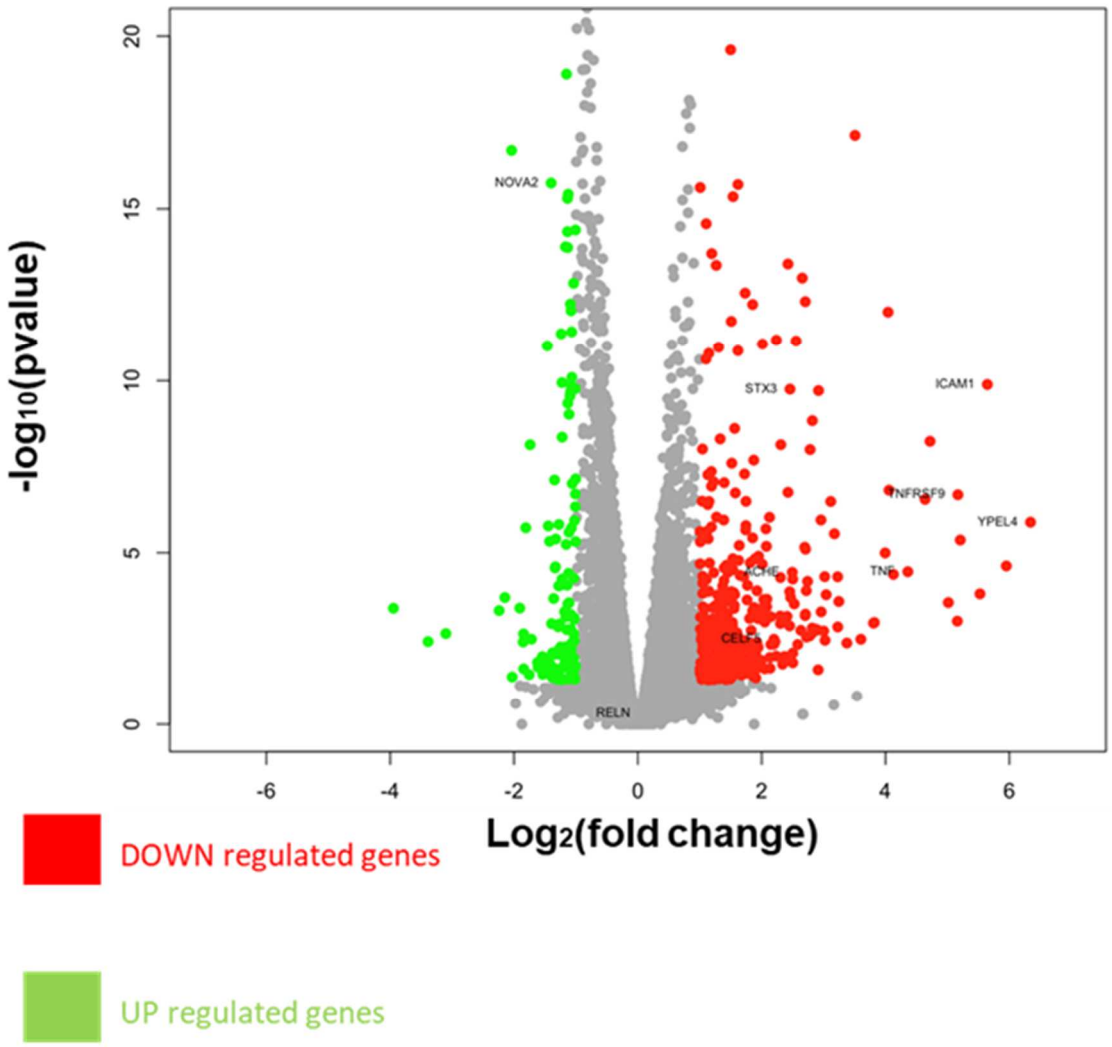

Figure 57 – Volcano plot representing the RNA sequencing data on SHSy5Y silenced for TDP-43. These data were extrapolated form the RNA sequence performed in 2017 after the paper of Appocher and colleagues (Appocher et al., 2017). Analysis performed by Sara Cappelli: data reported in her PhD thesis titled "Role of TDP-43 and hnRNP proteins in the regulation of different RNA targets", published by the Open University in 2019

As a result, the NPC RNA sequencing and the RNA seq on SHSy5Y cells with silenced TDP-43 data were merged in a volcano plot and from this combination, a total of 64 genes were discovered to be commonly misregulated. As apparent from this analysis, several of the most highly misregulated genes in NPC cells (LCP1, EPDR1, SHANK1, CDH18) are also regulated by TDP-43 levels. In particular, LPC1 is related to NF-kappa B signaling that has already been shown to play a role in the activation of apoptosis in NPC cells (Zampieri et al., 2009) whilst others are well known to play a role in synaptic activation, adhesion, axon growth, etc. (SHANK1, CDH18). Taken together these results strongly suggest that TDP-43 mislocalisation in patient cells could have a pathological effect on NPC neuronal cells function and survival.

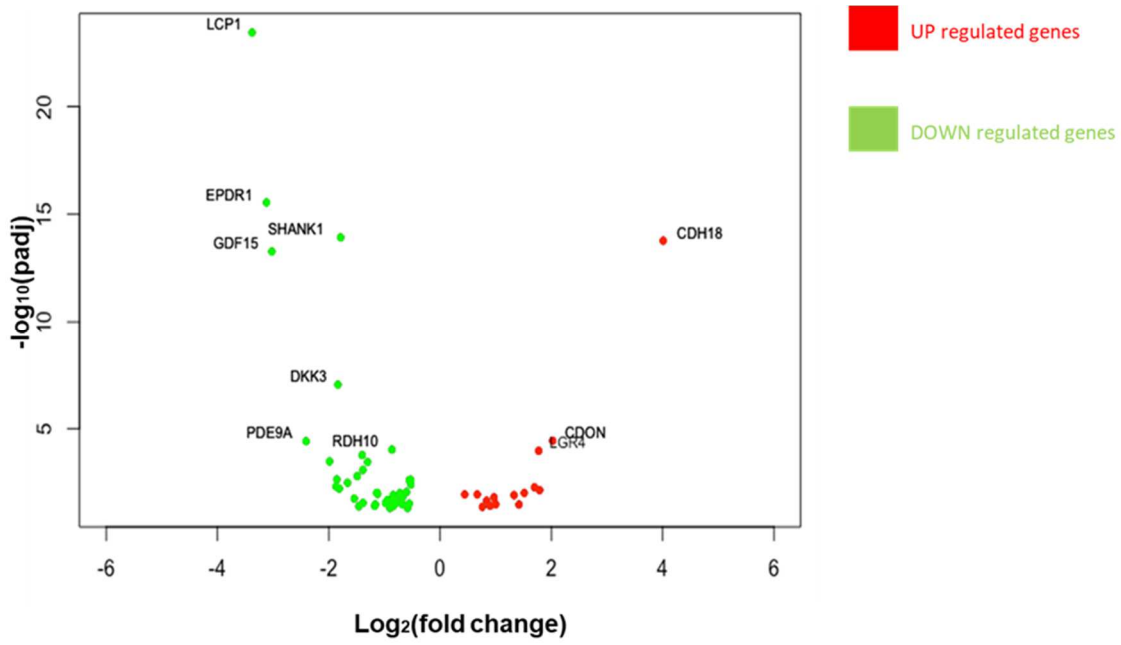

Figure 58 – Volcano plot of merged data between NPC RNA seq, and SH-SY-5Y cells silenced for TDP-43. The data were sorted for the p-value adjusted (pAdj<0.05) and for the fold change (FC>1.3 for the up-regulated genes; FC<0.7 for the down regulated genes).

4.2.2 RNA sequencing gene expression validation

Starting from the results obtained by merging the two RNA sequencing data-sets (**Fig.58**), I selected some genes based on their misregulation levels and their cellular function in order to validate the sequencing through Real Time Quantitative PCR. As

reported in Table 23, four down regulated genes and five up regulated genes were chosen for the validation analysis.

Gene Name	Gene Description	Gene Function
CDH18	Cadherin 18	Type II classical cadherin from the cadherin superfamily of integral membrane proteins that mediate calcium-dependent cell-cell adhesion. This particular cadherin is expressed specifically in the central nervous system and is putatively involved in synaptic adhesion, axon outgrowth and guidance.
DCLK1	Doublecortin Like Kinase 1	The protein encoded bind microtubules and regulate microtubule polymerization, and shows homology to Ca2+/calmodulin-dependent protein kinase mediating multiple protein-protein interactions. This protein is involved in several different cellular processes, including neuronal migration, retrograde transport, neuronal apoptosis and neurogenesis. This gene is up-regulated by brain-derived neurotrophic factor and associated with memory and general cognitive abilities.
DEPTOR	DEP Domain Containing MTOR Interacting Protein	Diseases associated with DEPTOR include Glycine N-Methyltransferase Deficiency and Metaphyseal Chondrodysplasia, Jansen Type. Among its related pathways are PI3K / Akt Signaling and Autophagy.
CDON	Cell Adhesion Associated, Oncogene Regulated	This protein is a member of a cell-surface receptor complex that mediates cell-cell interactions between muscle precursor cells and positively regulates myogenesis.
LGR4	Leucine Rich Repeat Containing G Protein-Coupled Receptor 4	It is a G-protein coupled receptor that binds R-spondins and activates the Wnt signaling pathway. This Wnt signaling pathway activation is necessary for proper development of many organs of the body.
ITPR1	Inositol 1,4,5-Trisphosphate Receptor Type 1	Upon stimulation by inositol 1,4,5-trisphosphate, this receptor mediates calcium release from the endoplasmic reticulum. Mutations in this gene cause spinocerebellar ataxia type 15, a disease associated with a heterogeneous group of cerebellar disorders.
LCP1	Lymphocyte Cytosolic Protein 1	Plastins are a family of actin-binding proteins. Diseases associated with LCP1 include B-Cell Non-Hodgkin Lymphoma and Noonan Syndrome 1. Among its related pathways are NF-kappaB Signaling.
SHANK1	SH3 And Multiple Ankyrin Repeat Domains 1	Members of this family act as scaffold proteins that are required for the development and function of neuronal synapses.
EPDR1	Ependymin Related 1	Type II transmembrane protein that is similar to two families of cell adhesion molecules, the protocadherins and ependymins. This protein may play a role in calcium-dependent cell adhesion. This protein is glycosylated, and the orthologous mouse protein is localized to the lysosome.

Table 23 – Selected genes for the RNA-sequencing validations. In red are highlight the up regulated genes; in green the down regulated items.

The validation was performed on neuronal cells differentiated from human multipoint adult stem cells isolated from the skin from NPC patients and healthy controls. Following the previous analysis, I tested three control (WT) and three NPC samples (NPC) in quantitative real-time PCR. As shown in **Figure 59**, differences in gene expression for all these genes are all statistically significant in comparison to the healthy control. Moreover, I included TDP-43 in the analysis that seemed to be slightly up-regulated in the NPC cells, presumably owing to the fact that a heavy mislocalization in the cytoplasm would induce the autoregulation mechanism to increase protein production in order to maintain normal levels in the nucleus.

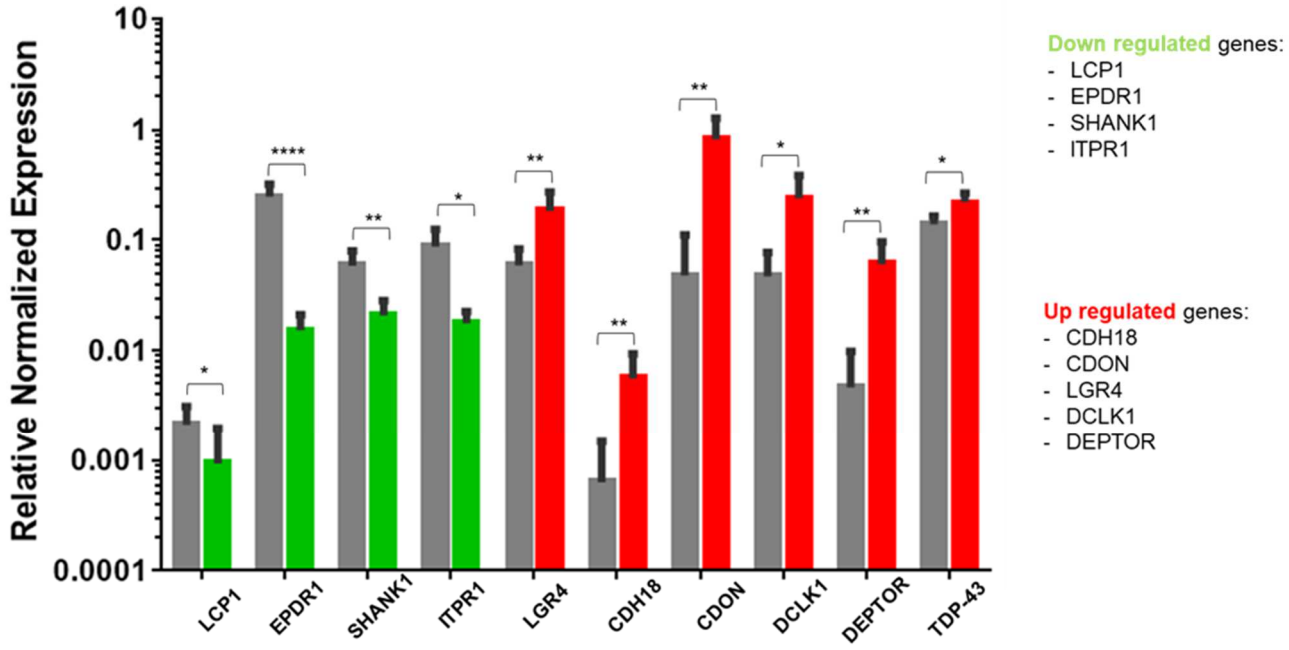

Figure 59 – Quantitative real-time PCR preliminary result on RNA sequencing validation. The statistical analysis was performed on three independent experiments each containing three technical replicates. The relative normalized expression levels were plotted in a grouped table and an unpaired t-test was performed using GraphPad software (GraphPad Software, La Jolla California, USA). In order to better visualize all the plotted data, the x axe was plotted in log_{10} scale.

4.2.3 RNA sequencing functional validation

Following the RNA sequencing gene expression validation, I performed a functional validation of the selected terms.

4.2.3.1 RNA immunoprecipitation assay

In order to establish whether direct binding of TDP-43 exists with the selected targets, an RNA immunoprecipitation assay was performed. As reported in **Figure 60**, *ITPR1* and *EPDR1* mRNAs were significantly enriched following TDP-43 immunoprecipitation compared to IgG control. The occurrence of correct transfection was controlled by Western blot, using tubulin as a loading control.

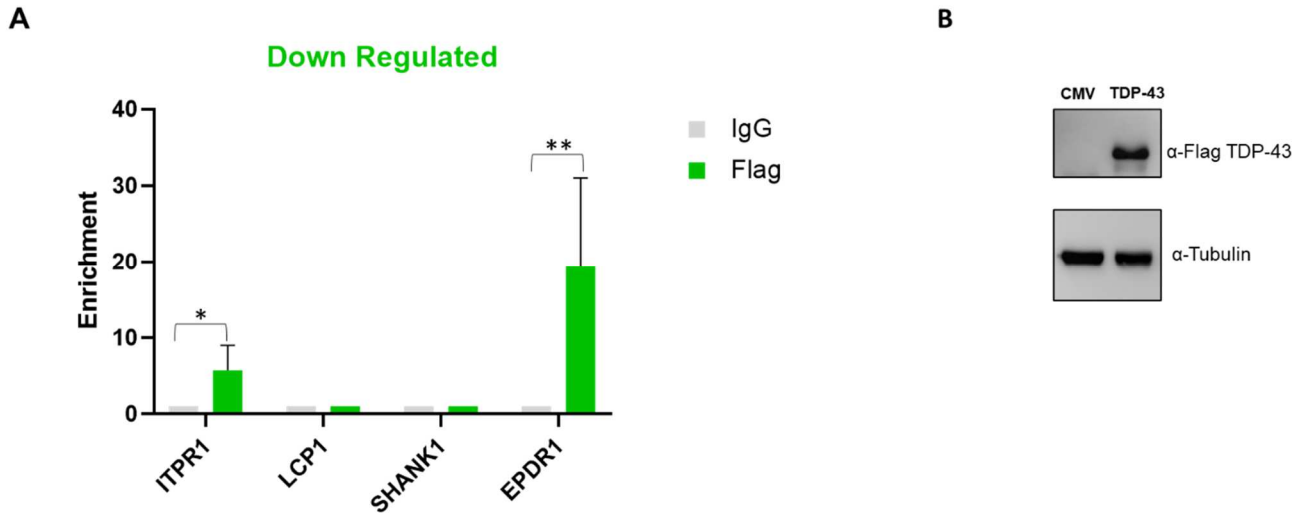

Figure 60 – RNA immunoprecipitation assay on down regulated genes. A) RNA immunoprecipitation analysis derived from quantitative real-time PCR. The obtained data were plotted in a grouped table and a multiple t-test was performed using GraphPad software (GraphPad Software, La Jolla California, USA). B) Western blot analysis was performed to check the transfection efficiency. A-flag M2 antibody was performed to check the presence of transfected TDP-43. Tubulin was used as standard loading control.

The same experiment was performed for the up-regulated selected genes. As for the down-regulated targets, correct transfection was tested first by western blot and the results showed that just *DCLK1* mRNA was significantly enriched upon TDP-43 overexpression (**Fig.61**).

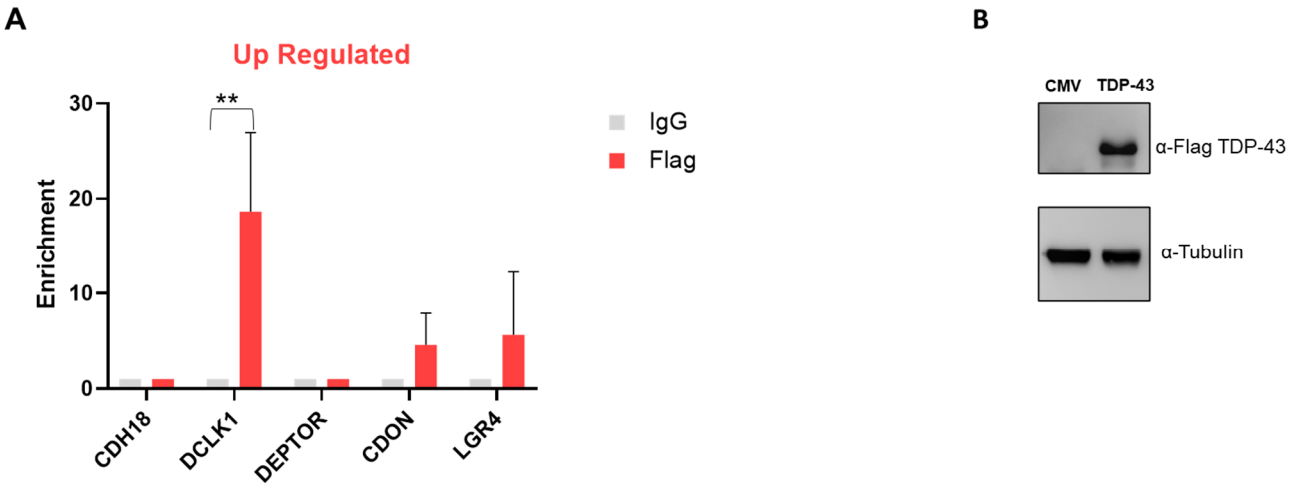

Figure 61 – RNA immunoprecipitation assay on up regulated genes. A) RNA immunoprecipitation analysis derived from quantitative real-time PCR. The obtained data were plotted in a grouped table and a multiple t-test was performed using GraphPad software (GraphPad Software, La Jolla California, USA). B) Western blot analysis was performed to check the transfection efficiency. A-flag M2 antibody was performed to check the presence of transfected TDP-43. Tubulin was used as standard loading control.

One question that may arise from these results is to determine the binding sites of TDP-43 for these mRNAs. From previous studies, it has been known that TDP-43 binds specifically the mRNA sequences that are UG/TG rich (Y. M. Ayala et al., 2008; Buratti and Baralle, 2001). Using Ensemble Genome Browser (Ensembl genome browser 102), a brief research of TG stretch was performed for *ITPR1*, *EPDR1*, and *DCLK1* genes. In all three cases, TG stretches could be found at exon/intron critical sites as well as in the flanking untranslated regions (5' and 3'UTRs). In particular, for the *EPDR1* gene I could see that the 3'UTR is strongly enriched in TG stretches. At the moment, functional experiments have not yet been performed to validate these potential binding sites. In the future, this will probably be necessary to determine exactly how TDP-43 direct binding can affect mRNA processing in these genes (i.e., splicing, stability, transport) and therefore their expression.

4.2.3.2 Down-regulated genes functional analysis

In order to establish a functional significance for the selected genes, I tested in SHSy5Y cell line the effect of up- or down-regulating the expression of these genes by silencing or overexpression.

I started the analysis with the down regulated genes because the production of a siRNA is faster than the cloning of a target in a plasmid for overexpression.

4.2.3.2.1 Down-regulated genes functional analysis: LDH release assay

Following the previous observations, I decided to test the following genes: *LCP1*, *EPDR1*, *SHANK1*, *ITPR1*). Then, after 24, 48, and 72 hours after siRNA treatment the cellular LDH levels were measured together with the gene expression levels in order to check the silencing efficiency. As shown in **Figure 62**, all the genes were significantly silenced compared to the negative control that was represented by the siRNA against the *Luciferase* (siLUC) (**Fig.62A**, **B**, and **C** right part). In the left part of all panels, cellular toxicity was reported compared to the control (siLUC). As shown in this figure, only *ITPR1* silencing showed a significant cellular toxicity at 48h that reach a maximum effect at 72 hours.

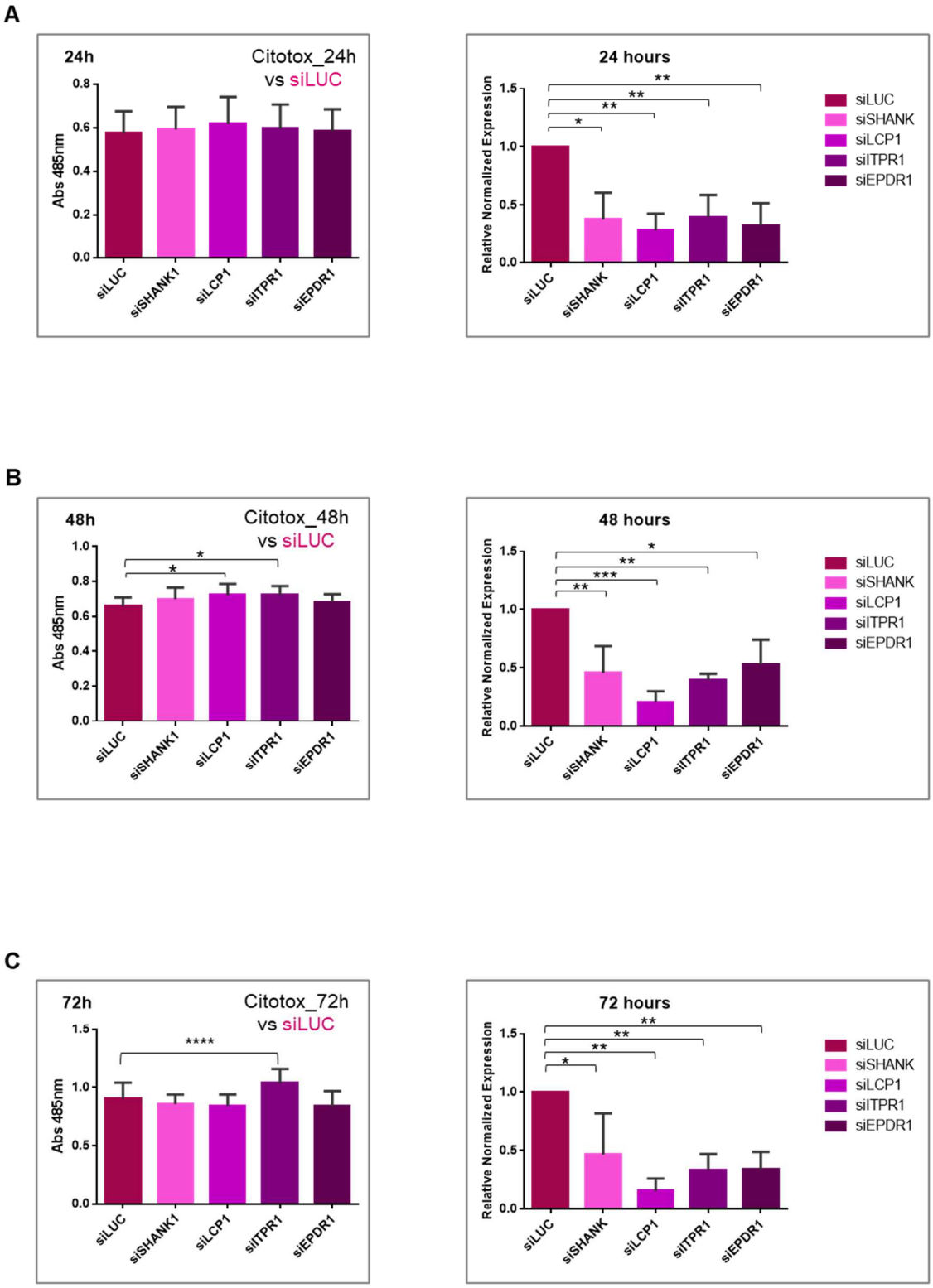

Figure 62 – LDH release assay. The absorbance at 485 nm is reported, and three-time laps (24 (A), 48 (B), and 72 (C) hours) were studied. In all panels the gene expression upon silencing tested by quantitative real-time PCR is also reported. The statistical analysis was performed on three independent experiment with multiple comparison one-way Anova with Bonferroni's correction using GraphPad software (GraphPad Software, La Jolla California, USA).

4.2.3.2.2 Down-regulated genes functional analysis: TDP-43 and pTDP-43 immunolocalization analysis upon *ITPR1* knockdown

Based on these preliminary results, *ITPR1* seemed to be the most promising target to further characterize in terms of its relationship with TDP-43. In order to establish a possible bi-functional correlation between ITPR1 and TDP-43 the localization of TDP-43 phosphorylated S409/S410 form was tested upon *ITPR1* knockdown. As reported in **Figure 64**, following *ITPR1* silencing the localization of TDP-43 was more cytoplasmic and its phosphorylated form was even more expressed compared to the control.

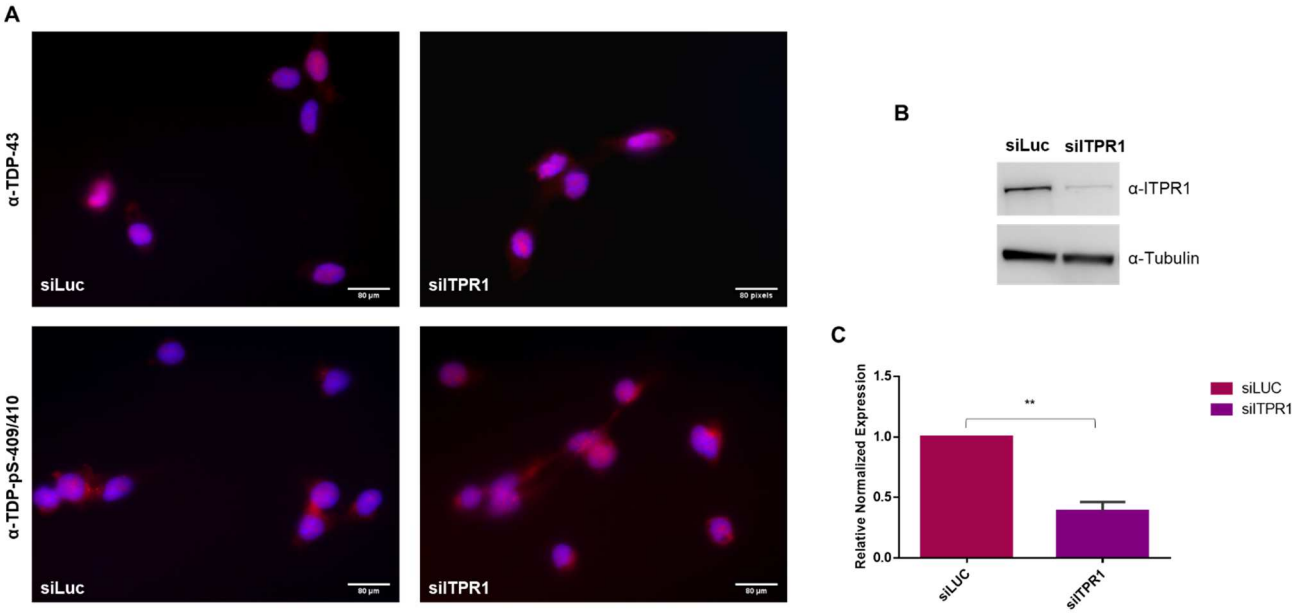

Figure 63 – TDP-43 and pS409/S410 TDP-43 immunostaining upon ITPR1 *silencing. A) TDP-43 and pS409/410 TDP-43 staining for the control (siLUC) and for* ITPR1 *knockdown. The merged images are showed. B) Western blot control of* ITPR1 *silencing efficiency. C) Quantitative real time PCR test of* ITPR1 *silencing performed in three independent experiments. The results were plotted in column table and a T-test analysis was performed using GraphPad software (GraphPad Software, La Jolla California, USA).*

5 DISCUSSION

The role of PTMs in controlling both physiological and pathological status of different proteins has been studied a long time in order to improve diagnostic, prognostic approaches and also for identifying new specific targets for a list of many heterogeneous disorders, including neurodegeneration (Buratti, 2018; Pagel et al., 2015).

In the work for my thesis, I have focused on TDP-43 phosphorylation that seems to play an important role in different neurodegenerative disorders and appears as a common aberrant feature in the ALS/FTD type of diseases as well as in metabolic disorders such as Niemann Pick C (Buratti, 2018; Dardis et al., 2016; Neumann et al., 2009; Weihl et al., 2008). In all of these pathological contexts, the balance between physiological and pathological status is very delicate, and for this reason I studied two different models in which TDP-43 phosphorylation is impaired: a disease-associated TDP-43 mutation in a particularly early-onset ALS patient and aberrant phosphorylation of TDP-43 in NPC disease.

5.1 Characterization of TDP-43 mutation in an ALS case affecting a potential phosphorylation site

Regarding ALS disease, together with a group in Indiana/Kansas University, I described for the first time a novel mutation in TDP-43 affecting a Serine residue changing in a Glycine in position 375 (S375G) that was present in a particularly early-onset ALS case, with upper and lower motoneuron involvement, and the presence of hyperphosphorylated TDP-43.

As already described in the Introduction chapter, TDP-43 mutations are quite rare events and it is not always easy to prove a clear relationship between the discovered variant and the disease (Buratti, 2015). However, looking at the literature, a lot of mutations with a clinical significance have been described over the years and many of them are affecting a potential phosphorylation site: by removing a potential site of phosphorylation, by inserting a Serine or a Threonine, thus adding a novel hypothetical phosphorylated residue, or by missense substitutions that introduce negatively charged aminoacids such as Glutamic or Aspartic acid, thus mimicking a phosphorylation event (Buratti, 2018). All of these alterations can change the protein-protein interaction profile of TDP-43, increase its aggregation, and affect half-life or its cytoplasmic localization. Taken together, these observations lead to the hypothesis that phosphorylation could play a key role between the physiological and pathological balance (Buratti, 2015, 2018; Newell et al., 2018).

In many respects, the S375G mutation that I described in this work could change any of these features and its molecular/functional analysis. It is therefore interesting to compare our results with the effects of other mutations already studied in literature that could involve changes in the phosphorylation status of TDP-43.

Starting with the disruption of a potential phosphorylation site, Corrado and colleagues in 2009 described a novel mutation (S396L) with a deleterious effect on the protein structure that was leading to the formation of low molecular weight fragments (around 32 KDa), probably after affecting TDP-43 stability (Corrado et al., 2009). In keeping with these results, it was interesting to note that the S375G mutation can also affect the protein structure and stability, but instead of promoting fragmentation it was promoting the TDP-43 self-association and its nuclear retention (Newell et al., 2018).

In another occurrence, Xiong and colleagues described a Serine changed to an Asparagine in position 292 and predicted the variation to be deleterious for protein function,

although no functional validation was provided (Buratti, 2015; Xiong et al., 2010). Similarly, the S375G mutation is disrupting the normal protein functions, in particular regarding the role played by TDP-43 in cell cycle regulation. Moreover, the structural analysis of S375 surrounding residues suggested that the ability of these mutations to alter TDP-43 localization in the nucleus (or in the cytoplasm for its phosphomimic mutant) could be specifically connected to S375 potential phosphorylation (Newell et al., 2018).

Nearer to the 375 position, previous works identified the insertion of a Threonine instead of a Serine in position 387. In this work, Solski and colleagues showed that S387T was inducing loss of nuclear TDP-43, correlating well with the formation of cytoplasmic inclusions upon induced stress (Solski et al., 2012). The Threonine is also a potential phosphorylated residue, and upon stress condition this post-translational modification can become aberrant (Buratti, 2018). This result is consistent with the one obtained with our S375E phosphomimic mutant, in which its cytoplasmic presence, compared to WT protein, was even more persistent upon sodium arsenate induced stress conditions (Newell et al., 2018). This is somewhat similar to the results of another mutations, A315E that was shown to increase TDP-43 cytoplasmic amount of TDP-43 following structural modifications (Zhu et al., 2014).

Importantly, many mutations that create a novel potential phosphorylated site were also described in literature to be related with aggregation. For example, N390S mutation was described to enhance TDP-43 aggregation and insolubility and the G295S mutation was found to induce twisted amyloid-like fibers that increased the aggregative status of TDP-43 (Jo et al., 2020; Gendron et al., 2013). These results are in contrast with our mutants, in which the protein seems to remain mainly soluble with the exception of the S375E phosphomimic upon arsenate treatment. Moreover, the presence of the negative charge promotes the disruption of the amyloid-like structure in the S375E mutant. This difference is interesting because it shows that mutations in TDP-43 phosphorylation may have a great variety of effects and will not necessarily overlap with each other. This is also confirmed by the description of other mutations such as R361S and N390S that were increasing the CTD truncated forms (Gendron et al., 2013). Also, in this case, this result differs from the one obtained in the S375E phosphomimic mutant where no truncated forms were revealed both in the transient transfection experiments as well as in the stable cell line.

Finally, another example is the A382T mutation that was described to induce a reduction in the ability of cells to respond to cellular stress leading to a TDP-43 loss of

function. There are also in this case some similarities with our S375 changes in terms of responding to cellular stress. However, there are also important differences as S375 can become toxic and aberrant in the pathological status through a gain of function mechanism (Newell et al., 2018; Orrù et al., 2016).

As shown from all these examples, the disruption or the insertion of a novel phosphorylated site can lead to different conditions. Due to the great variability of the effects observed, however, it is important to study how the potential phosphorylation status of each mutations is influencing the protein functions both in physiological, as well as in pathological conditions. In order to perform this, the employment of a phosphomimic variant is not new in the field, and in literature are reported many examples using this technique (Wang et al., 2018; Li et al., 2017; Kim et al., 2015; Brady et al., 2011; Guo et al., 2011). The single negative charge carried by the Glutamic Acid (or the Aspartic Acid) is sufficient to mimic the phospho-modification. I also took advantage of this technique in order to clarify the strong toxicity of the S375G mutation and its nuclear retention, assuming that the phosphorylation of this residue could balance the nuclear-cytoplasmic shuttle of TDP-43 (Newell et al., 2018). Therefore, I compared the two opposite conditions, such as the lack of the Serine (S375G) with its impossibility to be phosphorylated, and its constitutive aberrant phosphorylation imposing the negative charge of the Glutamic Acid (Newell et al., 2018). As already mentioned, the transiently transfected S375E phosphomimic mutant was more localized in the cytoplasm, but without compromising the splicing capability of the protein, an effect that could be explained due to the amount of S375E TDP-43 persisting in the nucleus, which was presumably sufficient to drive correct pre-mRNA processing. Due to a molecular dynamic simulation, the different subcellular localization within the two mutants was characterized: while the WT and the S375G TDP-43 form presented a strong amyloid-like structure, the phosphomimic appeared unstable due to the presence of the negative charge (Newell et al., 2018). The disruption of TDP-43 assembly was also described by Wang and colleague in 2018, using a phosphomimic of an N-terminal Serine in position 48 (Wang et al., 2018). This is supporting the idea that the phosphorylation of the protein could induce a destabilization of TDP-43 polymerization and its cytoplasmic shuttle.

In addition, it is still unclear which kinases are responsable for this phosphorylation event. In general, TDP-43 phosphorylation is probably linked to cellular stress if we consider that TDP-43 was described to strongly regulated by the MAPK/ERK kinase. Also in this case, phosphomimic variant were employed to study the response upon TDP-43 phosphorylation.

In particular the T153 and Y155 residues, identified as MEK phosphorylated sites, were substituted with a phosphomimic residue, increasing the heat shock response, that normally occures as a survival reaction to toxic conditions (Li et al., 2017). In contrast with the S375E phosphomimic, the T153 and Y155 phosphorylation could be affecting the GU- stretch recognition, imparing TDP-43 splicing capability (Newell et al., 2018; Li et al., 2017).

In addition, TDP-43 aberrant phosphorylation can become toxic and irreversible in disease condition. Supporting this idea, the negative charge of the S375E mutant is inducing cellular toxicity (Newell et al., 2018). This result is also supported by the literature, in which phosphomimic substitution have a toxic effect on the cells. For example, Ki Yoon Kin and colleagues studied three different TDP-43 phosphomimic mutants (S379E, S403/404E, and S409/410E) that were able to reduce Drosha stability, preventing protein-protein interaction and compromising TDP-43 function, and inducing neurotoxicity in Neuro 2A cell line (Kim et al., 2015). In comparison with this work, the S375E phosphomimic mutant did not show any compromise in the protein function that concerns TDP-43 splicing capability. However, toxicity was observed that may be linked to changes in the cell cycle, as reported in the stable clones' experiments.

Taken together, the obtained results showed that the phosphorylation of S375 might be a key aspect of TDP-43 assembly and it could play an important role in the nuclear-cytoplasmic balance. The potential phosphorylation of the Serine in position 375 could be involved in the physiological phosphorylation of TDP-43, promoting its dissociation and the cytoplasmic transport, which is necessary for TDP-43 to carry on its functions. Conversely, in the S375G mutant the lack of this Serine residue was shown to promote cellular toxicity because this TDP-43 form was more confined in the nucleus, presumably affecting cytoplasmic physiological activities. Moreover, the relevance of the S375 residue could also play a role in pathological TDP-43 phosphorylation, as shown in the sodium arsenate treatment of the transfected cells with the S375E phosphomimic.

In order to better clarify this physiological/pathological subtle balance, I created stable clones expressing the WT, S375G, and S375E (phosphomimic) TDP-43 forms. Again, the stable clones creation for TDP-43 functional study was already employed in the past permitting the study of protein aggregation (Budini et al., 2012). As with transient transfections, no significant changes were reported in splicing, autoregulation, or aggregation in these stable cell lines. However, a cell cycle analysis of the stable clones

showed that the number of cells in the G2 phase decreased in the two mutants compared to the WT that could be linked with activation of apoptosis.

It is known that the apoptosis is one of the key processes promoting neurodegeneration (Ekshyyan and Aw, 2005). In particular, the mitochondria apoptotic signal is one of the key players that mediates the proapoptotic signaling in neurodegeneration (De Conti et al., 2015; Shangguan et al., 2014; Shibata et al., 2009; Krantic et al., 2007; Ekshyyan and Aw, 2005; Kermer et al., 2004; Candé et al., 2002). As already reported, the CTD fragmentation is leading to a G2 phase drop compromising cellular survival and leading to apoptosis (Yamashita et al., 2014). In this contex, considering that TDP-43 aberrant phosphorylation is one of the early responses to cellular stress and that TDP-43 neurotoxicity can trigger the mitochondria pathway, we are considering this G2 phase decrease potentially linked to the mitochondria stress signaling, leading to cell death response. In particular the Apoptosis-inducing factor 1 (AIF1), a mitochondrial protein, was described to be consistently involved in neuronal death (Shibata et al., 2009; Krantic et al., 2007; Candé et al., 2002). Based on these assumptions, I performed an immunolocalization analysis of AIF1 mitochondrial protein, and I observed that AIF1 protein in the S375G and the S375E mutants was not confined anymore in the mitochondria, but it was found diffused inside the cell, especially in the nucleus. This is consistent with the literature and could represent a sign of an early apoptotic phase where the expression of these TDP-43 mutated forms could lead to mitochondria stress signaling, resulting in AIF1 release and its shuttle from the cytoplasm to the nucleus where it could induce an apoptotic signal (Candé et al., 2002). Further analysis will be required in the future to better characterize the involved pathways, and maybe mitochondrial stress could be used as a therapeutic strategy or as an early marker for the disease.

5.2 Involvement of TDP-43 in neurological defects of Niemann-Pick type C

Disfunction of the RNA metabolism or the involvement of RNA binding proteins in lysosomal storage disorders, is one of the putative cause of the neurodegenerative features related to this disorders (Paron et al., 2020). Considering TDP-43 role in other neurodegenerative disorders, in 2016 this was studied by Andrea Dardis and colleague relating to NPC disease. They found TDP-43 mislocalized and hyperphosphorylated in different NPC models (Dardis et al., 2016). This work prepared the foundation for my study, trying to better understand the molecular mechanisms that lead to TDP-43 pathological involvement and its phosphorylation in this disorder. For this reason, I performed an RNA sequencing analysis on human NPC cellular model, and I compared it to the list of changes detected in neuronal SHSy5Y cells depleted for TDP-43. From this analysis, 64 genes were commonly misregulated within NPC RNA sequencing and the one performed on SHSy5Y cells upon TDP-43 silencing. Between these 64 genes, I selected and validated some of them basing on their misregulation rate, and their cellular function. In particular, *LCP1* and *ITPR1* were already described to be involved in NPC disease. In particular LCP1 pathway is related to NF-kappaβ signaling, already known to induce apoptosis in NPC disease (Zampieri et al., 2009). *ITPR1* variant was described to worsen the ataxia phenotype in a NPC patient, consistently with *ITPR1* involvement in cerebellar ataxia 15 (Zeiger et al., 2018). Moreover, ITPR1 is also involve in calcium homeostasis, as well as DCLK1 and CDON. These two genes are able to modulate neuroplasticity, axon outgrowth and guidance, neuronal apoptosis and neurogenesis, and neuronal migration through calcium homeostasis. Instead, *EPDR1* is involved calcium homeostasis to promote cellular adhesion. *SHANK1* is also involved in neuronal pathways, like the development of synapses, and CDON regulates myogenesis. Like *ITPR1* and *DCLK1*, also *DEPTOR* and *LGR4* are involved in important cellular pathways, such as the PI3K/Akt and the Wnt signaling, respectively (GeneCards - Human Genes | Gene Database | Gene Search).

After the validation, I performed a functional analysis testing the RNA immunoprecipitation of the selected genes within TDP-43 overexpression, in order to establish a link between TDP-43 and the selected genes. This analysis showed *ITPR1*, *EPDR1*, and *DCLK1* enrichment, leading to the hypothesis that the mRNAs of these three targets were directly bound by TDP-43. Indeed, for all these three genes, TG stretches were found both in exons/introns critical sites as well as in the untranslated regions. This supports

the idea that TDP-43 could be involved in *ITPR1*, *EPDR1*, and *DCLK1* regulation, inducing alternative splicing, by binding to exons/introns critical sites; or in mRNA degradation or instability, by recognizing TG stretches in the untranslated regions. Further analyses will be necessary in order to clarify the mechanism of action.

Together with the RNA immunoprecipitation assay, I performed a functional analysis on the down-regulated genes by testing their cellular toxicity and measuring the LDH release in the medium after silencing the down regulated genes of interest. From the LDH release cytotoxicity assay, just *ITPR1* gene showed a cytotoxic effect at 48 and 72 hours, adding another evidence to the RNA immunoprecipitation assay, and leading to the hypothesis that *ITPR1* could be somehow involved and linked to TDP-43 neuropathogenesis. Indeed, calcium pathways and Cyclic adenosine monophosphate (cAMP) homeostasis related to oxidative stress, were already described to be associated biomarkers in another neurodegenerative disorder, such as FTLD (Palluzzi et al., 2017). In addition, different papers were published coupling TDP-43 neuronal toxicity and its sub-cellular localization with ITPR1 as a modifier of this condition (Zhan et al., 2013; Kim et al., 2012). Moreover, supporting our results, *ITPR1* was already described in literature as a down-regulated item upon TDP-43 knockdown (Štalekar et al., 2015; Polymenidou et al., 2011). Also, ITPR1 potentially involvement in NPC was described by William Zeiger and colleagues, reporting a NPC patient with a novel *ITPR1* variant that leads to an autosomal dominant spinocerebellar ataxia that worsen the phenotype (Zeiger et al., 2018). Therefore, *ITPR1* down regulation could be a phenotype modifier in NPC disease, related to TDP-43 misregulation and hyperphosphorylation. Based on these preliminary results, I performed an immunolocalization analysis showing that *ITPR1* knockdown was promoting TDP-43 cytoplasmic localization and its phosphorylation. This could be an important starting point for investigating strategies that will allow the rescue of proper TDP-43 localization in the nucleus and thus recovery of proper gene expression, in particular kinase inhibitors compounds already approved for clinical applications.

Further experiments should be performed in order to test also the up-regulated genes and the effects of their overexpression. In addition, there is also work that remains to be done with regards to better characterizing the aberrant phosphorylation process of TDP-43 in NPC. In my experiments, I have focused on the well-known S409/S410 phosphorylation sites that are also found in the ALS/FTD pathway. However, it is also possible that in the NPC model the aberrantly localized TDP-43 may carry some novel

phosphorylation events that have yet to be described. To address this issue, I therefore plan to immunoprecipitated TDP-43 from our NPC model cell lines and perform mass-spec analysis to identify the phosphorylation sites of TDP-43 in NPC cells. To do this, we will use the mass-spec facility at ICGEB that has a long-standing expertise in this kind of analysis.

Another question that remains open is the identification of kinases that are involved in the phosphorylation of TDP-43 in NPC. Are they the same or are they different from ALS/FTD disease? To address this issue, I plan to overexpress various kinases in our model cell lines to address the mislocalization properties of phosphorylated TDP-43. For example, this could be done using lentiviral vectors with genes cloned under the control of ubiquitous or neuron-specific promoters (for example, HB9, a lower MN-specific transcription factor). In parallel, from the SIGMA MISSION shRNA library I might obtain lentiviruses carrying three different shRNAs that specifically target selected human kinases. After target gene overexpression or silencing, any modifications to the phosphorylation status and behavior of TDP-43 will be evaluated together with their consequences on the cellular phenotype.

6 CONCLUSIONS

Following the discussion and the reported results, the two disease models have revealed distinct aspects that could be employed for novel strategies and to add new information regarding TDP-43 pathogenic mechanism.

First of all, the work I have performed has pointed out that the study of a single point mutation can lead to discover new features of proteins, that might represent a novel link to disease. The analysis of this Serine in position 375, revealed its relevance in both physiological and pathological conditions, opening a new window in cell cycle/apoptosis related phosphorylation. In conclusion the S375 phosphorylation seemed to promote the cytoplasmic shuttle of TDP-43 protein in physiological conditions; instead, the pathological status was induced by the lack of phosphorylation as well as its abnormal modification. This could be linked to mitochondria apoptotic pathway, and in future it could be exploited as a novel therapeutic target for ALS and, more in general, for neurodegenerative disorders.

Following this, the importance of phosphorylation in regulating TDP-43 functions has been highlighted by my study on its pathological role in Niemann Pick type C. In particular, this work has allowed the identification of a novel potential modifier, namely *ITPR1*. The downregulation of this gene seems to worsen the TDP-43 related phenotype, especially regarding the phosphorylation pattern of the protein. Further studies will therefore be performed to check if *ITPR1* could possibly represent a potential target or biomarker of the disease not just NPC, but also other TDP-43 related neurodegenerative disorders. Moreover, ITPR1 involvement in kinase pathways could represent a novel target for already approved kinase inhibitors, as new strategies for the treatment of neurological disorders.

In conclusion, this work is looking at phosphorylation as a common target between heterogenous neurodegenerative diseases, underlying the relevance of the physiological/pathological subtle balance, as well as the importance of potential modifiers.

7 FUTURE PERSPECTIVES

For both models, further analysis will be necessary.

To better understand the potential second modifiers of the physiological/pathological balance, an RNA sequencing analysis on the S375G and S375E stable clones will be performed. The results from this analysis could be interesting in order to add new information about what is regulating the toxicity of this specific PTM and to better characterize the cell cycle/mitochondrial apoptosis involvement. Moreover, the obtained data from this sequencing can then be merged with the one obtained with NPC with the hope of finding the common features that regulate the phosphorylation status. It will also be interesting to start analyzing the differences between ALS and NPC1, thus identifying specific characteristics relating to the different diseases. Moreover, the RNA sequencing data will add some functional information about the normal cell division/apoptosis signal, that could be rescued by treating the cells with small compounds known to be able to rescue the pathway, both in normal and in stress conditions.

Regarding the NPC model, a lot is still needed to be added. First of all, the exact positions where TDP-43 binding with *ITPR1*, *EPDR1*, and *DCLK1* is occurring should be clarified. This is important in order to establish how these genes are regulated by TDP-43, if they are alternative spliced or if TDP-43 induces mRNA destabilization by binding the untranslated regions. To study the potential alternative splicing, a deeper analysis of the RNA sequences should be performed. Moreover, specific primers should be designed on exons that could potentially undergo to TDP-43 splicing regulation. On the other hand, the mRNA stability will be studied through transcription block, using for example actinomycin D. The half-life of the mRNA will be then tested with quantitative real time PCR, in order to check if TDP-43 binding is performing the mRNA degradation.

Regarding ITPR1 analysis as a potential modifier of the disease, already clinical approved kinase inhibitors can be tested. Upon *ITPR1* knockdown, kinase inhibitors will be administered to the cells and TDP-43 localization and phosphorylation will be monitored, in order to check if some of the compounds are able to rescue the wild-type phenotype.

Moreover, the functional analysis on up-regulated genes will be performed. The selected targets will be cloned in the pCMV4 vector in frame with the flag tag. The overexpression in SHSy5Y ECACC cell line will be performed and their toxicity effects will be tested through the LDH release assay. Based on the results obtained with the cytotoxicity

experiment, together with the results following the RNA immunoprecipitation, we hope to find other potential targets that could represent another therapeutic option or it could add new information about the pathogenic mechanism.

Finally, the two disease models could reveal different phosphorylation patterns and kinase involvement. In this context, it will be important to determine the putative TDP-43 phosphorylated sites also in an NPC cellular model, in order to compare them with the ones found in ALS/FTLD spectrum (Kametani et al., 2016). Also, the identification of the kinases involved could help to address the mislocalization properties of phosphorylated TDP-43. This could be answered by overexpressing different kinases, under the control of ubiquitous or neuron-specific promoters, or to silence them by using shRNAs that specifically target selected human kinases. Both could be address by using lentiviral vectors. This will be useful to evaluate TDP-43 phospho-status and behavior and to potentially exploit it as a novel potential target.

Bibliography

Abhyankar, M. M., Urekar, C. and Reddi, P. P. (2007) 'A novel CpG-free vertebrate insulator silences the testis-specific SP-10 gene in somatic tissues: role for TDP-43 in insulator function.', *The Journal of biological chemistry*, vol. 282, no. 50, pp. 36143–54 [Online]. DOI: 10.1074/jbc.M705811200 (Accessed 13 August 2019).

Achi, E. Y. and Rudnicki, S. A. (2012) 'ALS and Frontotemporal Dysfunction: A Review.', *Neurology research international*, vol. 2012, p. 806306 [Online]. DOI: 10.1155/2012/806306 (Accessed 28 September 2018).

Appocher, C., Mohagheghi, F., Cappelli, S., Stuani, C., Romano, M., Feiguin, F. and Buratti, E. (2017) 'Major hnRNP proteins act as general TDP-43 functional modifiers both in Drosophila and human neuronal cells', *Nucleic Acids Research*, vol. 45, no. 13, pp. 8026–8045 [Online]. DOI: 10.1093/nar/gkx477 (Accessed 26 April 2019).

Arai, T., Hasegawa, M., Akiyama, H., Ikeda, K., Nonaka, T., Mori, H., Mann, D., Tsuchiya, K., Yoshida, M., Hashizume, Y. and Oda, T. (2006) 'TDP-43 is a component of ubiquitin-positive tau-negative inclusions in frontotemporal lobar degeneration and amyotrophic lateral sclerosis', *Biochemical and Biophysical Research Communications*, vol. 351, no. 3, pp. 602–611 [Online]. DOI: 10.1016/j.bbrc.2006.10.093 (Accessed 28 September 2018).

Ayala, Youhna M, Misteli, T. and Baralle, F. E. (2008) 'TDP-43 regulates retinoblastoma protein phosphorylation through the repression of cyclin-dependent kinase 6 expression.', *Proceedings of the National Academy of Sciences of the United States of America*, vol. 105, no. 10, pp. 3785–9 [Online]. DOI: 10.1073/pnas.0800546105 (Accessed 25 September 2018).

Ayala, Y. M., Pantano, S., D'Ambrogio, A., Buratti, E., Brindisi, A., Marchetti, C., Romano, M. and Baralle, F. E. (2005) 'Human, Drosophila, and C.elegans TDP43: Nucleic Acid Binding Properties and Splicing Regulatory Function', *Journal of Molecular Biology*, vol. 348, no. 3, pp. 575–588 [Online]. DOI: 10.1016/j.jmb.2005.02.038 (Accessed 13 August 2019).

Ayala, Y. M., Zago, P., D'Ambrogio, A., Xu, Y.-F., Petrucelli, L., Buratti, E. and Baralle, F. E. (2008) 'Structural determinants of the cellular localization and shuttling of TDP-43', *Journal of Cell Science*, vol. 121, no. 22, pp. 3778–3785 [Online]. DOI: 10.1242/jcs.038950.

Bahr, B. A. and Bendiske, J. (2002) ‘The neuropathogenic contributions of lysosomal dysfunction.’, *Journal of neurochemistry*, vol. 83, no. 3, pp. 481–9 [Online]. DOI: 10.1046/j.1471-4159.2002.01192.x (Accessed 26 July 2019).

Banks, G. T., Kuta, A., Isaacs, A. M. and Fisher, E. M. C. (2008) ‘TDP-43 is a culprit in human neurodegeneration, and not just an innocent bystander’, *Mammalian Genome*, vol. 19, no. 5, pp. 299–305 [Online]. DOI: 10.1007/s00335-008-9117-x (Accessed 19 September 2018).

Barmada, S. J. and Finkbeiner, S. (2010) ‘Pathogenic TARDBP mutations in amyotrophic lateral sclerosis and frontotemporal dementia: disease-associated pathways.’, *Reviews in the neurosciences*, vol. 21, no. 4, pp. 251–72 [Online]. Available at http://www.ncbi.nlm.nih.gov/pubmed/21086759 (Accessed 28 September 2018).

Bergamin, N., Dardis, A., Beltrami, A., Cesselli, D., Rigo, S., Zampieri, S., Domenis, R., Bembi, B. and Beltrami, C. A. (2013) ‘A human neuronal model of Niemann Pick C disease developed from stem cells isolated from patient’s skin’, *Orphanet Journal of Rare Diseases*, Orphanet J Rare Dis, vol. 8, no. 1 [Online]. DOI: 10.1186/1750-1172-8-34 (Accessed 5 January 2021).

Björkhem, I., Meaney, S. and Fogelman, A. M. (2004) ‘Brain Cholesterol: Long Secret Life behind a Barrier’, *Arteriosclerosis, Thrombosis, and Vascular Biology*, Arterioscler Thromb Vasc Biol, vol. 24, no. 5 [Online]. DOI: 10.1161/01.ATV.0000120374.59826.1b (Accessed 28 December 2020).

Boshart, M., Weber, F., Jahn, G., Dorsch-Hler, K., Fleckenstein, B. and Schaffner, W. (1985) ‘A very strong enhancer is located upstream of an immediate early gene of human cytomegalovirus’, *Cell*, Cell, vol. 41, no. 2, pp. 521–530 [Online]. DOI: 10.1016/S0092-8674(85)80025-8 (Accessed 5 January 2021).

Brady, O. A., Meng, P., Zheng, Y., Mao, Y. and Hu, F. (2011) ‘Regulation of TDP-43 aggregation by phosphorylation andp62/SQSTM1’, *Journal of Neurochemistry*, J Neurochem, vol. 116, no. 2, pp. 248–259 [Online]. DOI: 10.1111/j.1471-4159.2010.07098.x (Accessed 25 January 2021).

Braun, R. J., Sommer, C., Carmona-Gutierrez, D., Khoury, C. M., Ring, J., Büttner, S. and Madeo, F. (2011) ‘Neurotoxic 43-kDa TAR DNA-binding protein (TDP-43) triggers mitochondrion-dependent programmed cell death in yeast’, *Journal of Biological*

Chemistry, vol. 286, no. 22, pp. 19958–19972 [Online]. DOI: 10.1074/jbc.M110.194852.

Brown, M. S. and Goldstein, J. L. (1986) 'A receptor-mediated pathway for cholesterol homeostasis', *Science*, Science, vol. 232, no. 4746, pp. 34–47 [Online]. DOI: 10.1126/science.3513311 (Accessed 28 December 2020).

Budini, M. and Buratti, E. (2011) 'TDP-43 Autoregulation: Implications for Disease', *Journal of Molecular Neuroscience*, vol. 45, no. 3, pp. 473–479 [Online]. DOI: 10.1007/s12031-011-9573-8 (Accessed 25 September 2018).

Budini, M., Romano, V., Avendaño-Vázquez, S. E., Bembich, S., Buratti, E. and Baralle, F. E. (2012) 'Role of selected mutations in the Q/N rich region of TDP-43 in EGFP-12xQ/N-induced aggregate formation.', *Brain research*, vol. 1462, pp. 139–50 [Online]. DOI: 10.1016/j.brainres.2012.02.031 (Accessed 23 September 2018).

Buratti, E. (2015) 'Functional Significance of TDP-43 Mutations in Disease', in *Advances in genetics*, vol. 91, pp. 1–53 [Online]. DOI: 10.1016/bs.adgen.2015.07.001 (Accessed 29 September 2018).

Buratti, E. (2018) 'TDP-43 post-translational modifications in health and disease.', *Expert opinion on therapeutic targets*, vol. 22, no. 3, pp. 279–293 [Online]. DOI: 10.1080/14728222.2018.1439923 (Accessed 29 September 2018).

Buratti, E. and Baralle, F. E. (2001) 'Characterization and functional implications of the RNA binding properties of nuclear factor TDP-43, a novel splicing regulator of CFTR exon 9.', *The Journal of biological chemistry*, vol. 276, no. 39, pp. 36337–43 [Online]. DOI: 10.1074/jbc.M104236200 (Accessed 23 September 2018).

Buratti, E. and Baralle, F. E. (2008) 'Multiple roles of TDP-43 in gene expression, splicing regulation, and human disease.', *Frontiers in bioscience : a journal and virtual library*, vol. 13, pp. 867–78 [Online]. Available at http://www.ncbi.nlm.nih.gov/pubmed/17981595 (Accessed 19 September 2018).

Buratti, E. and Baralle, F. E. (2012) 'TDP-43: gumming up neurons through protein-protein and protein-RNA interactions.', *Trends in biochemical sciences*, vol. 37, no. 6, pp. 237–47 [Online]. DOI: 10.1016/j.tibs.2012.03.003 (Accessed 19 September 2018).

Candé, C., Cecconi, F., Dessen, P. and Kroemer, G. (2002) 'Apoptosis-inducing factor (AIF): Key to the conserved caspase-independent pathways of cell death?', *Journal of Cell Science*, vol. 115, no. 24, pp. 4727–4734 [Online]. DOI: 10.1242/jcs.00210.

Cappelli, S., Romano, M. and Buratti, E. (2018) 'Systematic Analysis of Gene Expression Profiles Controlled by hnRNP Q and hnRNP R, Two Closely Related Human RNA Binding Proteins Implicated in mRNA Processing Mechanisms', *Frontiers in Molecular Biosciences*, vol. 5 [Online]. DOI: 10.3389/fmolb.2018.00079 (Accessed 26 April 2019).

Chiang, H. H., Andersen, P. M., Tysnes, O. B., Gredal, O., Christensen, P. B. and Graff, C. (2012) 'Novel TARDBP mutations in Nordic ALS patients', *Journal of Human Genetics*, vol. 57, no. 5, pp. 316–319 [Online]. DOI: 10.1038/jhg.2012.24 (Accessed 14 April 2020).

Colombrita, C., Zennaro, E., Fallini, C., Weber, M., Sommacal, A., Buratti, E., Silani, V. and Ratti, A. (2009) 'TDP-43 is recruited to stress granules in conditions of oxidative insult', *Journal of Neurochemistry*, vol. 111, no. 4, pp. 1051–1061 [Online]. DOI: 10.1111/j.1471-4159.2009.06383.x.

Conlon, E. G. and Manley, J. L. (2017) 'RNA-binding proteins in neurodegeneration: mechanisms in aggregate', *Genes & Development*, vol. 31, no. 15, pp. 1509–1528 [Online]. DOI: 10.1101/gad.304055.117 (Accessed 16 July 2019).

Cooper-Knock, J., Kirby, J., Highley, R. and Shaw, P. J. (2015) 'The Spectrum of C9orf72-mediated Neurodegeneration and Amyotrophic Lateral Sclerosis', *Neurotherapeutics*, Springer New York LLC, vol. 12, no. 2 [Online]. DOI: 10.1007/s13311-015-0342-1 (Accessed 7 April 2020).

Corrado, L., Ratti, A., Gellera, C., Buratti, E., Castellotti, B., Carlomagno, Y., Ticozzi, N., Mazzini, L., Testa, L., Taroni, F., Baralle, F. E., Silani, V. and D'Alfonso, S. (2009) 'High frequency of TARDBP gene mutations in italian patients with amyotrophic lateral sclerosis', *Human Mutation*, Wiley-Liss Inc., vol. 30, no. 4, pp. 688–694 [Online]. DOI: 10.1002/humu.20950 (Accessed 14 April 2020).

D'Ambrogio, A., Buratti, E., Stuani, C., Guarnaccia, C., Romano, M., Ayala, Y. M. and Baralle, F. E. (2009) 'Functional mapping of the interaction between TDP-43 and hnRNP A2 in vivo.', *Nucleic acids research*, vol. 37, no. 12, pp. 4116–26 [Online]. DOI: 10.1093/nar/gkp342 (Accessed 13 August 2019).

Dardis, A., Zampieri, S., Canterini, S., Newell, K. L., Stuani, C., Murrell, J. R., Ghetti, B., Fiorenza, M. T., Bembi, B. and Buratti, E. (2016) 'Altered localization and functionality of TAR DNA Binding Protein 43 (TDP-43) in niemann- pick disease type C.', *Acta neuropathologica communications*, vol. 4, no. 1, p. 52 [Online]. DOI: 10.1186/s40478-016-

0325-4 (Accessed 3 October 2018).

De Conti, L., Akinyi, M. V., Mendoza-Maldonado, R., Romano, M., Baralle, M. and Buratti, E. (2015) 'TDP-43 affects splicing profiles and isoform production of genes involved in the apoptotic and mitotic cellular pathways', *Nucleic Acids Research*, Oxford University Press, vol. 43, no. 18, p. 8990 [Online]. DOI: 10.1093/NAR/GKV814 (Accessed 16 April 2019).

Ekshyyan, O. and Aw, T. (2005) 'Apoptosis: A Key in Neurodegenerative Disorders', *Current Neurovascular Research*, Bentham Science Publishers Ltd., vol. 1, no. 4, pp. 355–371 [Online]. DOI: 10.2174/1567202043362018 (Accessed 29 April 2020).

Estiu, G., Khatri, N. and Wiest, O. (2013) 'Computational Studies of the Cholesterol Transport between NPC2 and the N-Terminal Domain of NPC1 (NPC1(NTD))', *Biochemistry*, vol. 52, no. 39, pp. 6879–6891 [Online]. DOI: 10.1021/bi4005478 (Accessed 23 July 2019).

Fiesel, F. C., Voigt, A., Weber, S. S., Van Den Haute, C., Waldenmaier, A., Görner, K., Walter, M., Marlene, A. L., Kern, J. V., Rasse, T. M., Schmidt, T., Springer, W., Kirchner, R., Bonin, M., Neumann, M., Baekelandt, V., Alunni-Fabbroni, M., Schulz, J. B. and Kahle, P. J. (2010) 'Knockdown of transactive response DNA-binding protein (TDP-43) downregulates histone deacetylase 6', *EMBO Journal*, EMBO J, vol. 29, no. 1, pp. 209–221 [Online]. DOI: 10.1038/emboj.2009.324 (Accessed 28 December 2020).

Fiesel, F. C., Weber, S. S., Supper, J., Zell, A. and Kahle, P. J. (2012) 'TDP-43 regulates global translational yield by splicing of exon junction complex component SKAR', *Nucleic Acids Research*, Nucleic Acids Res, vol. 40, no. 6, pp. 2668–2682 [Online]. DOI: 10.1093/nar/gkr1082 (Accessed 22 January 2021).

Fiorenza, M. T., Moro, E. and Erickson, R. P. (2018) 'The pathogenesis of lysosomal storage disorders: beyond the engorgement of lysosomes to abnormal development and neuroinflammation.', *Human molecular genetics*, vol. 27, no. R2, pp. R119–R129 [Online]. DOI: 10.1093/hmg/ddy155 (Accessed 24 July 2019).

Gendron, T. F., Rademakers, R. and Petrucelli, L. (2013) 'TARDBP mutation analysis in TDP-43 proteinopathies and deciphering the toxicity of mutant TDP-43.', Perry, G., Zhu, X., Smith, M. A., Sorensen, A., and Avila, J. (eds), *Journal of Alzheimer's disease : JAD*, vol. 33 Suppl 1, no. s1, pp. S35-45 [Online]. DOI: 10.3233/JAD-2012-129036 (Accessed 27 September 2018).

Guo, W., Chen, Y., Zhou, X., Kar, A., Ray, P., Chen, X., Rao, E. J., Yang, M., Ye, H., Zhu, L., Liu, J., Xu, M., Yang, Y., Wang, C., Zhang, D., Bigio, E. H., Mesulam, M., Shen, Y., Xu, Q., Fushimi, K. and Wu, J. Y. (2011) 'An ALS-associated mutation affecting TDP-43 enhances protein aggregation, fibril formation and neurotoxicity', *Nature Structural and Molecular Biology*, Nat Struct Mol Biol, vol. 18, no. 7, pp. 822–831 [Online]. DOI: 10.1038/nsmb.2053 (Accessed 25 January 2021).

Hasegawa, M., Arai, T., Nonaka, T., Kametani, F., Yoshida, M., Hashizume, Y., Beach, T. G., Buratti, E., Baralle, F., Morita, M., Nakano, I., Oda, T., Tsuchiya, K. and Akiyama, H. (2008) 'Phosphorylated TDP-43 in frontotemporal lobar degeneration and amyotrophic lateral sclerosis', *Annals of Neurology*, vol. 64, no. 1, pp. 60–70 [Online]. DOI: 10.1002/ana.21425 (Accessed 1 October 2018).

Higgins, M. E., Davies, J. P., Chen, F. W. and Ioannou, Y. A. (1999) 'Niemann-Pick C1 is a late endosome-resident protein that transiently associates with lysosomes and the trans-Golgi network.', *Molecular genetics and metabolism*, vol. 68, no. 1, pp. 1–13 [Online]. DOI: 10.1006/mgme.1999.2882 (Accessed 15 July 2019).

Janas, A. M., Sapoń, K., Janas, Teresa, Stowell, M. H. B. and Janas, Tadeusz (2016) 'Exosomes and other extracellular vesicles in neural cells and neurodegenerative diseases', *Biochimica et Biophysica Acta (BBA) - Biomembranes*, Elsevier, vol. 1858, no. 6, pp. 1139–1151 [Online]. DOI: 10.1016/J.BBAMEM.2016.02.011 (Accessed 31 July 2019).

Jellinger, K. A. (2009) 'Recent advances in our understanding of neurodegeneration.', *Journal of neural transmission (Vienna, Austria : 1996)*, vol. 116, no. 9, pp. 1111–62 [Online]. DOI: 10.1007/s00702-009-0240-y (Accessed 17 July 2019).

Jo, M., Lee, S., Jeon, Y. M., Kim, S., Kwon, Y. and Kim, H. J. (2020) 'The role of TDP-43 propagation in neurodegenerative diseases: integrating insights from clinical and experimental studies', *Experimental and Molecular Medicine*, Springer Nature, vol. 52, no. 10 [Online]. DOI: 10.1038/s12276-020-00513-7 (Accessed 25 January 2021).

Kametani, F., Obi, T., Shishido, T., Akatsu, H., Murayama, S., Saito, Y., Yoshida, M. and Hasegawa, M. (2016) 'Mass spectrometric analysis of accumulated TDP-43 in amyotrophic lateral sclerosis brains', *Scientific Reports*, Nature Publishing Group, vol. 6, no. March [Online]. DOI: 10.1038/srep23281.

Kermer, P., Liman, J., Weishaupt, J. H. and Bähr, M. (2004) 'Neuronal apoptosis in neurodegenerative diseases: From basic research to clinical application', *Neurodegenerative Diseases*, vol. 1, no. 1 [Online]. DOI: 10.1159/000076665.

Kim, K. Y., Lee, H. W., Shim, Y. M., Mook-Jung, I., Jeon, G. S. and Sung, J. J. (2015) 'A phosphomimetic mutant TDP-43 (S409/410E) induces Drosha instability and cytotoxicity in Neuro 2A cells', *Biochemical and Biophysical Research Communications*, Academic Press Inc., vol. 464, no. 1, pp. 236–243 [Online]. DOI: 10.1016/j.bbrc.2015.06.125 (Accessed 25 January 2021).

Kim, S. H., Zhan, L., Hanson, K. A. and Tibbetts, R. S. (2012) 'High-content RNAi screening identifies the Type 1 inositol triphosphate receptor as a modifier of TDP-43 localization and neurotoxicity.', *Human molecular genetics*, Oxford University Press, vol. 21, no. 22, pp. 4845–56 [Online]. DOI: 10.1093/hmg/dds321 (Accessed 10 January 2020).

King, O. D., Gitler, A. D. and Shorter, J. (2012) 'The tip of the iceberg: RNA-binding proteins with prion-like domains in neurodegenerative disease.', *Brain research*, vol. 1462, pp. 61–80 [Online]. DOI: 10.1016/j.brainres.2012.01.016 (Accessed 16 July 2019).

Krantic, S., Mechawar, N., Reix, S. and Quirion, R. (2007) 'Apoptosis-inducing factor: A matter of neuron life and death', *Progress in Neurobiology*, vol. 81, no. 3 [Online]. DOI: 10.1016/j.pneurobio.2006.12.002.

Krecic, A. M. and Swanson, M. S. (1999) 'hnRNP complexes: composition, structure, and function', *Current Opinion in Cell Biology*, vol. 11, no. 3, pp. 363–371 [Online]. DOI: 10.1016/S0955-0674(99)80051-9 (Accessed 19 September 2018).

Lagier-Tourenne, C., Polymenidou, M. and Cleveland, D. W. (2010) 'TDP-43 and FUS/TLS: emerging roles in RNA processing and neurodegeneration', *Human Molecular Genetics*, vol. 19, no. R1, pp. R46–R64 [Online]. DOI: 10.1093/hmg/ddq137 (Accessed 23 September 2018).

Lee, E. B., Lee, V. M.-Y. and Trojanowski, J. Q. (2012) 'Gains or losses: molecular mechanisms of TDP43-mediated neurodegeneration', *Nature Reviews Neuroscience*, vol. 13, no. 1, pp. 38–50 [Online]. DOI: 10.1038/nrn3121 (Accessed 25 September 2018).

Lee, E. B., Lee, V. M. Y. and Trojanowski, J. Q. (2011) 'Gains or losses : molecular mechanisms of TDP43 - mediated neurodegeneration', Nature Publishing Group, vol. 13, no. January 2012 [Online]. DOI: 10.1038/nrn3121.

Li, W., Reeb, A. N., Lin, B., Subramanian, P., Fey, E. E., Knoverek, C. R., French, R. L., Bigio, E. H. and Ayala, Y. M. (2017) 'Heat shock-induced phosphorylation of TAR DNA-binding protein 43 (TDP-43) by MAPK/ERK kinase regulates TDP-43 function', *Journal of Biological Chemistry*, American Society for Biochemistry and Molecular Biology Inc., vol. 292, no. 12, pp. 5089–5100 [Online]. DOI: 10.1074/jbc.M116.753913 (Accessed 25 January 2021).

Mompeán, M., Romano, V., Pantoja-Uceda, D., Stuani, C., Baralle, F. E., Buratti, E. and Laurents, D. V. (2016) 'The TDP-43 N-terminal domain structure at high resolution', *The FEBS Journal*, John Wiley & Sons, Ltd, vol. 283, no. 7, pp. 1242–1260 [Online]. DOI: 10.1111/febs.13651 (Accessed 19 February 2021).

Murrell, J., Farlow, M., Ghetti, B. and Benson, M. D. (1991) 'A mutation in the amyloid precursor protein associated with hereditary Alzheimer's disease', *Science*, American Association for the Advancement of Science, vol. 254, no. 5028, pp. 97–99 [Online]. DOI: 10.1126/science.1925564 (Accessed 6 January 2021).

Nelson, J. A., Reynolds-Kohler, C. and Smith, B. A. (1987) 'Negative and positive regulation by a short segment in the 5'-flanking region of the human cytomegalovirus major immediate-early gene.', *Molecular and Cellular Biology*, American Society for Microbiology, vol. 7, no. 11, pp. 4125–4129 [Online]. DOI: 10.1128/mcb.7.11.4125 (Accessed 5 January 2021).

Neumann, M., Kwong, L. K., Lee, E. B., Kremmer, E., Flatley, A., Xu, Y., Forman, M. S., Troost, D., Kretzschmar, H. A., Trojanowski, J. Q. and Lee, V. M.-Y. (2009) 'Phosphorylation of S409/410 of TDP-43 is a consistent feature in all sporadic and familial forms of TDP-43 proteinopathies.', *Acta neuropathologica*, vol. 117, no. 2, pp. 137–49 [Online]. DOI: 10.1007/s00401-008-0477-9 (Accessed 30 September 2018).

Neumann, M., Sampathu, D. M., Kwong, L. K., Truax, A. C., Micsenyi, M. C., Chou, T. T., Bruce, J., Schuck, T., Grossman, M., Clark, C. M., McCluskey, L. F., Miller, B. L., Masliah, E., Mackenzie, I. R., Feldman, H., Feiden, W., Kretzschmar, H. A., Trojanowski, J. Q. and Lee, V. M.-Y. (2006) 'Ubiquitinated TDP-43 in Frontotemporal Lobar Degeneration and Amyotrophic Lateral Sclerosis', *Science*, vol. 314, no. 5796, pp. 130–133 [Online]. DOI: 10.1126/science.1134108 (Accessed 27 September 2018).

Newell, K., Paron, F., Mompean, M., Murrell, J., Salis, E., Stuani, C., Pattee, G., Romano, M., Laurents, D., Ghetti, B. and Buratti, E. (2018) 'Dysregulation of TDP-43 intracellular

localization and early onset ALS are associated with a *TARDBP* S375G variant', *Brain Pathology* [Online]. DOI: 10.1111/bpa.12680 (Accessed 22 February 2019).

O'Gorman, S., Fox, D. T. and Wahl, G. M. (1991) 'Recombinase-mediated gene activation and site-specific integration in mammalian cells', *Science*, Science, vol. 251, no. 4999, pp. 1351–1355 [Online]. DOI: 10.1126/science.1900642 (Accessed 5 January 2021).

Ong, W.-Y., Kumar, U., Switzer, R., Sidhu, A., Suresh, G., Hu, C.-Y. and Patel, S. (2001) 'Neurodegeneration in Niemann-Pick type C disease mice', *Experimental Brain Research*, vol. 141, no. 2, pp. 218–231 [Online]. DOI: 10.1007/s002210100870 (Accessed 15 July 2019).

Origone, P., Caponnetto, C., Bandettini Di Poggio, M., Ghiglione, E., Bellone, E., Ferrandes, G., Mancardi, G. L. and Mandich, P. (2010) 'Enlarging clinical spectrum of FALS with TARDBP gene mutations: S393L variant in an Italian family showing phenotypic variability and relevance for genetic counselling', *Amyotrophic Lateral Sclerosis*, vol. 11, no. 1–2, pp. 223–227 [Online]. DOI: 10.3109/17482960903165039.

Orrù, S., Coni, P., Floris, A., Littera, R., Carcassi, C., Sogos, V. and Brancia, C. (2016) 'Reduced stress granule formation and cell death in fibroblasts with the A382T mutation of TARDBP gene: Evidence for loss of TDP-43 nuclear function', *Human Molecular Genetics*, Oxford University Press, vol. 25, no. 20, pp. 4473–4483 [Online]. DOI: 10.1093/hmg/ddw276 (Accessed 25 January 2021).

Ou, S. H., Wu, F., Harrich, D., García-Martínez, L. F. and Gaynor, R. B. (1995) 'Cloning and characterization of a novel cellular protein, TDP-43, that binds to human immunodeficiency virus type 1 TAR DNA sequence motifs.', *Journal of virology*, vol. 69, no. 6, pp. 3584–96 [Online]. Available at http://www.ncbi.nlm.nih.gov/pubmed/7745706 (Accessed 19 September 2018).

Pagani, F., Buratti, E., Stuani, C. and Baralle, F. E. (2003) 'Missense, nonsense, and neutral mutations define juxtaposed regulatory elements of splicing in cystic fibrosis transmembrane regulator exon 9', *Journal of Biological Chemistry*, J Biol Chem, vol. 278, no. 29, pp. 26580–26588 [Online]. DOI: 10.1074/jbc.M212813200 (Accessed 5 January 2021).

Pagel, O., Loroch, S., Sickmann, A. and Zahedi, R. P. (2015) 'Current strategies and findings in clinically relevant post-translational modification-specific proteomics', *Expert*

Review of Proteomics, Expert Reviews Ltd., vol. 12, no. 3 [Online]. DOI: 10.1586/14789450.2015.1042867.

Palluzzi, F., Ferrari, R., Graziano, F., Novelli, V., Rossi, G., Galimberti, D., Rainero, I., Benussi, L., Nacmias, B., Bruni, A. C., Cusi, D., Salvi, E., Borroni, B. and Grassi, M. (2017) 'A novel network analysis approach reveals DNA damage, oxidative stress and calcium/cAMP homeostasis-associated biomarkers in frontotemporal dementia', Skoulakis, E. M. C. (ed), *PLOS ONE*, vol. 12, no. 10, p. e0185797 [Online]. DOI: 10.1371/journal.pone.0185797 (Accessed 10 January 2020).

Paron, F., Dardis, A. and Buratti, E. (2020) 'Pre-mRNA splicing defects and RNA binding protein involvement in Niemann Pick type C disease', *Journal of Biotechnology*, Elsevier B.V., vol. 318 [Online]. DOI: 10.1016/j.jbiotec.2020.03.012 (Accessed 28 December 2020).

Polymenidou, M., Lagier-Tourenne, C., Hutt, K. R., Huelga, S. C., Moran, J., Liang, T. Y., Ling, S.-C., Sun, E., Wancewicz, E., Mazur, C., Kordasiewicz, H., Sedaghat, Y., Donohue, J. P., Shiue, L., Bennett, C. F., Yeo, G. W. and Cleveland, D. W. (2011) 'Long pre-mRNA depletion and RNA missplicing contribute to neuronal vulnerability from loss of TDP-43', *Nature Neuroscience*, vol. 14, no. 4, pp. 459–468 [Online]. DOI: 10.1038/nn.2779 (Accessed 10 January 2020).

Potashkin, J. A. and Meredith, G. E. (2006) 'The Role of Oxidative Stress in the Dysregulation of Gene Expression and Protein Metabolism in Neurodegenerative Disease', *Antioxidants & Redox Signaling*, Mary Ann Liebert, Inc. 2 Madison Avenue Larchmont, NY 10538 USA , vol. 8, no. 1–2, pp. 144–151 [Online]. DOI: 10.1089/ars.2006.8.144 (Accessed 8 August 2019).

Praline, J., Vourc'H, P., Guennoc, A. M., Veyrat-Durebex, C. and Corcia, P. (2012) 'Co-occurrence of progressive anarthria with an S393L TARDBP mutation and ALS within a family', *Amyotrophic Lateral Sclerosis*, vol. 13, no. 1, pp. 155–157 [Online]. DOI: 10.3109/17482968.2011.598168.

Rabinovici, G. D. and Miller, B. L. (2010) 'Frontotemporal lobar degeneration: epidemiology, pathophysiology, diagnosis and management.', *CNS drugs*, vol. 24, no. 5, pp. 375–98 [Online]. DOI: 10.2165/11533100-000000000-00000 (Accessed 28 September 2018).

Sauer, B. (1994) 'Site-specific recombination: developments and applications', *Current*

Opinion in Biotechnology, Curr Opin Biotechnol, vol. 5, no. 5, pp. 521–527 [Online]. DOI: 10.1016/0958-1669(94)90068-X (Accessed 5 January 2021).

Schmittgen, T. D. and Livak, K. J. (2008) 'Analyzing real-time PCR data by the comparative CT method', *Nature Protocols*, Nat Protoc, vol. 3, no. 6, pp. 1101–1108 [Online]. DOI: 10.1038/nprot.2008.73 (Accessed 8 January 2021).

Seelaar, H., Rohrer, J. D., Pijnenburg, Y. A. L., Fox, N. C. and van Swieten, J. C. (2011) 'Clinical, genetic and pathological heterogeneity of frontotemporal dementia: a review.', *Journal of neurology, neurosurgery, and psychiatry*, vol. 82, no. 5, pp. 476–86 [Online]. DOI: 10.1136/jnnp.2010.212225 (Accessed 14 August 2019).

Sephton, C. F. and Yu, G. (2015) 'The function of RNA-binding proteins at the synapse: implications for neurodegeneration', *Cellular and Molecular Life Sciences*, Springer Basel, vol. 72, no. 19, pp. 3621–3635 [Online]. DOI: 10.1007/s00018-015-1943-x (Accessed 2 August 2019).

Shangguan, W. J., Li, H. and Zhang, Y. H. (2014) 'Induction of G2/M phase cell cycle arrest and apoptosis by ginsenoside Rf in human osteosarcoma MG-63 cells through the mitochondrial pathway', *Oncology Reports*, Oncol Rep, vol. 31, no. 1, pp. 305–313 [Online]. DOI: 10.3892/or.2013.2815 (Accessed 8 October 2020).

Shibata, N., Kakita, A., Takahashi, H., Ihara, Y., Nobukuni, K., Fujimura, H., Sakoda, S., Sasaki, S., Yamamoto, T. and Kobayashi, M. (2009) 'Persistent cleavage and nuclear translocation of apoptosis-inducing factor in motor neurons in the spinal cord of sporadic amyotrophic lateral sclerosis patients', *Acta Neuropathologica*, vol. 118, no. 6, pp. 755–762 [Online]. DOI: 10.1007/s00401-009-0580-6.

Solski, J. A., Yang, S., Nicholson, G. A., Luquin, N., Williams, K. L., Fernando, R., Pamphlett, R. and Blair, I. P. (2012) 'A novel TARDBP insertion/deletion mutation in the flail arm variant of amyotrophic lateral sclerosis', *Amyotrophic Lateral Sclerosis*, vol. 13, no. 5, pp. 465–470 [Online]. DOI: 10.3109/17482968.2012.662690 (Accessed 14 April 2020).

Štalekar, M., Yin, X., Rebolj, K., Darovic, S., Troakes, C., Mayr, M., Shaw, C. E. and Rogelj, B. (2015) 'Proteomic analyses reveal that loss of TDP-43 affects RNA processing and intracellular transport.', *Neuroscience*, vol. 293, pp. 157–70 [Online]. DOI: 10.1016/j.neuroscience.2015.02.046 (Accessed 10 January 2020).

Storch, J. and Xu, Z. (2009) 'Niemann–Pick C2 (NPC2) and intracellular cholesterol trafficking', *Biochimica et Biophysica Acta (BBA) - Molecular and Cell Biology of Lipids*, vol. 1791, no. 7, pp. 671–678 [Online]. DOI: 10.1016/j.bbalip.2009.02.001 (Accessed 15 July 2019).

Stover, C. M., Lynch, N. J., Hanson, S. J., Windbichler, M., Gregory, S. G. and Schwaeble, W. J. (2004) 'Organization of the MASP2 locus and its expression profile in mouse and rat.', *Mammalian genome : official journal of the International Mammalian Genome Society*, vol. 15, no. 11, pp. 887–900 [Online]. Available at http://www.ncbi.nlm.nih.gov/pubmed/15672593 (Accessed 13 August 2019).

Strong, M. J., Volkening, K., Hammond, R., Yang, W., Strong, W., Leystra-Lantz, C. and Shoesmith, C. (2007) 'TDP43 is a human low molecular weight neurofilament (hNFL) mRNA-binding protein.', *Molecular and cellular neurosciences*, vol. 35, no. 2, pp. 320–7 [Online]. DOI: 10.1016/j.mcn.2007.03.007 (Accessed 23 September 2018).

Ticozzi, N., LeClerc, A. L., van Blitterswijk, M., Keagle, P., McKenna-Yasek, D. M., Sapp, P. C., Silani, V., Wills, A. M., Brown, R. H. and Landers, J. E. (2011) 'Mutational analysis of TARDBP in neurodegenerative diseases', *Neurobiology of Aging*, vol. 32, no. 11, pp. 2096–2099 [Online]. DOI: 10.1016/j.neurobiolaging.2009.11.018 (Accessed 14 April 2020).

Udan, M. and Baloh, R. H. (2011) 'Implications of the prion-related Q/N domains in TDP-43 and FUS.', *Prion*, vol. 5, no. 1, pp. 1–5 [Online]. DOI: 10.4161/pri.5.1.14265 (Accessed 13 August 2019).

Vanderweyde, T., Youmans, K., Liu-Yesucevitz, L. and Wolozin, B. (2013) 'Role of Stress Granules and RNA-Binding Proteins in Neurodegeneration: A Mini-Review', *Gerontology*, vol. 59, no. 6, pp. 524–533 [Online]. DOI: 10.1159/000354170 (Accessed 16 July 2019).

Vanier, M. T. (2010) 'Niemann-Pick disease type C', *Orphanet Journal of Rare Diseases*, vol. 5, no. 1, p. 16 [Online]. DOI: 10.1186/1750-1172-5-16 (Accessed 15 July 2019).

Vanier, M. T., Duthel, S., Rodriguez-Lafrasse, C., Pentchev, P. and Carstea, E. D. (1996) 'Genetic heterogeneity in Niemann-Pick C disease: a study using somatic cell hybridization and linkage analysis.', *American journal of human genetics*, vol. 58, no. 1, pp. 118–25 [Online]. Available at http://www.ncbi.nlm.nih.gov/pubmed/8554047 (Accessed 15 July 2019).

Vanier, M. T. and Millat, G. (2004) 'Structure and function of the NPC2 protein', *Biochimica*

et Biophysica Acta (BBA) - Molecular and Cell Biology of Lipids, vol. 1685, no. 1–3, pp. 14–21 [Online]. DOI: 10.1016/j.bbalip.2004.08.007 (Accessed 15 July 2019).

Wang, A., Conicella, A. E., Schmidt, H. B., Martin, E. W., Rhoads, S. N., Reeb, A. N., Nourse, A., Ramirez Montero, D., Ryan, V. H., Rohatgi, R., Shewmaker, F., Naik, M. T., Mittag, T., Ayala, Y. M. and Fawzi, N. L. (2018) 'A single N-terminal phosphomimic disrupts TDP-43 polymerization, phase separation, and RNA splicing', *The EMBO Journal*, EMBO, vol. 37, no. 5 [Online]. DOI: 10.15252/embj.201797452 (Accessed 25 January 2021).

Wang, H.-Y., Wang, I.-F., Bose, J. and Shen, C.-K. J. (2004) 'Structural diversity and functional implications of the eukaryotic TDP gene family.', *Genomics*, vol. 83, no. 1, pp. 130–9 [Online]. Available at http://www.ncbi.nlm.nih.gov/pubmed/14667816 (Accessed 19 September 2018).

Weihl, C. C., Temiz, P., Miller, S. E., Watts, G., Smith, C., Forman, M., Hanson, P. I., Kimonis, V. and Pestronk, A. (2008) 'TDP-43 accumulation in inclusion body myopathy muscle suggests a common pathogenic mechanism with frontotemporal dementia', *Journal of Neurology, Neurosurgery and Psychiatry*, vol. 79, no. 10, pp. 1186–1189 [Online]. DOI: 10.1136/jnnp.2007.131334 (Accessed 17 April 2020).

Winton, M. J., Igaz, L. M., Wong, M. M., Kwong, L. K., Trojanowski, J. Q. and Lee, V. M.-Y. (2008) 'Disturbance of Nuclear and Cytoplasmic TAR DNA-binding Protein (TDP-43) Induces Disease-like Redistribution, Sequestration, and Aggregate Formation', *Journal of Biological Chemistry*, vol. 283, no. 19, pp. 13302–13309 [Online]. DOI: 10.1074/jbc.M800342200 (Accessed 21 September 2018).

Xiong, H. L., Wang, J. Y., Sun, Y. M., Wu, J. J., Chen, Y., Qiao, K., Zheng, Q. J., Zhao, G. xian and Wu, Z. Y. (2010) 'Association between novel TARDBP mutations and Chinese patients with amyotrophic lateral sclerosis', *BMC Medical Genetics*, BioMed Central, vol. 11, no. 1, p. 8 [Online]. DOI: 10.1186/1471-2350-11-8 (Accessed 14 April 2020).

Yamashita, M., Nonaka, T., Hirai, S., Miwa, A., Okado, H., Arai, T., Hosokawa, M., Akiyama, H. and Hasegawa, M. (2014) 'Distinct pathways leading to TDP-43-induced cellular dysfunctions', *Human Molecular Genetics*, vol. 23, no. 16, pp. 4345–4356 [Online]. DOI: 10.1093/hmg/ddu152.

Zampieri, S., Mellon, S. H., Butters, T. D., Nevyjel, M., Covey, D. F., Bembi, B. and Dardis,

A. (2009) ‘Oxidative stress in NPC1 deficient cells: protective effect of allopregnanolone.’, *Journal of cellular and molecular medicine*, vol. 13, no. 9B, pp. 3786–96 [Online]. DOI: 10.1111/j.1582-4934.2008.00493.x (Accessed 29 October 2019).

Zarei, S., Carr, K., Reiley, L., Diaz, K., Guerra, O., Altamirano, P., Pagani, W., Lodin, D., Orozco, G. and Chinea, A. (2015) ‘A comprehensive review of amyotrophic lateral sclerosis’, *Surgical Neurology International*, vol. 6, no. 1, p. 171 [Online]. DOI: 10.4103/2152-7806.169561 (Accessed 27 September 2018).

Zeiger, W. A., Jamal, N. I., Scheuner, M. T., Pittman, P., Raymond, K. M., Morra, M. and Mishra, S. K. (2018) ‘Probable diagnosis of a patient with niemann–pick disease type C: Managing pitfalls of exome sequencing’, in *JIMD Reports*, Springer, vol. 41, pp. 47–51 [Online]. DOI: 10.1007/8904_2018_90 (Accessed 16 April 2020).

Zhan, L., Hanson, K. A., Kim, S. H., Tare, A. and Tibbetts, R. S. (2013) ‘Identification of genetic modifiers of TDP-43 neurotoxicity in Drosophila.’, Tear, G. (ed), *PloS one*, vol. 8, no. 2, p. e57214 [Online]. DOI: 10.1371/journal.pone.0057214 (Accessed 10 January 2020).

Zhu, L., Xu, M., Yang, M., Yang, Y., Li, Y., Deng, J., Ruan, L., Liu, J., Du, S., Liu, X., Feng, W., Fushimi, K., Bigio, E. H., Mesulam, M., Wang, C. and Wu, J. Y. (2014) ‘An ALS-mutant TDP-43 neurotoxic peptide adopts an anti-parallel β-structure and induces TDP-43 redistribution’, *Human molecular genetics*, Hum Mol Genet, vol. 23, no. 25, pp. 6863–6877 [Online]. DOI: 10.1093/hmg/ddu409 (Accessed 25 January 2021).

Zou, Z. Y., Peng, Y., Wang, X. N., Liu, M. S., Li, X. G. and Cui, L. Y. (2012) ‘Screening of the TARDBP gene in familial and sporadic amyotrophic lateral sclerosis patients of Chinese origin’, *Neurobiology of Aging*, Elsevier Inc., vol. 33, no. 9, p. 2229.e11-2229.e18 [Online]. DOI: 10.1016/j.neurobiolaging.2012.03.014 (Accessed 14 April 2020).